Copyright

by

Bo Yang

2004

The Dissertation Committee for Bo Yang certifies that this is the approved version of the following dissertation:

Development of New Membranes for Proton Exchange Membrane and Direct Methanol Fuel Cells

Committee:

Arumugam Manthiram, Supervisor

David L. Bourell

Ofodike A. Ezekoye

Desiderio Kovar

Harovel G. Wheat

Development of New Membranes for Proton Exchange Membrane and Direct Methanol Fuel Cells

by

Bo Yang, B. E.; M. E.

Dissertation

Presented to the Faculty of the Graduate School of

The University of Texas at Austin

in Partial Fulfillment

of the Requirements

for the Degree of

Doctor of Philosophy

The University of Texas at Austin

August, 2004

Dedication

To my parents

Acknowledgements

I would like to express my deepest appreciation to my dissertation advisor, Dr. Arumugam Manthiram, for his supervision throughout the duration of this work. His guidance and encouragement have fostered independent thinking and individual initiative, yet he has always been available for consultation. I would also like to thank my supervisory committee, Dr. Desiderio Kovar, Dr. David L. Bourell, Dr. Ofodike A. Ezekoye, and Dr. Harovel G. Wheat, for serving on my committee and providing helpful advice and support during this study.

I also wish to take this opportunity to thank past and present members of Dr. Manthiram's group for the exchange of ideas and friendship. It has been a pleasure working with and learning from them during this work. In particular, I would like to thank Dr. A. M. Kannan, a former postdoctoral researcher in Dr. Manthiram's group, for all his help during the initial work of this project.

Lastly, and most importantly, I wish to thank my family, for all their support with love. It takes many efforts to finish this long course, and it would not have been possible without them.

This work was supported by the Welch Foundation Grant F-1254.

Development of New Membranes for Proton Exchange Membrane and Direct Methanol Fuel Cells

Publication No._____

Bo Yang, Ph. D.

The University of Texas at Austin, 2004

Supervisor: Arumugam Manthiram

Proton exchange membrane fuel cells (PEMFC) and direct methanol fuel cells (DMFC) are drawing much attention as alternative power sources for transportation, stationary, and portable applications. Nafion membranes are presently used in both PEMFC and DMFC as electrolytes, but are confronted with a few difficulties: (i) high cost, (ii) limited operating temperature of < 100 °C, and (iii) high methanol permeability. With an aim to overcome some of the problems encountered with the Nafion membranes, this dissertation focuses on the design and development of a few materials systems for use in PEMFC and/or DMFC.

The incorporation of hydrous $Ta_2O_5 \cdot nH_2O$ into Nafion membrane as well as the electrodes is shown to help the cell to retain water to higher temperatures. Membrane-electrode assembly (MEA) consisting of the composite membrane shows better cell performance at 100 and 110 °C than that with plain Nafion membrane, and a high power density of ~ 650 mW/cm^2 at 100 °C is obtained with

H_2 - CO mixture as the fuel due to a significant alleviation of the CO poisoning of the catalysts.

Sulfonated poly(etheretherketone) (SPEEK) membranes with various sulfonation levels are prepared and investigated in DMFC. With a sulfonation level of ~ 50 %, the SPEEK membranes exhibit low methanol permeability and electrochemical performance comparable to that of Nafion at around 60 °C, making it an attractive low-cost alternative to Nafion. From a comparative study of the structural evolutions with temperature in 2 M methanol solution, it is found that the lower methanol permeability of SPEEK membranes is related to the less connected and narrower pathways for water/methanol permeation.

The dry proton conductor $CsHSO_4$ shows a high proton conductivity of ~ 10^{-3} S/cm at temperatures > 140 °C and water is not needed for proton conduction. However, it is found that $CsHSO_4$ decomposes to Cs_2SO_4 and H_2S at 150 °C in H_2 atmosphere in contact with the Pt/C catalyst. Thus, new catalyst materials need to be explored for $CsHSO_4$ to be used in practical high temperature PEMFC.

Thin self-humidifying Nafion membranes with dispersed Pt/C catalyst powder are prepared and tested in PEMFC with dry H_2 and O_2. The Pt/C particles provide sites for catalytic recombination of H_2 and O_2 permeating from the anode and cathode, and the water produced at these sites directly humidifies the membrane. The performance of the cell with the self-humidifying membrane operated with dry reactants is ~ 90 % of that obtained with well humidified H_2 and O_2.

Table of Contents

Acknowledgements ..... **v**

Abstract ..... **vi**

List of Tables ..... **xiii**

List of Figures ..... **xiv**

Chapter 1 Introduction **1**

1.1 FUEL CELLS 1

1.1.1 Proton Exchange Membrane Fuel Cell (PEMFC) 4

1.1.2 Direct Methanol Fuel Cell (DMFC) 5

1.2 PROTON EXCHANGE MEMBRANE MATERIALS - NAFION 7

1.2.1 Structure of Nafion 7

1.2.2 Difficulties Associated with Nafion Membranes 9

1.3 PROTON CONDUCTION MECHANISMS 12

1.4 DEVELOPMENT OF HIGH TEMPERATURE PROTON EXCHANGE MEMBRANES 14

1.4.1 Modification of Nafion with Nanometer-size Hygroscopic Particles 14

1.4.2 Development of Alternative Sulfonated Polymers and Their Composite Membranes 17

1.4.2.1 Sulfonation of alternative polymers and their properties 18

1.4.2.2 Organic-inorganic composite membranes 21

1.4.3 Exploration of Anhydrous Proton Conducting Electrolytes 23

1.4.3.1 Acid doped membranes 23

1.4.3.2 Anhydrous polymeric proton conductors 26

1.4.3.3 Inorganic proton conductors 28

1.5 DEVELOPMENT OF PROTON EXCHANGE MEMBRANES WITH REDUCED METHANOL PERMEABILITY 29
1.5.1 Modification of Nafion Membranes 30
1.5.2 Development of Alternative Polymer Membranes 31
1.6 OBJECTIVES OF THIS DESSERTATION 32

Chapter 2 Experimental Procedures 35

2.1 MATERIAL AND MEMBRANE PREPARATIONS 35
2.1.1 Recast Method for Preparing Nafion Based Membranes [13] ... 35
2.1.2 Pre-treatment of Nafion Based Membranes 36
2.1.3 Homemade Pt/C Catalyst 36
2.2 MATERIALS CHARACTERIZATION 37
2.2.1 Scanning Electron Microscopy (SEM) 37
2.2.2 X-ray Diffraction (XRD) 37
2.2.3 Thermogravimetric Analysis (TGA) 37
2.2.4 Differential Scanning Calorimeter (DSC) 38
2.2.5 Liquid Uptake of Polymer Membranes 38
2.2.6 Proton Conductivity Measurement 38
2.3 MEMBRANE-ELECTRODE ASSEMBLY (MEA) PREPARATION 40
2.3.1 Electrode Preparation 40
2.3.2 Membrane-Electrode Assembly (MEA) Preparation 41
2.4 ELECTROCHEMICAL TESTING 41
2.4.1 Fuel Cell Performance Evaluation 41
2.4.1.1 H_2/O_2 fuel cell test 42
2.4.1.2 Low temperature DMFC test 42
2.4.2 Methanol Crossover Evaluation 43

Chapter 3 Hydrous $Ta_2O_5 \cdot nH_2O$ Modified Membrane-Electrode Assemblies for Proton Exchange Membrane Fuel Cells **44**

3.1 INTRODUCTION 44

3.2 EXPERIMENTAL 48

3.3 RESULTS AND DISCUSSION 50

3.3.1 Characterization of Hydrous $Ta_2O_5 \cdot nH_2O$ Particles 50

3.3.2 Membrane Characterization 53

3.3.3 H_2/O_2 PEMFC Performance 58

3.3.4 Effects of CO poisoning 66

3.3.5 Discussion of the Role of the Hydrous Oxides 73

3.4 CONCLUSIONS 76

Chapter 4 Polymer Electrolyte Membranes Based on Sulfonated Poly(etheretherketone) for Direct Methanol Fuel Cells **77**

4.1 INTRODUCTION 77

4.2 EXPERIMENTAL 79

4.3 RESULTS OF SPEEK MEMBRANES AND A COMPARISON WITH NAFION MEMBRANES 81

4.3.1 Sulfonation of PEEK 81

4.3.2 Determination of the Ion Exchange Capacity (IEC), Degree of Sulfonation (DS), and the Liquid Uptake 83

4.3.3 Thermal Stability: TGA Studies 87

4.3.4 Proton Conductivity 88

4.3.5 DMFC Tests and Methanol Crossover Evaluation 92

4.4 MULTILAYERED MEMBRANES 97

4.5 CONCLUSIONS 105

Chapter 5 Comparison of the *In-situ* Small Angle X-ray Scattering and Impedance Spectroscopic Studies of Sulfonated Poly(etheretherketone) and Nafion Membranes for Direct Methanol Fuel Cells **107**

5.1 INTRODUCTION 107

5.2 EXPERIMENTAL 110

5.3 RESULTS AND DISCUSSION 111

5.3.1 SAXS Profiles in Dry States 111

5.3.2 Influence of Sulfonation Level on SAXS Profile 114

5.3.3 Influence of Temperature on Bragg Spacing 117

5.3.4 Impedance Spectroscopic Studies 119

5.3.5 Relationship between SAXS and Fuel Cell Performance Data 127

5.4 CONCLUSIONS 128

Chapter 6 Dry Proton Conductor $CsHSO_4$ and Its Stability in Hydrogen Atmosphere **130**

6.1 INTRODUCTION 130

6.2 EXPERIMENTAL 135

6.3 RESULTS AND DISCUSSION 138

6.3.1 Characterizations of $CsHSO_4$ and PVDF/$CsHSO_4$ Composite Membranes 138

6.3.2 Chemical Stability Investigation of $CsHSO_4$ 142

6.3.3 Challenge in Preparing Dense Thin Membrane with $CsHSO_4$ 145

6.4 CONCLUSIONS 148

Chapter 7 Operation of Thin Nafion Based Self-Humidifying Membrane in Proton Exchange Membrane Fuel Cell with Dry H_2 and O_2 ..... **149**

7.1 INTRODUCTION 149

7.2 EXPERIMENTAL 151

7.3 RESULTS AND DISCUSSION 152

7.3.1 Cell Resistance vs. Current Density 152

7.3.2 Relationship Between the Cell Voltage Output and Water Management 155
7.3.3 PEMFC Performance 160
7.4 CONCLUSIONS 164

Chapter 8 Summary 165

Bibliography 171

List of Tables

Table 1.1: Essential and operational characteristics of different types of fuel cells [4,5]. 3

Table 1.2: Summary of the conductivity (σ) properties of some non-fluorinated polymer membranes. 21

Table 1.3: Summary of organic-inorganic composite membranes. 22

Table 4.1: Ion exchange capacity (IEC), degree of sulfonation (DS), proton conductivity (σ), and water uptake of SPEEK membranes obtained with different sulfonation reaction times. 85

Table 4.2: Comparison of the liquid uptake of SPEEK and Nafion membranes in methanol solution at different temperatures. 86

Table 4.3: Multilayered membranes and their thickness. 97

Table 4.4: Comparison of the open-circuit voltages (OCV) of the MEAs fabricated with the various multilayered membranes 102

Table 6.1: Comparison of the weight losses experienced by $CsHSO_4$, Pt/C, and $CsHSO_4$-Pt/C mixture on heating at 150 ^oC for 48 h. 137

Table 7.1: Comparison of the open circuit voltages (OCV) of cells fabricated with the plain N-N and the composite N-NPtC membranes at different temperatures with humidified H_2 and O_2. 156

Table 7.2: Comparison of the fraction of current density delivered by a PEMFC fabricated with the plain N-N and the composite N-NPtC membranes on operating with dry H_2/O_2. 162

List of Figures

Figure 1.1: Proton exchange membrane fuel cell. 4

Figure 1.2: Phenomenological sketch of Yeager's three-phase model structure of Nafion solid polymer electrolyte; A: perfluorinated backbone, B: interfacial zone, and C: ionic clusters [10]. 8

Figure 1.3: Langumuir-type adsorption of H_2 and CO on a smooth platinum surface as a function of temperature. These adsorption isobars are computed for 100 ppm CO in 1 bar H_2, based on the adsorptio equilibrium constants for CO and h on Pt (111) surfaces [13]. 11

Figure 1.4: Schematic illustration of the modes involved in proton conduction phenomena [20]. 13

Figure 1.5: Structure of some sulfonated polymers of interest as electrolytes for fuel cells. SPSU: sulfonated polysulfone; SPEEK: sulfonated poly(etheretherketone); SPES: sulfonated polyethersulfone; SPI: sulfonated polyimide; SPPBP: sulfonated poly(4-phenoxybenzoyl-1,4-phenylene)... 20

Figure 1.6: Structure of PBI. 25

Figure 1.7: Schematic representation of a polymer with imidazole terminated side chains [112]. 27

Figure 2.1: Schematic representation of the cell components employed for impedance measurement. 39

Figure 2.2: Single cell fuel cell test station used in this study. 41

Figure 2.3: Schematic diagrams showing the methanol permeation measurement in the DMFC configuration. For the permeation measurement, the humidified oxygen feed in DMFC is replaced by the humidified nitrogen feed and the electro-oxidation of methanol permeated through the membrane/electrode assembly takes place at the membrane/electrode interface at the cathode [144]. 43

Figure 3.1: Schematic of PEMFC illustrating modes of water, proton, and electron transports. 47

Figure 3.2: X-ray diffraction patterns of hydrous $Ta_2O_5 \cdot nH_2O$ before and after heating at various temperatures for 2 h. 50

Figure 3.3: A Scanning electron micrograph of the as-prepared $Ta_2O_5 \cdot nH_2O$ sample. 51

Figure 3.4: TGA curves of $Ta_2O_5 \cdot nH_2O$ before drying (as-prepared) and after drying at 150 °C for 2 h. The plots were recorded at a heating rate of 5 °C/min in a flowing dry air atmosphere. 52

Figure 3.5: Variations of water uptake of the membranes with temperature. ... 53

Figure 3.6: Typical impedance diagrams of Nafion/3 wt% $Ta_2O_5 \cdot nH_2O$ composite membrane: (a) at 80 °C and various relative humidities, and (b) at 100 % relative humidity and various temperatures. 54

Figure 3.7: Proton conductivities of native recast Nafion and composite membranes: (a) variation with relative humidity at 80 °C and (b) variation with temperature at 100 % R.H..... 55

Figure 3.8: Variations of the cell voltage and temperature with time with H_2 fuel for various MEAs: (a) native recast Nafion membrane and unmodified electrodes without $Ta_2O_5 \cdot nH_2O$, (b) Nafion-$Ta_2O_5 \cdot nH_2O$ composite membrane and unmodified electrodes without $Ta_2O_5 \cdot nH_2O$, (c) Nafion-$Ta_2O_5 \cdot nH_2O$ membrane and electrodes with $Ta_2O_5 \cdot nH_2O$, and (d) Nafion-$Ta_2O_5 \cdot nH_2O$ membrane and electrodes with $Ta_2O_5 \cdot nH_2O$ at 60 and 80 °C. The membrane thickness and the current density were kept constant at, respectively, 150 μm and 400 mA/cm^2. 60

Figure 3.9: Water balance cycle which may cause the observed periodic fluctuations in cell voltage during the operation of a PEMFC at a constant high current under conditions involving dehydration of the MEA. 61

Figure 3.10: Polarization curves and power density variations recorded with H_2 fuel and 50 μm thick membranes: (a) MEAs composed of electrodes with $Ta_2O_5 \cdot nH_2O$ and unmodified recast Nafion membrane and (b) MEAs composed of electrodes with $Ta_2O_5 \cdot nH_2O$ and Nafion membrane with $Ta_2O_5 \cdot nH_2O$. 64

Figure 3.11: Variations of the cell voltage with time at 100 and 110 °C with H_2 fuel for an MEA consisting of 50 μm thick modified Nafion membrane with $Ta_2O_5 \cdot nH_2O$ and electrodes with $Ta_2O_5 \cdot nH_2O$. 65

Figure 3.12: Variations of the cell voltage with time at 60 °C and 240 mA/cm^2 upon applying H_2-CO fuel (150 ppm CO). Both the cathode and anode sides were purged with the inert N_2 gas before applying the fuel and oxidant. 66

Figure 3.13: Polarization curves and power density variations recorded with H_2-CO fuel (150 ppm CO) and 50 μm thick membranes: (a) MEAs composed of electrodes with $Ta_2O_5 \cdot nH_2O$ and unmodified recast Nafion membrane and (b) MEAs composed of electrodes with $Ta_2O_5 \cdot nH_2O$ and Nafion membrane with $Ta_2O_5 \cdot nH_2O$. 67

Figure 3.14: Impedance plots recorded at (a) 0.85 and (b) 0.75 V with H_2 fuel and MEAs composed of modified Nafion (50 μm thick) membrane with $Ta_2O_5 \cdot nH_2O$ and electrodes with $Ta_2O_5 \cdot nH_2O$. 70

Figure 3.15: Impedance plots recorded at (a) 0.85 and (b) 0.75 V with H_2-CO fuel (150 ppm CO) and MEAs composed of modified Nafion (50 μm thick) membrane with $Ta_2O_5 \cdot nH_2O$ and electrodes with $Ta_2O_5 \cdot nH_2O$. 71

Figure 3.16: Schematic representation of the $Ta_2O_5 \cdot nH_2O$ structure and proton transport involved. 75

Figure 4.1: Sulfonation of PEEK polymer. 82

Figure 4.2: Thermogravimetric analysis of PEEK, SPEEK, and Nafion in flowing N_2 atmosphere at a heating rate of 5 °C/min. 88

Figure 4.3: Impedance spectra of SPEEK-44 membrane at 80 °C and various relative humidities. 91

Figure 4.4: Arrhenius plots of the variations of proton conductivity of Nafion and SPEEK membranes with relative humidity at 80 °C. 92

Figure 4.5: Comparison of the polarization characteristics of the SPEEK membranes with that of Nafion in DMFC: (a) 65 °C and (b) 80 °C. The data were collected with a methanol flow rate of 2.5 mL/m at the anode and a O_2 flow rate of 600 mL/m with a pressure of 40 psi at the cathode and the humidifier temperature for O_2 was same as the cell temperature. (Anode: 4 mg/cm^2 PtRu, Cathode: 3 mg/cm^2 Pt).. 94

Figure 4.6: Comparison of the variations of methanol crossover current density for SPEEK and Nafion membranes at different temperatures. The data were collected with a methanol flow rate of 2.5 mL/m at the anode and a N_2 flow rate of 600 mL/min and a P_{N_2} = 40 psi at the cathode. (Anode: 4 mg/cm^2 PtRu, Cathode: 3 mg/cm^2 Pt). The applied potential step is 1 mV/s 95

Figure 4.7: Comparison of the variations of methanol crossover current density for the multilayered membranes with a thickness of 135 µm at 60 and 80 °C. anode: 2.0 M methanol, 8 mL/min, cathode: N_2 flow rate = 600 ml/min, P = 15 psi. The applied potential step is 1 mV/s. 98

Figure 4.8: Comparison of the variations of methanol crossover current density for the multilayered membranes with a thickness of 115 µm at 60 and 80 °C. anode: 2.0 M methanol, 8 mL/min, cathode: N_2 flow rate = 600 ml/min, P = 15 psi. The applied potential step is 1 mV/s. 99

Figure 4.9: Cell voltage variation of MEA with N-S54-N(135) multilayered membrane after the cell is changed from the full current load to open circuit . T_{cell} = 60 °C, anode: 2.0 M methanol, 8 mL/min; cathode: oxygen flow rate = 600 ml/min, P = 15 psi. 101

Figure 4.10: Comparison of the polarization characteristics of the multilayered membranes with a thickness of (a) 135 µm and (b) 115 µm at 60 and 80 °C. The data were collected with a methanol solution (2 M) flow rate of 8 mL/min at the anode and a N_2 flow rate of 600 mL/min with a pressure of 15 psi at the cathode. (Anode catalyst: 0.6 mg/cm^2 PtRu, cathode: 1 mg/cm^2 Pt). 104

Figure 5.1: Comparison of the SAXS profiles of dry Nafion and SPEEK membranes. 112

Figure 5.2: Comparison of the SAXS profiles of sodium and cesium neutralized SPEEK membranes. 112

Figure 5.3: Comparison of the SAXS profiles of SPEEK and Nafion membranes after equilibrating in 2 M methanol solution at (a) 40 °C, (b) 50 °C, (c) 60 °C, (d) 70 °C, and (e) 80 °C. 116

Figure 5.4: Comparison of the SAXS profiles of SPEEK-44 and SPEEK-54 membranes after equilibrating in 2 M methanol solution at 40 ° C.. 117

Figure 5.5: Variations of the Bragg distance d with the equilibrating temperature in 2 M methanol solution for the SPEEK and Nafion membranes. 118

Figure 5.6: Impedance diagrams of the Nafion 115 membrane at 80 °C and various relative humidities. 121

Figure 5.7: Impedance diagrams of the SPEEK-54 membrane at 80 °C and various relative humidities. 122

Figure 5.8: Impedance diagrams of the SPEEK-58 membrane at 80 °C and various relative humidities. 123

Figure 5.9: Equivalent circuits, indicating the evolution of the cluster networks in the SPEEK-54 membranes with relative humidity at 80 °C: (a) 20 % R.H., (b) 70 % R.H., (c) 90 % R. H., and (d) 100 % R.H.. $R_{cluster}$, $R_{channel}$, and $R_{membrane}$ refer to the resistance of, respectively, the cluster, channel, and membrane. 125

Figure 6.1: Structures of $CsHSO_4$: (a) Phase III ($p2_1/c$), (b) Phase II ($p2_1/c$), and (c) Phase I ($I4_1/amd$) [182]. 132

Figure 6.2: X-ray diffraction patterns of (a) as-prepared $CsHSO_4$ after drying at 100 °C in air and (b) $CsHSO_4$ Pt/C mixture after heating at 150 °C in H_2 atmosphere for 48 h. All the reflections in (a) correspond to $CsHSO_4$ (Phase II) and the unmarked reflections in (b) correspond to Cs_2SO_4. 138

Figure 6.3: DSC plots of (a) as-prepared $CsHSO_4$, (b) $CsHSO_4$ after heating at 150 °C in H_2 atmosphere for 48 h, (c) $CsHSO_4$-Pt/C mixture before heating, (d) $CsHSO_4$-Pt/C mixture after heating at 150 °C in H_2 atmosphere for 48 h, and (e) $CsHSO_4$-Pt/C mixture after heating at 150 °C in air for 48 h. 139

Figure 6.4: Typical impedance diagrams of PVDF/$CsHSO_4$ composite membrane consisting of 70vol% $CsHSO_4$: (a) below the superprotonic transition temperature, (b) above the superprotonic transition temperature. 140

Figure 6.5: Arrhenius plots of the variations of proton conductivity with temperature of $CsHSO_4$ - PVDF composite membranes: (a) 50 % $CsHSO_4$ - 50 % PVDF and (b) 70 % $CsHSO_4$ - 30 % PVDF 142

Figure 6.6: SEM photograph of the 70 % $CsHSO_4$/30 % PVDF composite membrane. 146

Figure 6.7: SEM photographs of the 80 wt% $CsHSO_4$/20 wt% SPEEK-54 composite membrane. 147

Figure 7.1: Variations of the cell resistance with the current density of the MEAs fabricated with the plain N-N and composite N-NPtC membranes and operated with dry H_2 and O_2 at 60 °C. 153

Figure 7.2: Variation of the cell resistance with the current density of the MEAs fabricated with the plain N-N and composite N-NPtC membranes and operated with humidified H_2 and O_2 at 60 °C. 154

Figure 7.3: Variations of the cell voltage output with time of the MEAs fabricated with the plain N-N and composite N-NPtC membranes operated with dry H_2 and O_2 at a constant current density of 1 A/cm^2. 155

Figure 7.4: Scheme of water transports in the cell and the corresponding performance of a PEMFC operated at a constant high current density of 1 A/cm^2 with dry H_2 and O_2. 158

Figure 7.5: Variations of the cell voltage output of the MEAs fabricated with the composite N-NPtC membrane on changing the humidification state of the reactants. The cell was operated at 60 °C and 1 A/cm^2. 159

Figure 7.6: Polarization characteristics of the MEAs fabricated with the (a) plain N-N membrane and (b) composite N-NPtC membrane and operated with humidified H_2 and O_2 at different temperatures. ... 160

Figure 7.7: Polarization characteristics of the MEAs fabricated with the (a) plain N-N membrane and (b) composite N-NPtC membrane and operated with dry H_2 and O_2 at different temperatures. 161

Chapter 1

Introduction

1.1 FUEL CELLS

The increase in environmental pollution due to internal combustion engines (ICE) used in road vehicles and the depletion of the earth's energy reserves such as fossil fuels have drawn much attention since the 1960s [1-3]. Alternative power sources other than non-renewable fossil fuels have been considered since then. Fuel cells, which can offer the possibility of zero emission at the point of use, have been widely advocated to be the best candidates capable of emulating internal combustion engines.

Fuel cells are electrochemical devices that convert chemical energy directly into electrical energy. They receive gaseous or liquid reactants from an external source and vent the reaction products. Fuel is fed to the anode and oxygen or air is fed to the cathode. The chemical reactions result in ionic flow through the electrolyte and electron flow through the external circuit between the anode and cathode, and provide electrical energy similar to a traditional power generator. Unlike batteries that require recharging when the chemical reaction ceases and the stored energy is all used up, fuel cells do not require the time consuming process of recharging and can provide electricity continuously as long as the fuel and oxidant are supplied.

The other advantages associated with fuel cells include [1] (i) higher energy density and efficiency compared to internal combustion engines, (ii) simplicity due to the

absence of moving parts such as pistons and crankshafts, and (iii) low or zero emission with water being the only exhaust if hydrogen is used as the fuel.

Based on the type of electrolyte used, fuel cells can be classified into several types: proton exchange membrane fuel cell (PEMFC), direct methanol fuel cell (DMFC), alkaline fuel cell (AFC), phosphoric acid fuel cell (PAFC), molten carbonate fuel cell (MCFC), and solid oxide fuel cell (SOFC). A summary of some of the essential and operational characteristics of these fuel cell systems is given in Table 1.1.

Among the various kinds of fuel cells listed in Table 1.1, the PEMFC and DMFC are being considered as the most promising types of fuel cells for transportation and portable applications because of their high efficiencies, compact size, ease of construction, absence of liquid electrolyte, rapid startup time, low operating temperatures, and easier maintenance.

Table 1.1 Essential and operational characteristics of different types of fuel cells [4,5].

Characteristic	Type of fuel cell					
	PEMFC	**DMFC**	**AFC**	**PAFC**	**MCFC**	**SOFC**
Electrolyte	Proton exchange membrane	Proton exchange membrane	Potassium hydroxide	Phosphoric acid (85% - 100%)	Molten carbonates (Li, K, Na)	Solid oxide (ZrO_2-Y_2O_3)
Operating temperature	50 - 90 °C	50 - 90 °C (≤ 130 °C)	50 - 250 °C	180 - 200 °C	650 °C	600 - 1000 °C
Charge carrier	H^+	H^+	OH^-	H^+	CO_3^{2-}	O^{2-}
Catalyst	Pt	Pt and PtRu	Pt, Ni/NiO_x	Pt	$Ni/LiNiO_x$	Ni/Perovskites
Fuel	H_2 (pure or reformed)	CH_3OH	H_2	H_2 (reformed)	H_2 and CO (reformed) and CH_4	H_2 and CO (reformed) and hydrocarbons
Poison	CO >10 ppm	Adsorbed intermediates	CO, CO_2	CO > 1 % H_2S > 50 ppm	H_2S > 0.5 ppm	H_2S > 1 ppm
Efficiency (% HHV)[a]	32 - 45 (indirect) > 50 (direct)	~ 40	> 50 (direct)	36 - 45	43 - 55	43 - 55
Startup time (h)[b]	< 0.1	< 0.1	< 0.1	1 - 4	5 - 10	-
Applications	Transportation, stationary	Portable, transportation	Space	Power generation, cogeneration, transportation	Power generation, cogeneration	Power generation, cogeneration

[a] HHV: higher heating value, i.e., the total heat released including the latent heat of vaporization of the water formed by the oxidation process.
[b] For fuel-stack only, i.e., does not include response time for a fuel processor, if present.

1.1.1 Proton Exchange Membrane Fuel Cell (PEMFC)

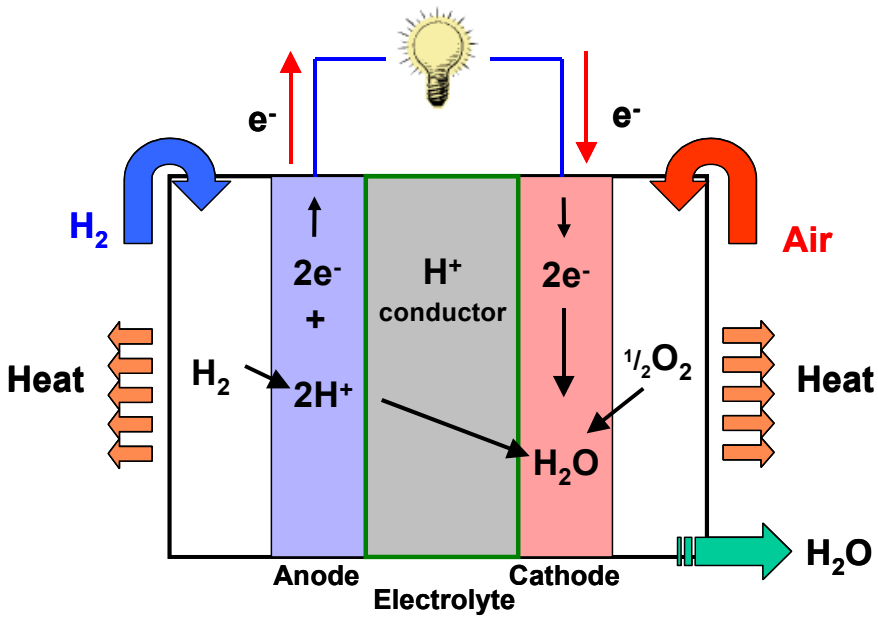

Figure 1.1 Proton exchange membrane fuel cell.

The state-of-the-art PEMFC operates at relatively low temperatures (~ 80 °C). It offers high power density (~ 700mW/cm^2) and can vary the output quickly to meet shifts in power demand. It is well suited for automobiles compared to other type of fuel cells as it can offer a quick startup. PEMFC consists of two bipolar graphite plates that hold a membrane-electrode assembly (MEA). MEA is the core part of the PEMFC and each MEA consists of two electrodes (anode and cathode) that are made of thin porous carbon cloth/paper with the catalyst (e.g. platinum and its alloy) deposited on them and an electrolyte membrane sandwiched between the two electrodes (Fig. 1.1). Hydrogen

and oxygen gases are supplied to the anode and cathode, respectively. The hydrogen is oxidized at the anode to hydrogen ions (protons) and free electrons. These electrons flow through the external circuit producing electrical energy by means of the external load, and arrive at the cathode to participate in the oxygen reduction reaction producing oxide anions. The protons diffuse through the membrane to the cathode side and combine with the oxide anions to form water. PEMFCs generally perform optimally with pure hydrogen fuel due to its extremely high electrochemical reactivity and practically zero pollution level. However, the storage and transportation of hydrogen pose complex problems. In this regard, on-board reforming of fuels such as methanol or gasoline to generate hydrogen has been a choice. However, the hydrogen gas stream thus produced usually contains some impurities such as carbon monoxide, which may poison the platinum, decrease the activity of platinum, and lower the cell performance dramatically.

1.1.2 Direct Methanol Fuel Cell (DMFC)

DMFC is similar to PEMFC in that they both use a polymer exchange membrane as the electrolyte. However, in the DMFC, liquid or vapor methanol instead of hydrogen is used as the fuel. Efficiencies of about 40 % are expected with this type of fuel cell. DMFC can either be operated at a temperature around 60 °C when liquid methanol is used or above 100 °C when methanol vapor is used.

Low-temperature DMFCs utilize liquid methanol fuel directly, eliminating the tedious tasks of fuel reforming and storage and transportation of gaseous hydrogen. Thus DMFC offers ease in refueling and simplified system design [4]. These advantages together with the high energy density of methanol and the recent advances in fabricating miniaturized fuel cells make DMFC systems attractive to replace the currently used lithium ion batteries in cellular phones, laptop computers, military back power packs, and other advanced mobile electronic devices.

In a DMFC, methanol is electrochemically oxidized at the anode and oxygen is electrochemically reduced at the cathode as shown below, involving the emission of CO_2 at the anode and H_2O at the cathode.

$$\text{Anode reaction: } CH_3OH + H_2O \rightarrow CO_2 + 6\,H^+ + 6\,e^- \qquad [1.1]$$

$$\text{Cathode reaction: } 3/2\,O_2 + 6\,H^+ + 6\,e^- \rightarrow 3\,H_2O \qquad [1.2]$$

$$\text{Overall reaction: } CH_3OH + 3/2\,O_2 \rightarrow 2H_2O + CO_2 \qquad [1.3]$$

Both the methanol oxidation and oxygen reduction reactions are kinetically sluggish. Therefore, expensive noble metals such as platinum and its alloys are presently used to catalyze these reactions, and the loadings are usually much higher than that used in the hydrogen fuel based PEMFC.

Besides the low performance (maximum power density reported is ~ 300 mW/cm^2), another hurdle that lies ahead the widespread commercialization of DMFC technology is methanol crossover from the anode to the cathode side [6], which is directly related to the swelling of the electrolyte membrane in the methanol-water mixture. More

details about the adverse impacts of methanol crossover on cell performance will be discussed later in Section 1.2.2.

1.2 PROTON EXCHANGE MEMBRANE MATERIALS - NAFION

1.2.1 Structure of Nafion

The heart of the PEMFC and DMFC is the proton exchange membrane (PEM). Ideally, the membrane should have high proton conductivity without any electronic transport and exhibit good impermeability for all other gas or liquid molecules. Additionally, it has to have excellent chemical and thermal stabilities. Currently, polyperfluorosulfonic acids such as Nafion membranes (Dupont de Nemours and Co., U.S.A.) are almost exclusively used in both PEMFC and DMFC due to their excellent chemical, mechanical, and thermal stabilities and relatively high proton conductivity of around 0.08 $S \cdot cm^{-1}$ in the hydrated state [7,8]. Additionally, unsurpassed longevity (> 60,000 h) in a fuel cell environment has been reported [9].

The exact structure of Nafion is not understood well, but it is commonly accepted that it combines the extreme hydrophobicity of the perfluorinated polymer backbone with the extreme hydrophilicity of the terminal sulfonic acid ($-SO_3H$) groups. This leads to a spontaneous hydrophilic/hydrophobic nano-separation even in the dry state. In the presence of water, only the hydrophilic part of the microstructure is hydrated. The water then acts as a plasticizer mobilizing the polymer backbone, which leads to a

further phase separation. Fig. 1.2 shows the commonly accepted three-phase model of Nafion structure first proposed by Yeager [10].

The unique properties of Nafion membranes are believed to be closely related to such phase-separated structures. Their hydrophobic part provides relatively good mechanical stability, while the hydrated hydrophilic domains provide high proton conductivity. These properties make Nafion membrane suitable for low temperature proton exchange membrane fuel cells.

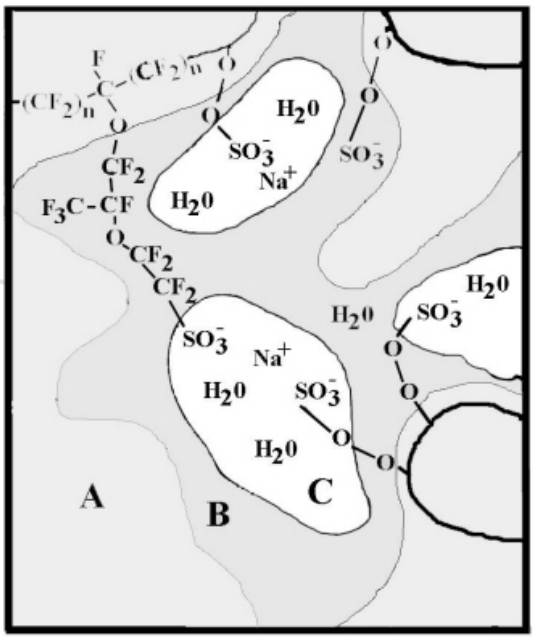

Figure 1.2 Phenomenological sketch of Yeager's three-phase model structure of Nafion solid polymer electrolyte; A: perfluorinated backbone, B: interfacial zone, and C: ionic clusters [10].

1.2.2 Difficulties Associated with Nafion Membranes

Despite the obvious advantages of the Nafion membranes, there are a few disadvantages in using them for PEMFC and DMFC applications.

High cost: The first disadvantage of Nafion is its high price (~ $780/m^2) [11], which contributes significantly to the overall cost of PEMFCs and DMFCs. The high cost of Nafion membranes is associated with the difficult synthesis of the monomers.

Limited operating temperature: Nafion membranes need to be humidified to provide satisfactory proton conductivity because of the hydrophilic nature of the sulfonic acid groups attached to the polymer backbone and the necessity to hydrate the ionic clusters. At ambient pressure, when the temperature exceeds the boiling point of water, the membrane dehydrates and experiences a dramatic decrease in the proton conductivity. Consequently, Nafion is regarded as unsuitable for fuel cell applications above 100 °C.

However, it would be desirable to operate the PEMFCs at temperatures as high as 150 °C because operation at elevated temperatures can provide several important advantages. For example, the higher operating temperature can provide faster reaction kinetics and possibly allow the use of less expensive non-platinum catalysts as the other normally less active catalysts could become active at higher temperatures. Most importantly, by increasing the operating temperature, the CO tolerance of Pt catalyst can be improved significantly. Hydrogen generated by reforming fuels such as methanol or gasoline usually has a CO level as high as 50 - 100 ppm. For the state-of-

the-art PEMFCs, which usually operate at around 80 °C, trace amount of CO as low as 10 - 20 ppm in the H_2 feed gas will result in a significant cell performance loss due to CO poisoning of the Pt anode electrocatalyst. In other words, CO is more easily adsorbed on the Pt catalyst, preventing the availability/accessibility of the electrode surface for H_2 adsorption. Therefore, careful purification of the reformed hydrogen is necessary to remove the CO traces, which are usually carried out by means of a water-gas shift reaction, preferential oxidation, membrane separation, or methanation [12]. However, the fuel cleanup unit increases the weight, cost, and the complexity of the system. Enhancement in the tolerance to higher levels of CO impurities in the fuel will not only simplify the power system by reducing the number of CO cleanup stages or even completely eliminating the cleanup units, but also lower the cost of the overall fuel cell system, enhancing the commercial viability.

An effective approach to gain CO tolerance is to take advantage of the fact that the free energy of adsorption of carbon monoxide on Pt has a larger positive temperature dependence than that of H_2. This effect is illustrated in Fig. 1.3, which shows the fractional coverage of CO and H on a Pt surface assuming competitive Langumuir-type adsorption [13]. It can be seen that the hydrogen coverage on Pt increases rapidly with increasing temperature while the coverage of CO drops dramatically. In other words, the CO tolerance will be significantly enhanced, from 10 - 20 ppm of CO at 80 °C to 1000 ppm at 130 °C, and up to 30,000 ppm at 200 °C [14]. This high CO tolerance makes it possible for a fuel cell to use hydrogen directly from a simple reformer, so that the CO cleanup unit can be eliminated from the fuel processing system. Therefore,

developing high temperature (> 100 °C) proton exchange membranes has been a key issue in the PEMFC area.

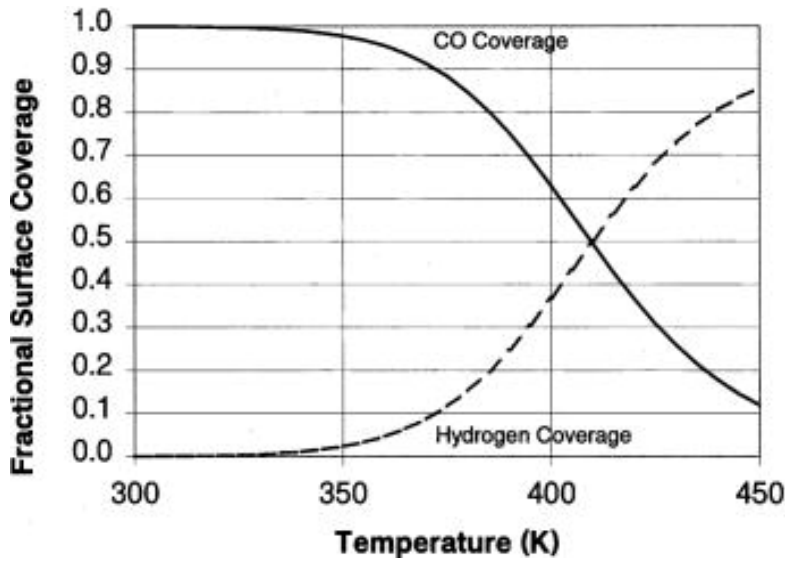

Figure 1.3 Langumuir-type adsorption of H_2 and CO on a smooth platinum surface as a function of temperature. These adsorption isobars are computed for 100 ppm CO in 1 bar H_2, based on the adsorption equilibrium constants for CO and H on Pt (111) surfaces [13].

High methanol permeability: Another problem arises when Nafion membrane is used in DMFC as methanol is easily transported through the Nafion membrane by means of (a) active transport along with the protons and their solvate water (electro-osmotic drag) and (b) diffusion through the Nafion membrane itself due to concentration gradient [15,16]. This phenomenon is usually called methanol crossover, and it not only wastes the fuel but also leads to an undesired reaction taking place at the cathode platinum catalyst: the oxidation of methanol permeating through the membrane at the cathode. This reaction leads to a mixed potential formation at the

cathode [17,18], which results in a severely reduced electrode potential, and therefore a severely reduced overall cell voltage and much poorer fuel cell performance.

These difficulties associated with the Nafion membranes have sparked enormous interest to develop alternative less expensive membranes that can offer a higher operating temperature (T > 100 °C) and/or lower methanol permeability. Generally, two strategies are being employed. The first strategy is to modify the currently used Nafion membranes to overcome some of the problems. The second strategy is to develop new membranes based on fluorine-free ionomers or anhydrous proton conductors.

According to these two strategies, various approaches are being actively investigated to overcome one or more of the problems associated with Nafion membrane. Before discussing the details of these approaches, it would be helpful to understand the mechanisms involved in proton conduction.

1.3 PROTON CONDUCTION MECHANISMS

Generally, there are two principal mechanisms involved in proton conduction: vehicle and Grotthuss mechanism [19,20], which are illustrated in Fig. 1.4 [20].

The most trivial case of proton migration requires the translational dynamics of bigger species: this is the vehicle mechanism. In this mechanism the proton diffuses through the medium together with a "vehicle" (e.g. as H_3O^+ and $H_5O_2^+$). The observed conductivity, therefore, is directly dependant on the vehicle diffusion rate Γ_D.

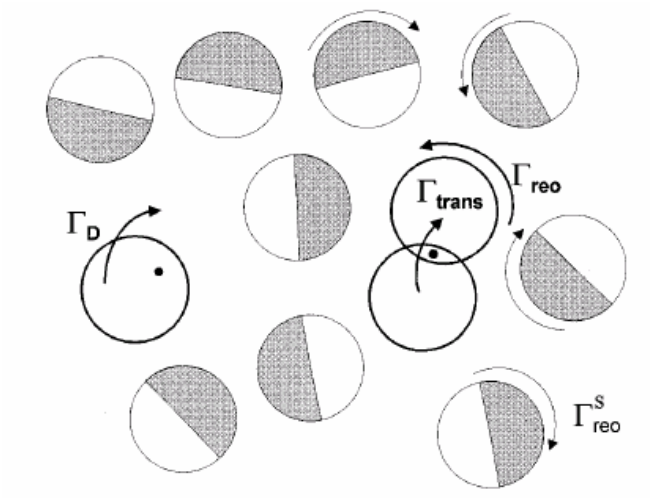

Figure 1.4 Schematic illustration of the modes involved in proton conduction phenomena [20].

In the Grotthuss mechanism, the vehicles show pronounced local dynamics but reside on their sites. The protons are transferred from one vehicle to the other through hydrogen bonds (proton hopping). In the meantime, reorganization of the proton environment, consisting of reorientation of individual species or even more extended ensembles, results in the formation of an uninterrupted path for proton migration. This reorganization usually involves the reorientation of solvent dipoles (e.g. H_2O), which is an inherent part of establishing the proton diffusion pathway. The proton transfer rate Γ_{trans} and reorganization rate Γ_{reo} of its environment affect directly this mechanism.

These two principle mechanisms essentially reflect the difference in the nature of the hydrogen bonds formed between the protonated species and their environment. In media that support strong hydrogen bonding, the Grotthuss mechanism is preferred; the vehicle mechanism is characteristic of species with weaker hydrogen bonding.

1.4 DEVELOPMENT OF HIGH TEMPERATRUE PROTON EXCHANGE MEMBRANES

To increase the operating temperature of the proton exchange membranes, a variety of alternative approaches have been pursued over the past two decades. They include (1) modification of Nafion membranes by incorporating nanometer-size hygroscopic particles (e.g. SiO_2 [13,21-25], TiO_2 [26,27], and $Zr(HPO_4)_2{\cdot}H_2O$ [28-30]) to help retain water at elevated temperatures, (2) development of alternative sulfonated polymers and their composite membranes [31,32], and (3) exploration of anhydrous polymeric [33] and inorganic proton conductors [34,35] which do not need water as the proton carrier.

1.4.1 Modification of Nafion with Nanometer-size Hygroscopic Particles

Hygroscopic particles such as SiO_2, TiO_2, and $Zr(HPO_4)_2{\cdot}H_2O$ can very easily adsorb water and the strongly hydrogen bonded lattice waters in these materials are kept at high temperatures (~ 200 °C). By introducing these particles into Nafion membranes, the hydrophilicity of the ionic clusters in the membrane is expected to be enhanced and water is kept to higher temperatures (> 100 °C).

Hygroscopic particles modified Nafion membranes can be prepared by two main procedures [30]:

(a) Dispersion of nanometer size filler particles or precursors in a Nafion solution followed by casting [13,27,36]. In the procedures of this type, nanometer size

powder is dispersed under strong stirring or ultrasonic blending in a Nafion solution and the membrane is obtained by casting the mixture followed by solvent elimination. The method is very simple, but it is usually difficult to avoid the formation of particle agglomerates inside the polymeric matrix, and thus membranes containing non-homogeneous dispersions of micro-size particles are usually obtained. To overcome this problem, appropriate precursors instead of preformed particles are mixed with the Nafion solution, and the precursors are converted into the final inorganic particle with a very uniform distribution during solvent elimination.

(b) *In-situ* formation of inorganic particles in preformed membranes [13,37-39]. This procedure is usually carried out in two steps: (1) introducing a filler precursor into the polymeric matrix by simple impregnation (if the filler is neutral) or by ion-exchange reaction (if the filler is a cationic species) and (2) converting the precursor into the final inorganic by treating the membrane with the necessary reactants. If this reaction is an acid-catalyzed hydrolysis, then the protogenic function of the ionomer itself can act as a catalyst, and external reactants are not necessary. A typical example is the impregnation of Nafion membranes with tetraethoxysilane (TEOS), which is then converted into the final filler, SiO_2. However, the stability of the particles in the membranes needs to be investigated.

Hygroscopic particle modified Nafion composites usually have higher water uptake than that of the plain Nafion. For example, Wang *et al.* [40] reported that composite membranes consisting of 5 wt% SiO_2 in Nafion could absorb 35 wt% water at room temperature compared to 26 wt% water for the pristine Nafion membrane.

Proton conductivity measurements of the hygroscopic particle modified Nafion membranes have also been carried out, but discrepancies exist among the results. Some studies showed higher proton conductivity for hybrid membranes compared to native Nafion membranes [41,42]. On the other hand, some results indicated that increased water uptake does not always result in a proportional increase in proton conductivity [22,28].

Hygroscopic particles modified Nafion composite membranes have also been tested in both H_2/O_2 PEMFC and DMFC at temperatures above 100 °C [13,21,23,28,43,44]. For example, at 130 °C under a pressure of 3 atm, a PEMFC based on an *in-situ* sol-gel formed Nafion 115/6 wt% SiO_2 membrane delivered a current density of ~ 850 mA/cm^2 at 0.4 V; this value is 3 times as that of unmodified Nafion 115 membranes [13]. Antonucci *et al.* [23] tested a DMFC at 145 °C under pressures of 4.5 atm for methanol-water and 5.5 atm for air, and obtained a peak power density of more than 200 mW/cm^2, which is a very encouraging result.

Although a lot of studies have been conducted on the development of Nafion/hygroscopic particle composite membranes, the functioning mechanisms of these particles are not very well understood. It is believed that the presence of these hygroscopic particles decreases the chemical potential of the water inside the membrane and thereby creates a continuous pathway for the proton conduction even at the reduced-humidity condition. At the same time, they provide hydrogen bonding sites for water in the membrane so that the hydration of the membrane will be increased and the transport and evaporation of water will be reduced. The enhanced water retention

enables low humidification and high temperature operation of both H_2/O_2 (air) PEMFC and DMFC.

However, little information is available towards using practical reformed H_2 reactant that includes impurities such as carbon monoxide, and the CO poisoning effect study at temperatures above 100 °C is sparse.

In addition, it should be noted that the performance of the modified membrane at higher temperatures (> 100 °C) was usually poorer than that of unmodified membrane at 80 °C and the power density was low. For transportation applications, it is highly desired that the PEMFCs deliver high power density. Therefore, the operating conditions need to be studied and optimized to obtain high power density with practical, reformed H_2 reactant.

1.4.2 Development of Alternative Sulfonated Polymers and Their Composite Membranes

A large number of polymer materials have been prepared and functionalized as membrane electrolytes for PEMFC. These materials were principally investigated to lower the membrane electrolyte cost for low-temperature operation [31,45-48]. Some of these materials, especially the sulfonated hydrocarbons, show interesting and promising features for a possible high-temperature operation [32,49]. In the meantime, more efforts are being made to develop organic-inorganic composites based on these alternative polymers due to the intrinsic limitations of the pristine materials [30,50].

1.4.2.1 Sulfonation of alternative polymers and their properties

For developing polymer electrolytes for fuel cells, many material systems have been widely investigated, including polysulfones (PSU) [51-55], polyethersulfones (PES) [56], various polyetherketones (PEKs) [31,57-63], polybenzimidazoles (PBI) [31,64,65], polyimides (PI) [66,67], poly(4-phenoxybenzoyl-1,4-phenylene) (PPBP) [31,58]. All these materials offer high temperature stability under steam/O_2 and steam/ H_2 atmospheres up to 200 °C [68], unlike Nafion which is not capable of withstanding those conditions.

Despite their thermohydrolytic stability, the proton conductivities of these polymers are inadequate. Proton conduction properties can be conferred by addition of a protogenic, generally a sulfonic acid, group. Sulfonation can be performed in several ways as follows: (1) direct sulfonation in concentrated sulfuric acid or chlorosulfonic acid [69-74], (2) radiation-grafting of monomers onto the polymer backbone followed by sulfonation [75], (3) chemical grafting of sulfonated monomers onto the polymer backbone [64], (4) synthesis from monomers bearing sulfonic acid groups [66], and (5) lithiation-sulfonaton-oxidation [76]. The structures of some sulfonated polymer materials are shown in Fig. 1.5. The sulfonation of these polymers leads to a marked improvement of the proton conduction properties. This is due to the enhancement of the density of the mobile protons, and the increased water-uptake that sulfonation allows.

The degree of sulfonation (DS) is critical to the performance and stability of the sulfonated polymers. Too low a sulfonation level may lead to insufficient proton

conductivity. However, too high a level of sulfonation can also be accompanied by an undesirable swelling of the polymer in water, or even water solubility. Therefore, the sulfonation level must be optimized to get the satisfactory proton conductivity as well as mechanical behavior.

A large number of results on the primary properties such as swelling behaviors and proton conductivities of these sulfonated polymers have been reported. Table 1.2 summarizes the proton conductivities of some sulfonated polymer membranes. It can be seen that decent proton conductivities have been obtained with these sulfonated polymers. However, it should be noted that the temperature and humidity dependences of the proton conductivity of most of the alternative sulfonated polymers are rarely different from those of the Nafion membrane, and they often have poorer thermal and chemical stabilities in the fuel cell environment compared to the Nafion membrane.

Despite the extensive studies of alternative sulfonated polymer membranes, very limited information is available on the long-term durability of them under practical fuel cell operations. Durability of at least 4000 h in a H_2/O_2 PEMFC was reported for SPEEK membranes, but at a low operation temperature of 50 °C [77]. Bauer *et al*. [57] tested SPEEK membranes discontinuously (shut-down overnight) at temperatures of 90 - 110 °C for several days.

SPSU

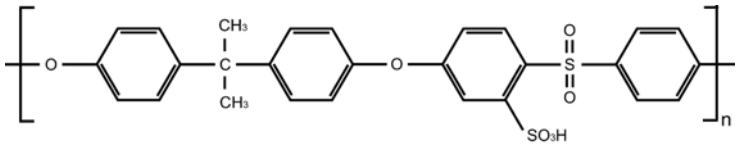

SPEEK

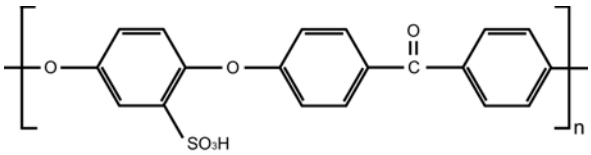

SPES

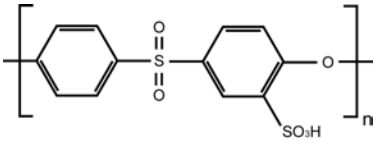

SPI

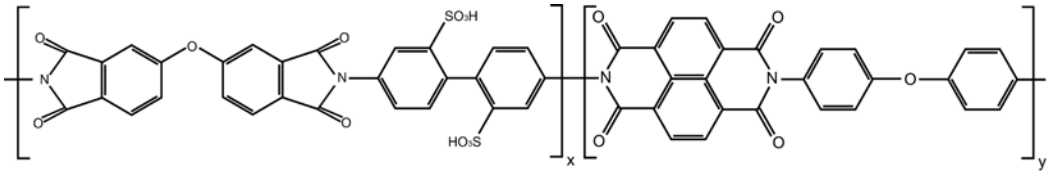

SPPBP

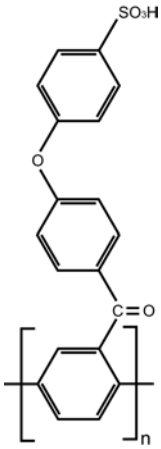

Figure 1.5 Structures of some sulfonated polymers of interest as electrolytes for fuel cells (SPSU: sulfonated polysulfone; SPEEK: sulfonated poly(etheretherketone); SPES: slulfonated polyethersulfone; SPI: sulfonated polyimide; SPPBP: sulfonated poly(4-phenoxybenzoyl-1,4-phenylene)).

Table 1.2 Summary of the conductivity (σ) properties of some non-fluorinated polymer membranes.

Membrane	IEC* (meq/g)	σ (S·cm^{-1})	Reference
SPEEK	1.6	0.04 (100 °C, 100 % R.H.)	[46,57]
	1.02	0.025(100 °C, 100 % R.H.)	[78]
	2.0 - 2.3	0.0067 - 0.076 (100 °C, 100 % R.H.)	[79]
	2.48	0.09 (100 °C, 100 % R.H.)	[49]
SPPBP	65 % DS**	0.005 (100 °C, 75 % R.H.)	[58]
SPSU	1.1	0.01 (80 °C, 100 % R.H.)	[51]
	1.07	0.002 (80 °C, 96 % R.H.)	[80]
SPI	1.6 - 2.7	0.09 - 0.21 (80 °C, 100 % R.H.)	[67,81]
	1.63	0.014 (100 °C, 100 % R.H.)	[82]
	1.98	0.037 (100 °C, 100 % R.H.)	[83]

* IEC: Ion exchange capacity
** DS: Degree of sulfonation

1.4.2.2 Organic-inorganic composite membranes

Aiming at higher operating temperatures, improved proton conductivity, and better mechanical properties, extensive efforts have been made to develop hydrocarbon polymer based organic-inorganic composites [30,39]. The principles and processes for preparing these composites are similar to those for Nafion based composites (Section 1.4.1), and the details will not be repeated here.

For preparing organic-inorganic composite membranes, the used polymer components include those without functional groups such as poly(ethyleneoxide)s

(PEO) and PBI, and those with functional groups such as sulfonated polysulfone (SPSU), sulfonated polyetheretherketone (SPEEK), and many others. Table 1.3 summarizes these developments with brief comments.

Table 1.3 Summary of inorganic-organic composite membranes.

Polymer	Inorganic filler**	Comments	Reference
SPEEK	SiO_2	3.4×10^{-2} S·cm^{-1} at 100 °C, 100% R.H; H_2/O_2 fuel cell test at 90 - 110 °C	[47]
SPEEK	$Zr(HPO_4)_{0.5}(O_3PC_6H_4SO_3H)_{1.5}$	4.0×10^{-2} S·cm^{-1} at 150 °C, 100% R.H, H_2/O_2 fuel cell test at 70 - 120 °C	[50]
SPEEK	HPA	1×10^{-1} S·cm^{-1} above 100 °C	[79]
SPEEK	BPO_4	5×10^{-1} S·cm^{-1} at 160 °C, fully hydrated	[59]
SPSU	PAA	2×10^{-2} S·cm^{-1} at 80 C, 98 % R.H.	[84]
SPSU	PAA	H_2/O_2 cell, 500 h at 80 °C and 4 atm	[25]
PBI	SiWA+ SiO_2	2.2×10^{-3} S·cm^{-1} at 160 °C, 100 % R.H.	[85]
PBI	PWA + SiO_2 + H_3PO_4	1.5×10^{-3} S·cm^{-1} at 150 °C, 100 % R.H.	[86]
GPTS*	SiWA + ZrP	1.9×10^{-2} S·cm^{-1} at 100 °C, 100 % R.H.	[87]
PEO	Tungsten acid	10^{-2} S·cm^{-1}at 120 °C;	[88]

* GPTS: 3-glycidoxypropyltrimethoxysilane.
** HPA: heteropolyacids; PAA: phosphatoantimonic acid; PWA: phosphotungstic acid; SiWA: silicotungstic acid; ZrP: zirconium hydrogen phosphate.

As can be seen from Table 1.3, some of these composite membranes exhibit promising conductivities at temperatures above 100 °C. However, most of these composite membranes have not been tested in fuel cells.

1.4.3 Exploration of Anhydrous Proton Conducting Electrolytes

For both Nafion and sulfonated hydrocarbon polymer based membranes to be used in PEMFCs, additional humidification system is required to obtain satisfactory proton conductivities; this increases the complexity of the fuel cell system and the cost and reduces the energy density. Hence, a high temperature (120 - 200 °C) fuel cell membrane that operates without humidifier system, but with high proton conductivity, would make the existing PEMFC technology much more attractive. In this regard, several fundamental approaches have been proposed and investigated. The first one is simply based on the substitution of the water with a strong acid that is capable of conducting protons in a similar way at higher temperatures. A second approach points toward fully polymeric systems that exhibit proton conductivity as an intrinsic property. The third approach involves the exploration of high temperature inorganic proton conductors.

1.4.3.1 Acid-doped membranes

It has been shown that substitution of water by strong acids such as phosphoric acid and sulfuric acid leads to proton conductivities comparable to the conductivities of hydrated polymers, but at temperatures between 150 and 250 °C. Phosphoric acid-doped membranes have been paid much attention because of the intrinsic property of phosphoric acid and ease in preparing blends with a large variety of polymers due to hydrogen bonding interaction. The acid-doped membranes can be prepared by [89] (1)

immersing the preformed polymer membrane in phosphoric acid solution or (2) directly casting from a solution of polymer and H_3PO_4 in a suitable solvent.

Several polymers such as poly(ethyleneoxide) (PEO) [90,91], poly(ethyleneimine) (PEI) [92,93], and poly(acrylamide) (PAAM) [94] have been used as the matrix for doping H_3PO_4 and reasonable proton conductivities have been reported for these systems at temperatures > 100 °C. However, these materials suffer from either thermomechanical or thermochemical limitations.

In 1995, Wainright *et al.* [95] proposed a blend of poly(benzimidazole) (PBI) and phosphoric acid as the electrolyte for H_2/O_2 PEMFC and DMFC for the first time. Usually, the term PBI refers to the structure shown in Fig. 1.6; however, several related polymers have been prepared. PBI is an amorphous, basic polymer of extraordinary thermal stability with a glass transition temperature of about 430 °C. Compared to the Nafion membranes, PBI is about 100 times less expensive. A considerably higher mechanical strength of H_3PO_4 doped PBI compared to that of Nafion has been reported [96]. The electroosmotic drag coefficient of water and methanol measured at different water activities, current densities, and temperatures up to 200 °C is essentially zero [97,98], whereas for Nafion, a drag number of 0.6 to 2 makes continuous humidification essential [99,100].

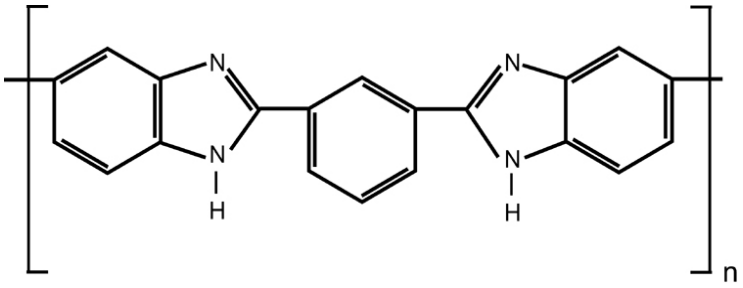

Figure 1.6 Structure of PBI.

Generally, the phosphoric acid molecules interact with PBI mainly by hydrogen bonding. Hydrogen bonds immobilize the anions and form a network for proton transfer by the Grutthuss mechanism. The proton hopping from one N-H site to phosphoric acid anions contributes significantly to the conductivity.

The presence of free or unbound acid is necessary to improve the conductivity and the proton conductivity of PBI/H_3PO_4 is found to be strongly dependent on the temperature and acid doping level [89,101]. At a doping level of 2 mol of H_3PO_4 per repeat unit, the conductivity of the membrane is about 2.5×10^{-2} S·cm^{-1} at 200 °C [102]. At a acid-doping level of 5.7 mol H_3PO_4, the measured conductivity is 4.6×10^{-3} S·cm^{-1} at room temperature, 4.8×10^{-2} S·cm^{-1} at 170 °C, and 7.9×10^{-2} S·cm^{-1} at 200 °C [102].

Although high proton conductivities of PBI/H_3PO_4 have been reported in dry conditions, it has been observed that at a given temperature, an increase in the relative humidity leads to higher proton mobility and conductivity [95].

The performance of PBI/H_3PO_4 membranes in fuel cells appears to be very promising based on the following data: power densities of 250 mW/cm^2 at 150 °C for a H_2/O_2 fuel cell [103] and 100 mW/cm^2 at 200 °C for a DMFC [104] have been achieved. Recently, Li *et al.* [105] reported a power density of 500 mW/cm^2 at 200 °C using methanol reformate as fuel without humidification. However, whether humidification of PBI fuel cells is necessary for long-term operation remains an open question. Also, the retention of H_3PO_4 in the fuel cells under long-term operating conditions still needs to be confirmed.

In the field of phosphoric acid-based materials, PBI blends currently seem to be unrivaled because all blends using alternative polymers suffer from inferior stability. Unfortunately, research on PBI-based membranes has shifted to a large extent from academic institutions to industry, and little information is available on recent developments, fuel cell performance, or long-term stability.

1.4.3.2 Anhydrous polymeric proton conductors

Another interesting group of solvents with potential to replace water is the nitrogen-containing aromatic heterocycles such as imidazole, pyrazole, and benzimidazole. These materials contain both proton donor (NH) and acceptor (N) and have extraordinary thermal and/or chemical stabilities. They exhibit moderate conductivities in the liquid state, which was ascribed to some degree of self-dissociation. In general, the behaviors of these heterocycles towards protons are very similar to that of water [33]. They can form hydrogen bonded networks similar to that

in water, and the transport properties in the liquid state are also similar to water, but at about 100 °C higher.

Based on the above facts of the heterocycles, a totally new strategy has been proposed recently and several model material systems have been investigated [106-112]. Such heterocycles can be tethered in appropriate way to soft side chains linked to a polymer network, and they may still aggregate to form a dynamic hydrogen bonded network with high mobility although they have become a constituent of the polymer's architecture (Fig. 1.7). Melting of such hierarchic architectures commences at different temperatures in different parts of the macromolecule (side chains may melt at lower temperatures than the entire polymer). The liquid-like domain then provides the proton conductivity while the solid-like part gives the material morphological stability.

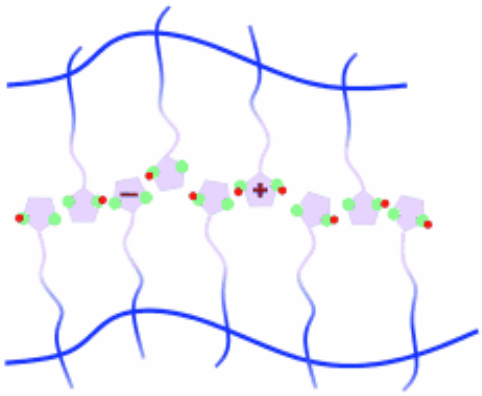

Figure1.7 Schematic representation of a polymer with imidazole terminated side chains [112].

Proton mobility in an environment of immobilized heterocycles must completely rely on Grotthuss mechanism comprising proton transfer between heterocycles and their reorganization. Recently, a set of imidazole-terminated ethylene oxide oligomers (Imi-2/-3/-5) have been studied as model systems [110,111]. Investigations have shown a close relation between conductivity and T_g, suggesting that the rate of intermolecular proton transfer depends on the available free volume, which in turn governs the local mobility of the heterocycle units. Proton conductivities of up to 5×10^{-3} S·cm^{-1} at 120 °C in the completely water-free materials have been obtained [111].

However, the developments based on this single-phase proton-conducting polymers strategy are still in the state of basic research rather than close to the application stage due to the difficulty of tethering the heterocycles onto appropriate polymer networks to obtain stable membranes with high proton conductivity at high temperatures. The step from a proof of concept to a stable, optimized membrane remains to be a challenge.

1.4.3.3 Inorganic proton conductors

Exploring dry inorganic proton conductors is another interesting approach of developing electrolyte materials for high temperature PEMFC. In this regard, solid acids such as $CsHSO_4$ [34,113] and CsH_2PO_4 [35] have been paid much attention since they can offer a significantly higher operating temperature of 150 - 200 °C. For example, $CsHSO_4$ transforms at around 140 °C into a superionic phase exhibiting a high proton conductivity of 10^{-3} - 10^{-2} S·cm^{-1}. With an operating temperature of 150 - 200 °C, it can alleviate the poisoning of the Pt-based catalysts by CO, simplify the

design of the fuel cell system without the need to have humidifiers as the proton conduction occurs in the absence of water.

However, the problems of the solubility in water and difficulties to fabricate thin membranes with these inorganic proton conductors need to be addressed before they can get any practical use in PEMFC applications. In addition, the chemical stability of these materials in the fuel cell environment needs to be fully assessed.

1.5 DEVELOPMENT OF PROTON EXCHANGE MEMBRANES WITH REDUCED METHANOL PERMEABILITY

In principle, enhancing the catalyst activity can alleviate the problem of methanol crossover. For example, operating the DMFC in an optimal manner such that all methanol can be consumed within the anode catalyst layer before reaching the membrane can alleviate the problem. Nevertheless, membrane with reduced methanol permeability is desirable to decrease the methanol crossover rate and to improve the dynamic cell response to a rapid change in load demand.

In this regard, two strategies have been employed to develop proton exchange membranes with reduced methanol permeability: (1) modification of Nafion membrane, and (2) exploration of alternative polymer materials.

1.5.1 Modification of Nafion Membranes

The high methanol permeability of Nafion membrane is believed to be related to the phase-separated structure. This unique structure provides a series of ion channels, which facilitate methanol permeation across the membrane.

Several polymers such as polypyrrole [114-116], polyaniline [117], and poly(1-methylpyrrole) [118] have been chemically or electrochemically impregnated into the nano-pores inside the Nafion membranes to form composites. For example, dried Nafion has been immersed in neat 1-methylpyrrole, rinsed with ethanol, and then soaked in ethanol. The 1-methylpyrrole within the membrane has then been polymerized by exposing the dried membrane to radiation from a UV lamp. The modified membrane thus obtained lowered methanol permeability by about 40 % compared to that with the plain Nafion membrane [118].

Instead of modifying the whole membrane, plasma [119-121] and electron beam (EB) [122,123] have been applied to modify only the surface structure of Nafion and create a thin methanol impermeable barrier at the membrane surface. By exposing Nafion 117 membranes to low dose EB irradiation with controlled accelerating voltage, the hydrophilic side chains and pendant SO_3H groups were removed increasingly from the polymer, leaving the PTFE backbone of the Nafion largely intact [122]. The modified membrane was shown to significantly reduce methanol crossover compared to the parent Nafion. Due to the effect of lowered methanol crossover, up to about 50 % increase in peak DMFC power output over native Nafion membrane was achieved.

These modified Nafion-based membranes have shown a potential for blocking the methanol transport. However, they generally suffer from a decrease in proton conductivity and some experience a loss in mechanical strength.

Hygroscopic particle modified Nafion membranes have also been applied to DMFC with a high operating temperature (> 100 °C) [23,44,124,125]. The kinetics of methanol oxidation reaction was improved at higher operating temperatures, offering the possibility to deliver higher current density. Thus, most of the methanol was consumed at the anode side before reaching the membrane, and the adverse effects of methanol crossover on the cathode catalyst was significantly alleviated. However, whether the hygroscopic particles in the Nafion membrane can help to block methanol in the low temperature DMFC remains a question due to the contradictory results reported in the literature [25,125,126].

1.5.2 Development of Alternative Polymer Membranes

Membranes based on some of the hydrocarbon polymers discussed in section 1.4.2.1 for high temperature PEMFC also show some interesting properties with respect to applications in DMFC. Among them, polyimide (PI) [66,81,127], polysulfones (PSU) [52,128], polyphenylene (PPO) [129-131], and various polyketones (PEK) [46,132-134] are actively being investigated.

Many studies have focused on the physical properties such as swelling, thermal stability, methanol permeability, and proton conductivity. The primary results show

that these materials are promising for DMFC applications. However, many of these performance features are not well understood mainly due to the complexity of the membrane structures arising from the phase separation when hydrated. In addition, little information is available on the performance of DMFC, and the long-term stabilities of these hydrocarbon polymers need to be investigated before they can get any practical use in DMFC. In the meantime, much attention is being paid to the development of composite membranes based on the above-mentioned polymers [30,135-139]. The preparation methods are similar to that of the Nafion based membranes, and so they will not be repeated here.

In addition, many efforts are being made to explore suitable membranes for DMFC by blending two or even three of the above-mentioned polymers [46,128,132,140-142]. By cross-linking the ionomer membranes covalently, the strong swelling of membranes at higher temperatures can be avoided.

1.6 OBJECTIVES OF THIS DISSERTATION

The general objective of this dissertation is to develop proton exchange membranes that can overcome some of the problems encountered with the conventional Nafion membrane. A few membrane systems are investigated systematically, and their advantages and limitations compared to Nafion are presented. The primary membrane characteristics such as proton conductivity, thermal stability, swelling behavior, and structural information are investigated. The membranes are tested in practical fuel cells

and based on the data, optimizations of the operating conditions are pursued. The knowledge gained can provide a better understanding of the proton conduction mechanisms and help in designing new membrane materials. In detail, the following are investigated:

(1) With an aim to increase the operating temperature and alleviate the CO poisoning effect in PEMFC, hydrous tantalum oxide ($Ta_2O_5 \cdot nH_2O$) modified membrane-electrode-assemblies are investigated at temperature > 100 °C. The incorporation of the hydrous oxide into both the Nafion membrane and the active layers of the electrodes is expected to help to retain the water to higher temperatures (> 100 °C). The cell performance with the modified membrane-electrode assemblies is evaluated with H_2 - CO mixture as the fuel and the effects of CO poisoning at different temperatures is studied. To better understand the roles of the hygroscopic particles in the membrane, a hydrous oxide structure model is employed to illustrate how the hydrous oxides involve in water retention and proton conduction in the Nafion membrane.

(2) With an aim to suppress methanol crossover, sulfonated poly(etheretherketone) (SPEEK) membranes with various sulfoantion levels are investigated in DMFC. The variations of % liquid uptake at different temperatures and methanol concentrations, proton conductivity, methanol crossover, and polarization data in DMFC with the degree of sulfonation are studied. The optimum condition under which the membrane will have acceptable proton conductivity and satisfactory mechanical property is identified.

In addition, the SPEEK and Nafion membranes are compared by investigating with the small angle X-ray scattering (SAXS) and electrochemical impedance spectroscopic techniques. Based on the scattering data and impedance diagrams, structural evolutions of these two kinds of membranes upon swelling are discussed.

(3) With an aim to explore membranes that can operate without external humidification, the chemical stability of the solid acid, cesium hydrogen sulfate ($CsHSO_4$) is studied in an environment similar to that of practical high temperature fuel cells. Additionally, the challenges in fabricating thin films with $CsHSO_4$ are addressed.

(4) With an aim to study the possibility of operating PEMFC with dry H_2 and O_2 reactants, a thin double-layer composite membrane consisting of one layer of Pt/C catalyst powder dispersed recast Nafion membrane and one layer of plain recast Nafion was investigated in PEMFC. The Pt/C particles in the membrane are expected to provide sites for catalytic recombination of permeating H_2 and O_2 from the anode and cathode; thus the crossover of the reactants was suppressed and water produced at these sites can directly humidify the membrane, leading to the proper operation of the PEMFC with dry reactants.

Chapter 2

Experimental Procedures

In this dissertation, all commercial chemicals were used as received without further purification unless stated otherwise.

2.1 MATERIAL AND MEMBRANE PREPARATIONS

Due to the variety of the materials systems used in this study, most of the material preparation methods and membrane fabrication processes will be described in the corresponding chapters. Some general procedures are given below.

2.1.1 Recast Method for Preparing Nafion Based Membranes [13]

A 1:2 volume ratio of commercial 5 wt% Nafion solution (DuPont Fluoroproducts) and isopropyl alcohol (99.9 %, Fisher Scientific) were ultrasonically mixed for 30 min. The mixture was then poured into a flat-bottom glass dish with a diameter of ~ 14 cm and dried at 90 °C for about 12 h. By adding deionized water into the dish, the formed membranes could be easily peeled off, and the membranes were flexible and strong. To prepare Nafion/oxide composite membranes, the same recast method was employed, excepting an appropriate amount of the oxide powder was mixed with the Nafion and isopropyl alcohol solution before casting and drying.

2.1.2 Pre-treatment of Nafion Based Membranes

Generally, both the commercial and recast Nafion membranes include some organic and heavy metal impurities and need to be purified before using. The common membrane cleaning procedure is given below. The membranes were boiled for over 1 h in 5 % hydrogen peroxide (H_2O_2) to get rid of the organic impurities. Then they were rinsed in deionized water several times and boiled in 1 M H_2SO_4 for another 1 h to dissolve the heavy metal impurities in the membrane. Finally, the membranes were rinsed in boiling deionized water for another 1 h. The membranes thus prepared in the acid form were stored in deionized water before use.

2.1.3 Homemade Pt/C Catalyst

Homemade Pt/C catalysts were prepared *in-situ* on high surface area Vulcan XC-72R support by reducing chloroplatinic acid (H_2PtCl_6) solution with 0.5 M sodium formate solution [143]. Typically, the reduction reaction was conducted at ~70 °C by simultaneously adding dropwise the chloroplatinic acid solution from one burette and the sodium formate solution from another burette into a constantly stirring carbon slurry that was prepared by suspending the Vulcan XC-72R in deionized water and ultrasonically mixing for 30 min. The reaction mixture was stirred for another 1 h after completing the addition of the solutions to ensure the completeness of the reaction. The solid mass was then filtered, washed with hot deionized water, and dried in an air oven at about 100 °C overnight.

2.2 MATERIALS CHARACTERIZATION

The general materials characterization methods used in this study will be discussed here briefly and the special details will be presented in the respective chapters.

2.2.1 Scanning Electron Microscopy (SEM)

Morphologies of the powder and membrane were investigated with a JEOL JSM-5610 scanning electron microscope. Before the SEM observation, the samples were coated with Au/Pd alloy to suppress charging effects.

2.2.2 X-ray Diffraction (XRD)

X-ray power diffraction was used to identify the phases present in the samples. A Phillips diffractometer with CuKα radiation was used to collect the diffraction data at a scan rate of 0.05° per 2 seconds between the 2θ values of 10 and 80°. The collected data were matched with the Joint Committee on Powder Diffraction Standards (JCPDS) files for phase identification.

2.2.3 Thermogravimetric Analysis (TGA)

A Perkin-Elmer series 7 thermogravimetric analyzer (TGA) was used to study the change in mass with temperature of the samples. Usually, the experiments were carried out at a heating rate of 5 °C/min in a specific flowing atmosphere.

2.2.4 Differential Scanning Calorimeter (DSC)

A Perkin-Elmer series 7 differential scanning calorimeter (DSC) was used to study the thermal behaviors such as phase transitions or decomposition. Usually, the experiments were conducted with around 10 mg of sample in N_2 atmosphere at a heating rate of 10 °C/min.

2.2.5 Liquid Uptake of Polymer Membranes

Liquid uptake of the polymer membrane was calculated by taking the difference between the dry mass (m_{dry}) and wet mass (m_{wet}) of a membrane sample. The dry weight was measured in a capped weighing bottle after the sample was dried at 100 °C in vacuum for 24 h. To obtain the wet mass, a membrane was equilibrated with deionized water or methanol solution at different temperatures for 24 h. The wet membrane was then blotted carefully with a filter paper to remove surface water droplets before being transferred to a capped weighing bottle for weighing. The percent liquid uptake was determined using the following formula:

$$PercentageUptake = \frac{(m_{wet} - m_{dry})}{m_{dry}} \times 100$$

2.2.6 Proton Conductivity Measurement

The proton conductivities of the membranes were calculated from the impedance data, which were collected with a computer interfaced HP 4192A LF Impedance

Analyzer, in the frequency range of 5 Hz - 13 MHz with an applied voltage of 10 mV. Measurements were carried out using a two-electrode setup and stainless steel was used as the blocking electrodes. In order to realize a good electrode/electrolyte contact, the electrode/membrane/electrode sandwich was pressed together by three screws. The components of the cell for impedance measurements are shown in Fig. 2.1.

For those measurements where humidity was needed, the sample fixture was put into an environmental chamber (Model 9000L, VWR Scientific), where the temperature and humidity could be controlled. The membrane area was chosen to be larger than that of the electrode holder to help the membrane equilibrate with the water vapor at each relative humidity (see Fig. 2.1). The data were collected after the equilibrium was obtained and the impedance reached a stable value.

The conductivity of the membrane is calculated using the equation,

$$\sigma = l / RA$$

where σ, l, R and A are, respectively, the ionic conductivity, thickness of the membrane, the resistance of the membrane, and the area of the electrode.

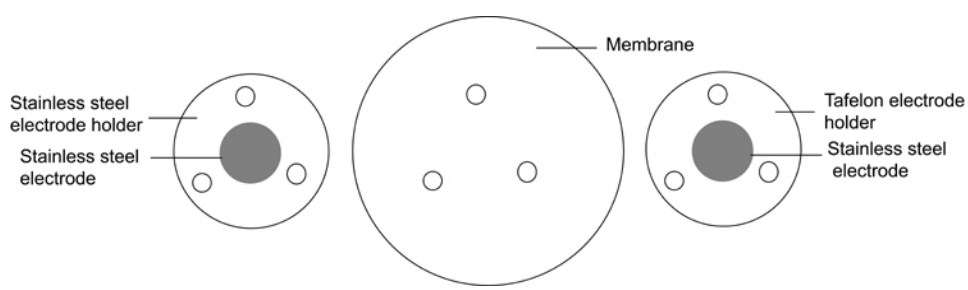

Figure 2.1 Schematic representation of the cell components employed for impedance measurement.

2.3 MEMBRANE-ELECTRODE ASSEMBLY (MEA) PREPARATION

2.3.1 Electrode Preparation

(a) Nafion-mixed electrodes: Both the anode and cathode electrodes for single cell testing consisted of gas-diffusion and catalyst layers. The gas diffusion layer was prepared by spraying a mixture of the Vulcan XC-72R carbon black, solvent (mixture of water and isopropyl alcohol in a volume ratio of 1:2), and 40 wt% PTFE onto a teflonized carbon cloth (Electrochem. Inc.) and sintering at 300 °C for 2 h. The catalyst layer was prepared by spraying a mixture of the required amount of either commercial or homemade carbon-supported catalyst, solvent (mixture of water and isopropyl alcohol in a volume ratio of 1:2), and commercial 5 wt% Nafion solution (with 33 wt % dry Nafion in the catalyst layer) onto the gas diffusion layer and drying in a vacuum oven at 90 °C for 1 h. In this dissertation, the electrodes thus prepared are called "Nafion-mixed electrodes".

(b) Nafion-impregnated electrodes: In this kind of electrodes, the gas-diffusion layer was prepared by exactly the same procedure as that for the "Nafion-mixed electrodes". The difference lies in the catalyst layer. Here, a mixture of the required amount of the carbon-supported catalyst and solvent (mixture of water and isopropyl alcohol in a volume ratio of 1:2) was sprayed onto the gas diffusion layer and sintered at 300 °C for 2 h. Then a mixture of commercial 5 wt% Nafion solution and isopropyl alcohol in a volume ratio of 1:2 was impregnated into the catalyst layer by the same

spraying technique and dried in a vacuum oven at 90 °C for 1 h. The electrodes thus prepared are called “Nafion-impregnated electrodes” in this study.

2.3.2 Membrane-Electrode Assembly (MEA) Preparation

To prepare the MEA, a piece of the polymer membrane was sandwiched between an anode and a cathode; then they were hot pressed uniaxially using a Chemplex SpectroPress. First, without pressure, the temperature was kept at 50 °C for 5 min, 75 °C for 3 min, 100 °C for 2 min, and 130 °C for 1 min. Then at the same temperature of 130 °C, the pressure was increased to 2000 psi and kept at this value for 2 min.

2.4 ELECTROCHEMICAL TESTING

2.4.1 Fuel Cell Performance Evaluation

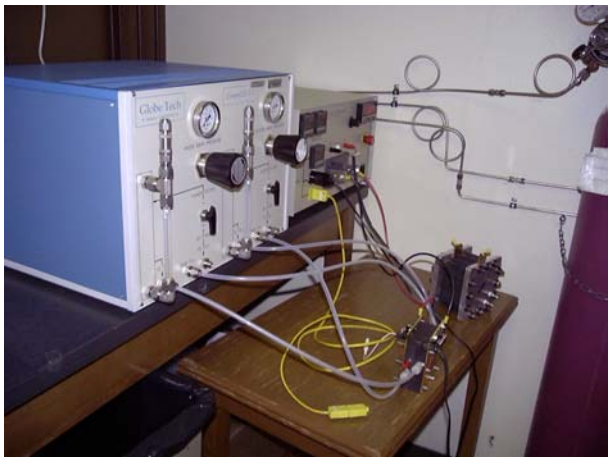

Figure 2.2 Single cell fuel cell test station used in this study.

The electrochemical performances of the MEAs in PEMFC and DMFC were evaluated with a commercial fuel cell test system (Compucell GT, Electrochem Inc.) using a single cell fixture having an active area of 5 cm^2 (Fig. 2.2). The experimental results were collected under steady-state conditions.

2.4.1.1 H_2/O_2 fuel cell test

High purity hydrogen (H_2) and oxygen (O_2) were fed, respectively, into the anode and cathode. The temperature, pressure, humidity, and gas flow rates could be controlled through the test station. In order to humidify the gases prior to the entry into the fuel cell, the H_2 and O_2 gases were bubbled through water contained in stainless steel bottles at a specified temperature.

2.4.1.2 Low temperature DMFC test

Around 1 liter methanol solution was stored in a glass tank which was heated with a heating mantle (Electrothermal Engineering Ltd.). The temperature in the tank was monitored and controlled. The tank has four ports at the top: one for a temperature probe, one for an outlet supplying methanol solution to the pump/cell, one for an air condenser, and the last one for the inlet return from the cell. Usually, the methanol solution was preheated to the same temperature as the cell and was fed into the anode at a certain flow rate controlled by a peristaltic pump without back pressurization. Oxygen was fed into the cathode side with controlled pressure, temperature, humidity, and flow rate.

2.4.2 Methanol Crossover Evaluation

Methanol crossover was evaluated in the same single DMFC by a qualitative method [144] in which methanol solution was fed into the anode side of the MEA while the cathode side was kept in an inert humidified N_2 atmosphere. By applying a positive potential at the cathode side (Fig. 2.3), the methanol permeation flux through the membrane could be calculated by measuring the transport-controlled limiting current of the methanol electro-oxidation process at the Pt/membrane interface at the cathode. During the measurement, the fuel cell was kept at open circuit state.

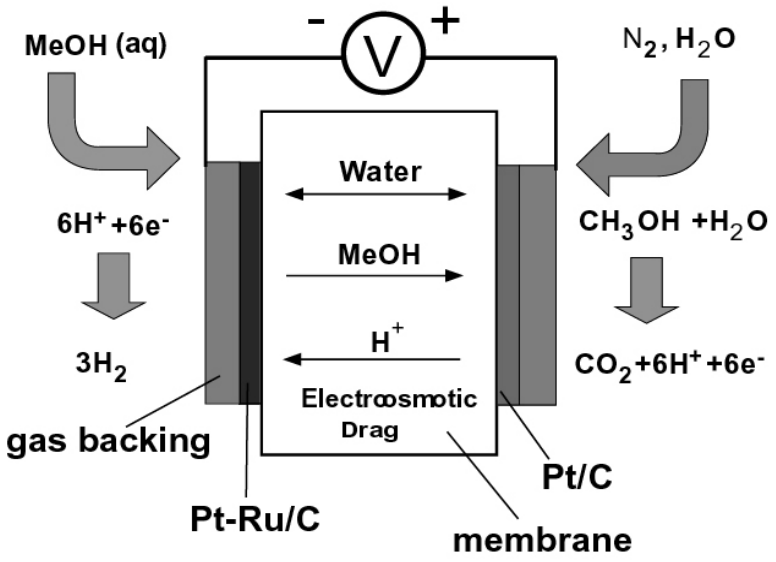

Figure 2.3 Schematic diagrams showing the methanol permeation measurement in the DMFC configuration. For the permeation measurement, the humidified oxygen feed in DMFC is replaced by the humidified nitrogen feed and the electro-oxidation of methanol permeated through the membrane/electrode assembly takes place at the membrane/electrode interface at the cathode [144].

Chapter 3

Hydrous $Ta_2O_5 \cdot nH_2O$ Modified Membrane-Electrode Assemblies for Proton Exchange Membrane Fuel Cells

3.1 INTRODUCTION

As discussed in chapter 1, several approaches are being actively investigated to develop high temperature proton exchange membranes for PEMFC applications. However, the proton conductivities of most of the alternative sulfonated polymers have similar temperature and humidity dependences as those of Nafion, and much poorer electrochemical performances are often observed for these membranes. On the other hand, the realization of mechanically strong membranes with high proton conductivity and good stability remains a challenge with the anhydrous proton conductors.

Nafion membranes thus still remain as a benchmark and appropriate modification (e.g., incorporation of hygroscopic nanometer size particles into the membrane) to increase their operating temperature is an attractive strategy. However, the performance of the modified membranes at higher temperatures (> 100 °C) was found to be usually poorer than that of the unmodified membranes at conventional operating temperature of around 80 °C and the power density was low[13,28].

On the operation aspect, the water balance in a PEMFC involves the following mechanisms (Fig. 3.1): (1) water supply from the fuel and oxidant through humidification, (2) water produced at the cathode due to cell reaction, (3) water drag

from the anode to the cathode by the protonic current, and (4) back diffusion of water from the cathode to the anode due to the concentration gradient. The water balance is essential for the proton conduction and the electrochemical performance of the fuel cell. If the MEA is too dry, the proton conductivity falls, resulting in reduced cell performance. An excess of water in the fuel cell leads to cathode flooding problems, also resulting in less than optimal performance.

As shown in Fig. 3.1, in order to keep the continuous cell reactions, good proton and electron transports must be achieved. Generally, electron transport is not an issue due to the high electronic conductivity of the support materials such as carbon in both the diffusion and catalyst layers. On the other hand, proton transport depends on the operating conditions such as reactants humidification levels, hydration state of the membrane, and the current density being delivered. Large-scale numerical investigation of PEMFC performances under both fully humidified gas feed and low-humidity operation also indicates that the ionic resistances in the anode and cathode catalyst layers were comparable to that in the membrane, indicating that the ionic conductivity of the catalyst layers need to be considered in optimizing PEMFC performance [145].

For transportation applications, the PEMFCs are expected to operate at high current densities in order to deliver a high power density. However, at high current densities, the anode side may suffer from a shortage of water due to the high electro-osmotic water drag coefficients of the protonic current. Thus, when operating at temperature > 100 °C, not only does the membrane dehydrate, but also the Nafion in the active layer

of the electrode dries out, causing an increased resistance and overpotential in the electrodes. To overcome this problem, hygroscopic particles have been impregnated to the catalyst layers as well to retain water at higher temperatures [146,147].

When the operating temperature of PEMFC is increased above 100 °C, the CO poisoning effect is reduced, but the proton conductivity may decrease. Therefore, the dependences of both CO poisoning and cell resistance on temperature must be considered to find the optimum operating condition that can offer high power density with the reformed H_2 fuel containing CO impurities.

Besides hydrous tetravalent oxides like $SiO_2 \cdot nH_2O$ and $TiO_2 \cdot nH_2O$, some hydrous pentavalent oxides such as $Sb_2O_5 \cdot nH_2O$ and $Ta_2O_5 \cdot nH_2O$ [19,148] are known to be good proton conductors. We present here the synthesis of nanometer size hydrous $Ta_2O_5 \cdot nH_2O$, its incorporation into the Nafion membrane as well as the active layer of the electrodes, and an evaluation of the electrochemical performance of the MEA in PEMFC. The electrochemical data are collected at various temperatures with pure H_2 and H_2-CO mixture as the fuel and the results are compared with those obtained with pristine recast Nafion membranes.

Although extensive studies have been carried out on oxide modified Nafion membranes for PEMFC, the functions of these oxides are not still understood well. In this study, a hydrous oxide structure model is employed to illustrate how the hydrous oxides participate in water retention and proton conduction in Nafion membrane. This discussion may help to optimize the properties of the oxides and prepare better oxide-modified membranes for high temperature PEMFCs.

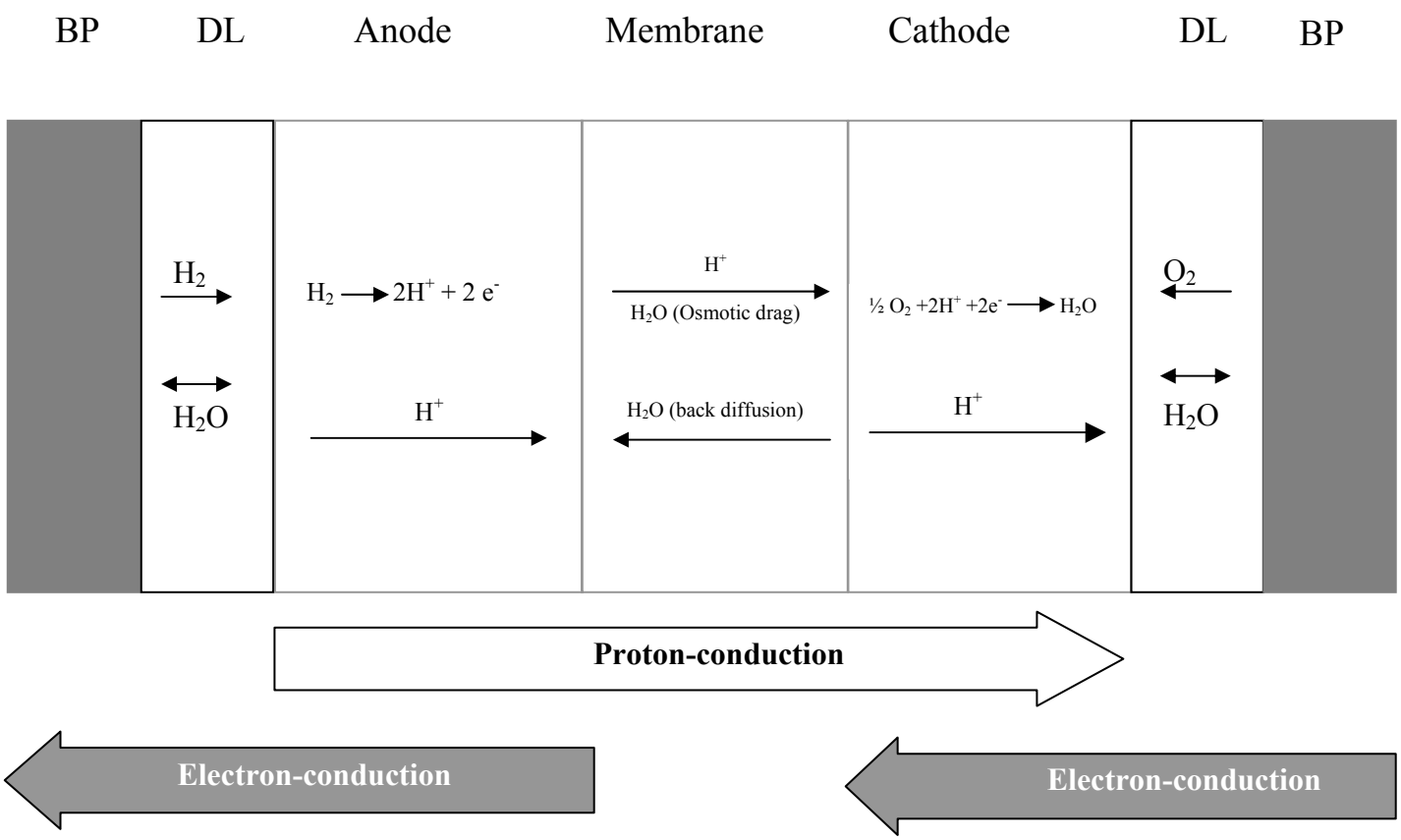

BP: bipolar plate DL: diffusion layer

Figure 3.1 Schematic of PEMFC illustrating modes of water, proton and electron transports.

3.2 EXPERIMENTAL

Nanometer size hydrous $Ta_2O_5 \cdot nH_2O$ was synthesized by dissolving Ta_2O_5 oxides in HF (49.25 % solution) at 70 °C for 24 h to get a clear solution, followed by a slow addition of ammonium hydroxide, filtering the white precipitate formed, and washing with deionized water until the pH of the filtrate reduces to around 7. The hydrous $Ta_2O_5 \cdot nH_2O$ was then dried in air at ambient temperature. The sample was characterized by X-ray diffraction (XRD), scanning electron microscopy (SEM), and thermogravimetric analysis (TGA).

Composite Nafion/3 wt% $Ta_2O_5 \cdot nH_2O$ and plain Nafion membranes were prepared by the recast method and the thickness of the membrane was controlled by varying the amount of the recast mixture. All the membranes were post-treated following the cleaning procedure given in chapter 2.

Measurements of the water uptake and proton conductivity of the native recast Nafion and composite membranes were carried out, and the experimental details are given in chapter 2.

A commercial 20 wt% Pt on Vulcan XC-72R (E-TEK) catalyst was used both in the anode and cathode. "Nafion-mixed electrodes" (see section 2.3.1.1) were prepared for single cell tests. The carbon loading in the diffusion layers was 5 $mg \cdot cm^{-2}$ and dry Nafion percentage in the catalyst layers was 33 wt%. For the modified catalyst layers, a small amount of $Ta_2O_5 \cdot nH_2O$ was added to the catalyst and solvent mixture before ultrasonic blending and spraying. The Pt metal loading in all the electrodes was 0.4

mg·cm^{-2}. In the case of catalyst layers containing $Ta_2O_5 \cdot nH_2O$, the $Ta_2O_5 \cdot nH_2O$ loading was 0.2 mg·cm^{-2}.

The MEAs were fabricated by uniaxially hot-pressing the electrodes (anode and cathode) thus obtained onto the membrane at 130 °C for 2 min. The MEAs were evaluated in the H_2/O_2 and H_2 - CO (150 ppm CO)/O_2 PEMFC. The gas pressures at the anode and cathode were kept at 36 and 38 psi, respectively. The flow rates of the fuel (H_2 or H_2 - CO mixture) and oxidant (O_2) were ~ 50 mL/min, which corresponded to a stoichiometry of 1.5 at 1 A/cm^2 for H_2 and 3 at 1 A/cm^2 for O_2. When the cell temperature was < 100 °C, both the anode and cathode humidification temperatures were kept the same as the cell temperature. When the cell temperature was 100 °C, the humidification temperature was kept at 95 °C for both the cathode and anode. When the cell temperature was > 100 °C, the anode and cathode humidification temperatures were kept at 98 and 95 °C, respectively.

The *in-situ* ac impedance spectra of the single fuel cell were recorded with a VoltaLab PGZ402 potentiostat in the constant voltage mode in the frequency range of 1 mHZ to 100 kHZ.

3.3 RESULTS AND DISCUSSION

3.3.1 Characterization of Hydrous $Ta_2O_5 \cdot nH_2O$ Particles

The X-ray diffraction patterns of $Ta_2O_5 \cdot nH_2O$ before and after heating at various temperatures for 2 h are shown in Fig. 3.2. No discernible diffraction peaks are seen up to 500 °C, suggesting an amorphous nature. However, the formation of well crystalline hexagonal Ta_2O_5 (JCPDS card No. 19-1299) is seen after heating at 800 °C.

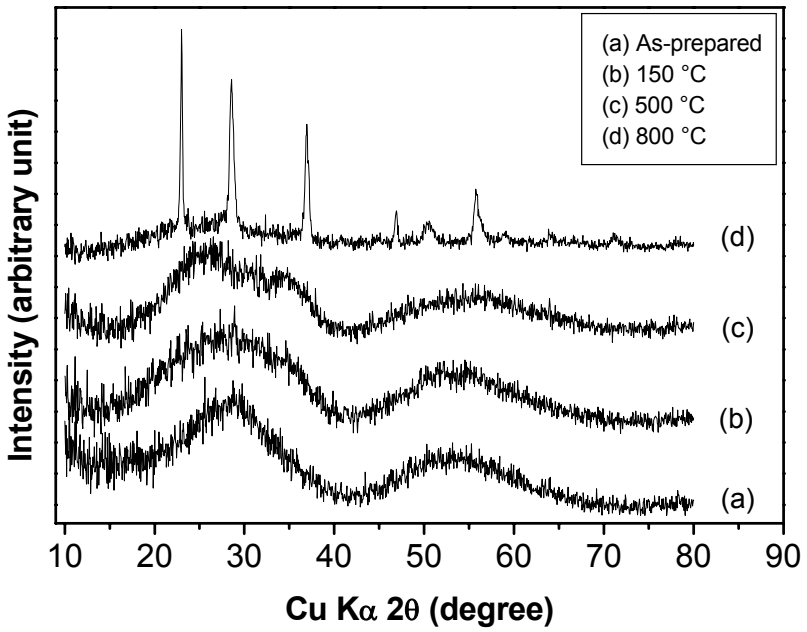

Figure 3.2 X-ray diffraction patterns of hydrous $Ta_2O_5 \cdot nH_2O$ before and after heating at various temperatures for 2 h.

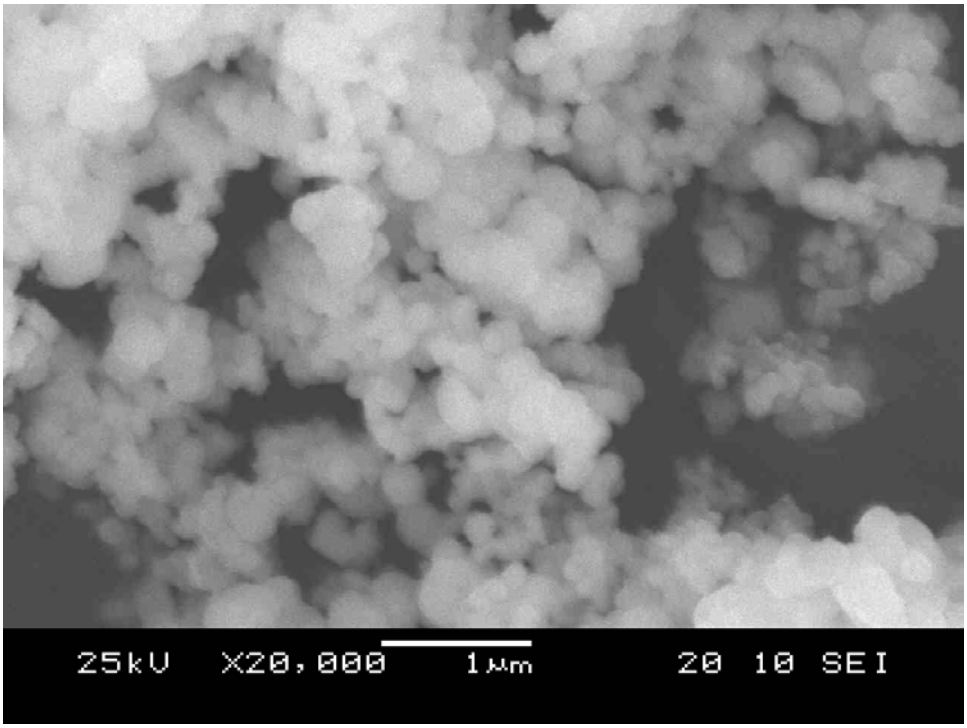

Figure 3.3 A scanning electron micrograph of the as-prepared $Ta_2O_5 \cdot nH_2O$ sample.

The typical morphology of as-prepared hydrous $Ta_2O_5 \cdot nH_2O$ powder is shown in Figure 3.3. It can be seen that the sample contains aggregates formed of very fine particles, which are in the sub-micron size range.

Figure 3.4 compares the TGA curves and the corresponding derivative plots (DTG curves) of $Ta_2O_5 \cdot nH_2O$ before and after drying at 150 °C. The sample without drying shows a huge weight loss below 200 °C, suggesting the presence of adsorbed and lattice water. The dried sample, on the other hand, shows smaller weight loss with two DTG peaks at < 100 and > 100 °C, which could be attributed to the loss of,

respectively, adsorbed and lattice water. This suggests that (i) the dried sample re-adsorbs water easily (hygroscopic) and (ii) the lattice water is not completely removed on drying at 150 °C. From the TGA data, the n value in $Ta_2O_5 \cdot nH_2O$ can be calculated to be 3.9 and 1.5, respectively, for the samples dried at ambient temperature and at 150 °C for 2 h in air. Both the samples show a small, broad peak in DTG at 350 - 500 °C, which could be attributed to the loss of small amount of ammonium groups that may have been incorporated during the synthesis [149].

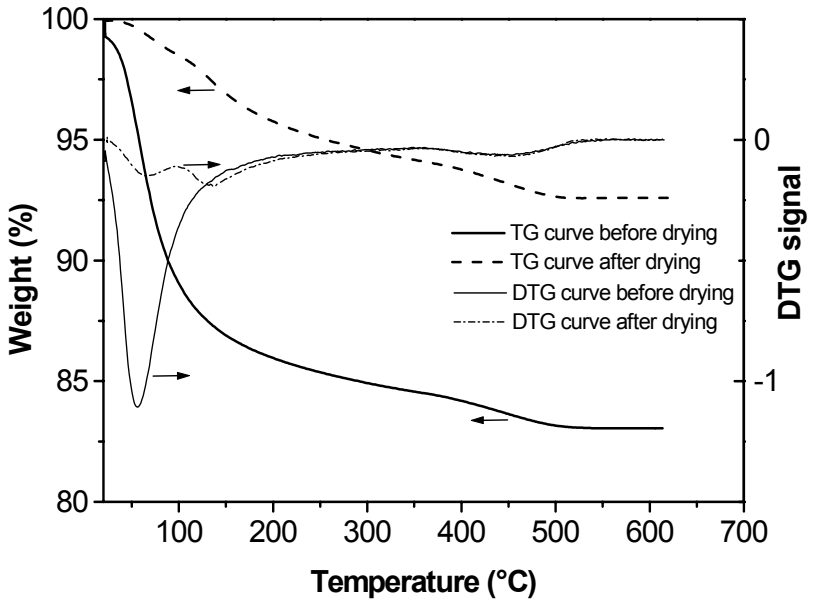

Figure 3.4 TGA curves of $Ta_2O_5 \cdot nH_2O$ before drying (as-prepared) and after drying at 150 °C for 2 h. The plots were recorded at a heating rate of 5 °C/min in a flowing dry air atmosphere.

3.3.2 Membrane Characterization

Water uptakes of the plain recast Nafion and Nafion/3 wt% $Ta_2O_5 \cdot nH_2O$ composite membranes were measured at various temperatures, and the results are given in Fig. 3.5. For both the membranes, the water uptake increases as the temperature increases; this is because the Nafion network is more swollen at high temperature. From Fig. 3.5, it can also be seen that at each temperature, the composite membrane adsorbs slightly more water than native recast membrane, indicating the hygroscopic property of the incorporated oxide particles.

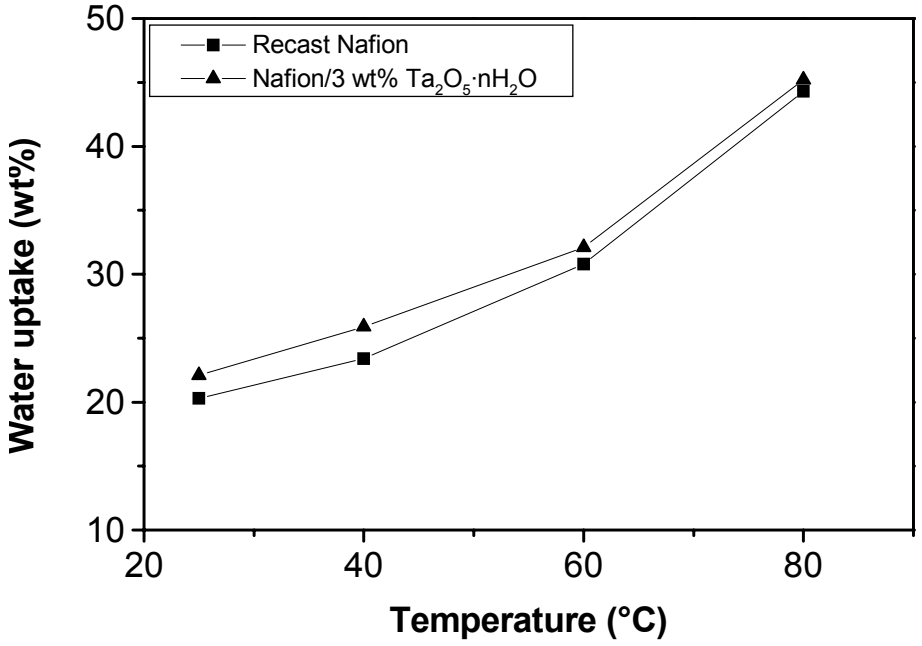

Figure 3.5 Variations of water uptake of the membranes with temperature.

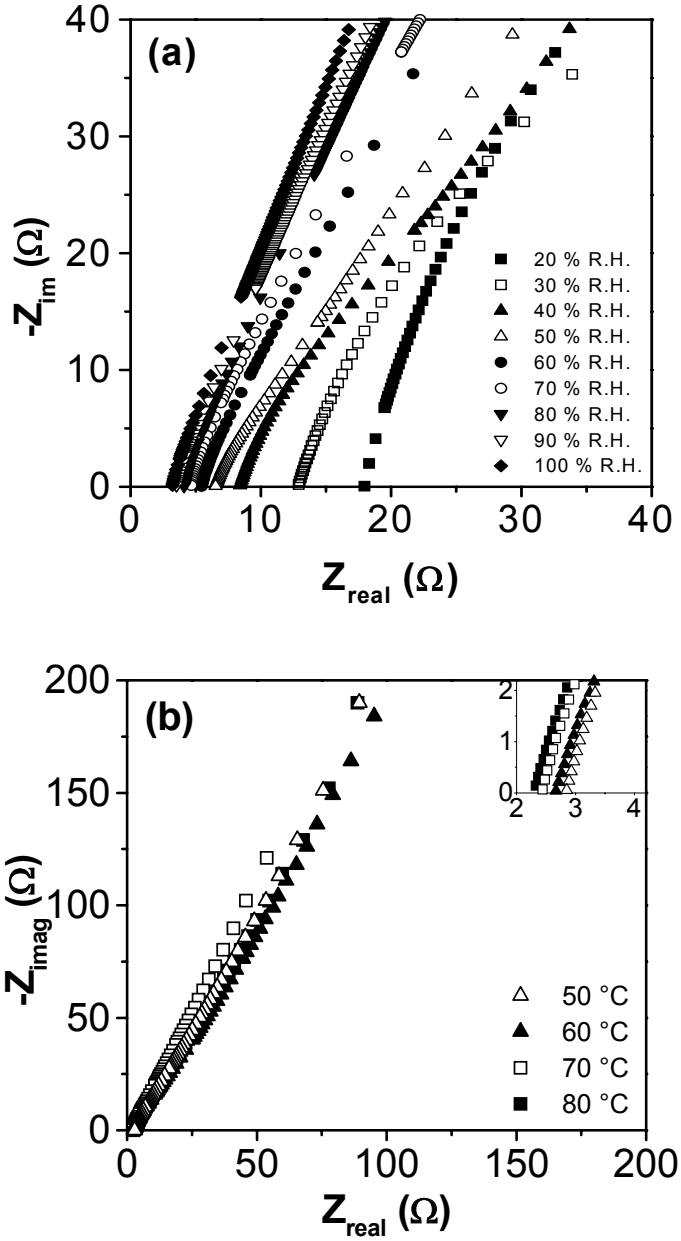

Figure 3.6 Typical impedance diagrams of Nafion/3 wt% $Ta_2O_5 \cdot nH_2O$ composite membrane: (a) at 80 °C and various relative humidities, and (b) at 100 % relative humidity and various temperatures.

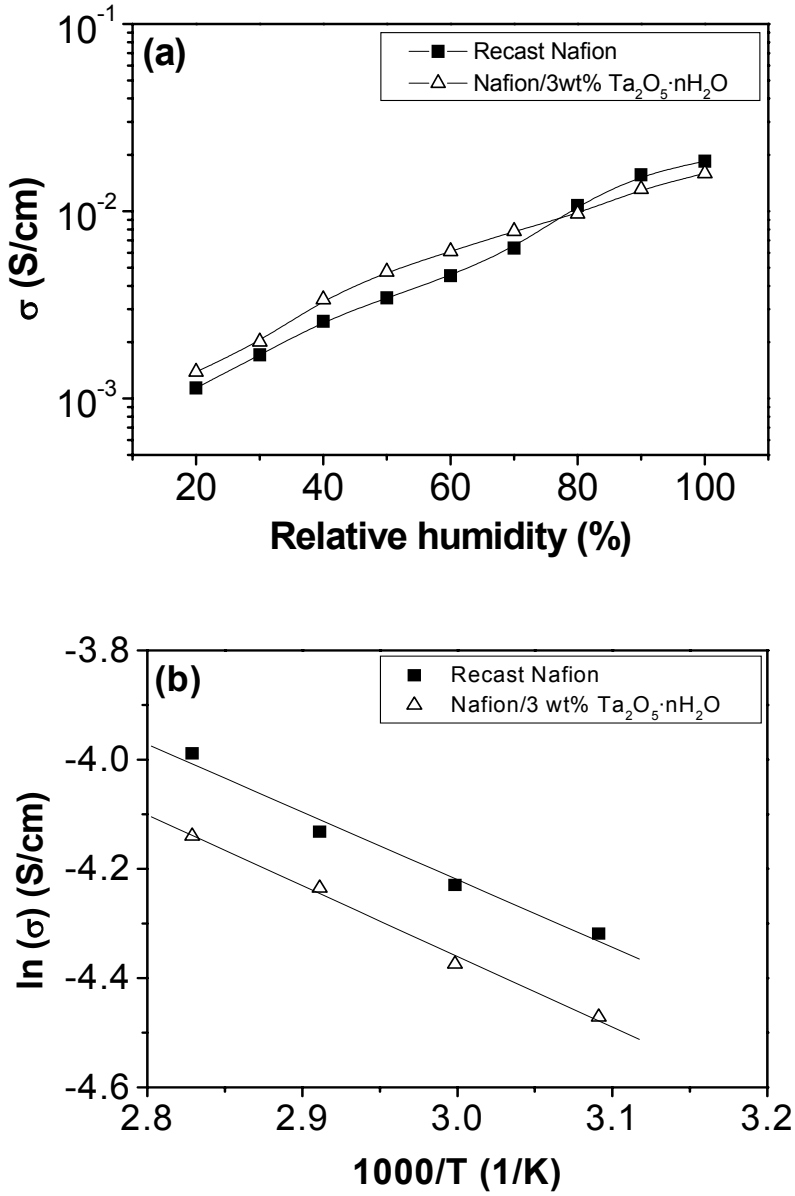

Figure 3.7 Proton conductivities of native recast Nafion and composite membranes: (a) variation with relative humidity at 80 °C and (b) variation with temperature at 100 % R.H.

The typical results for the electrical studies of Nafion/3 wt% $Ta_2O_5 \cdot nH_2O$ composite membrane are shown in Fig 3.6 in the form of complex impedance diagrams. As can be seen, at different measuring conditions, all the impedance diagrams appear to be slanted lines, intersecting with the real axis at different values. These kinds of impedance plots indicate that the protons can communicate freely between ionic clusters in the membrane and the membrane can be regarded as a pure resistor [150]. The value of the intersection is usually taken as the bulk resistance of the membrane. From Fig. 3.6a, it can be seen that, at 80 °C, the resistance of the membrane decreases with increasing R.H. as expected. It can also be observed that the resistance decrease step is larger in the low relative humidity range than that in the high relative humidity range. This indicates that Nafion-based membranes can easily absorb water from the humid environment. Fig. 3.6b shows the variation of the impedance of the $Ta_2O_5 \cdot nH_2O$ modified Nafion membrane with temperature at 100 % R.H. It can be seen that, the impedance decreases with increasing temperature, indicating the enhancement of the kinetics for proton conduction. However, the impedance variation with temperature at 100 % R.H. is very small, indicating that the proton conductivity of Nafion based membrane relies more on humidity than on temperature. The impedance diagrams of plain recast Nafion membrane are similar to those of the composite membranes.

The proton conductivities calculated from the measured impedances are shown in Fig. 3.7. Fig. 3.7a gives the comparison of the proton conductivities of pristine and composite membranes at 80 °C and various relative humidities. It can be seen that at

low R.H. (< 80 %), the proton conductivity of the $Ta_2O_5 \cdot nH_2O$ modified composite membrane is slightly higher than that of the plain recast Nafion membrane, indicating that at low relative humidity, the composite membrane may absorb more water than that of the plain Nafion membrane, facilitating the proton conduction. On the other hand, at higher R.H. (> 80 %), the composite membrane shows lower proton conductivity compared to the native membrane. This is possibly due to the low ion exchange capacity (IEC) of the additive and/or the blocking effect of the oxides for proton conduction. Water dissociates the protons from the sulfonic acid groups in Nafion membranes and its high dielectric constant enables the separation of charge between proton and sulfonate group, resulting in highly mobile protons. When the environmental humidity is above 80 %, both membranes absorb a large amount of water that is enough to create a continuous pathway for proton conduction. However, $Ta_2O_5 \cdot nH_2O$ additive with low IEC in the composite membrane may block the conduction of protons, leading to decreased proton conductivity.

The variation of proton conductivity with temperature at 100 % R.H. is shown in Fig. 3.7b. The overall mechanism for proton conduction involves an activation barrier and thus the relationship between the conductivity and temperature can be expressed by the Arrhenius law:

$$\sigma = A \exp(-E_a / RT)$$

where σ, A, E_a, R, and T are the proton conductivity, pre-exponential factor, activation energy for proton conduction, gas constant, and temperature. From Fig. 3.7b, an

activation energy of 10.3 kJ/mol for native recast Nafion and 10.7 kJ/mol for Nafion/$Ta_2O_5 \cdot nH_2O$ composite can be evaluated. These values are similar to those reported for commercial or composite Nafion membranes by other researchers [52,151,152]. The similar values of proton conductivity and activation energy for native Nafion and Nafion/$Ta_2O_5 \cdot nH_2O$ composite membranes indicate that the presence of $Ta_2O_5 \cdot nH_2O$ may not significantly change the proton conduction mechanism in well hydrated membranes. Again, the slightly lower conductivity of the composite membrane at 100 % R.H. and temperature below 80 °C indicates that the increased water uptake does not always result in a similar increase in conductivity due to the low IEC of the $Ta_2O_5 \cdot nH_2O$ additive and/or the blocking effect. However, it should be noted that some other studies showed higher proton conductivity for Nafion/oxide composite membranes compared to that for native Nafion membranes as discussed in Section 1.4.1. These conflicting results suggest the need for more investigation on the properties of hydrous oxides themselves.

3.3.3 H_2/O_2 PEMFC Performance

To determine whether the incorporation of the hydrous oxide $Ta_2O_5 \cdot nH_2O$ into the Nafion membrane could help to increase the operating temperature, preliminary PEMFC experiments were carried out with 150 μm thick membranes. Figure 3.8 compares the evolution of the cell voltage with time for various MEAs at 100 and 110 °C under a constant current density of 400 mA/cm^2 with pure hydrogen as the fuel.

When the MEA is composed of native recast Nafion and electrodes without the hydrous oxide, the cell voltage exhibits a large periodic fluctuation at 100 °C (Fig. 3.8a), indicating a poor water management in the cell. On the other hand, when the MEA is composed of Nafion/$Ta_2O_5 \cdot nH_2O$ composite membrane and electrodes without the hydrous oxide, the voltage output increases and the fluctuation decreases significantly (Fig. 3.8b). The data in Figs. 3.8a and 3.8b also reveal that the cell voltage drops dramatically on increasing the temperature from 100 to 110 °C. This is due to the dehydration of the membrane and the drying out of the anode, which lead to an increase in the cell resistance and the anode activation over-potential. The kinetics of the overall hydrogen oxidation process is linked to the ion-hydration step, and the lack of water at the anode can hinder the proton transport. In fact, when the hydrous $Ta_2O_5 \cdot nH_2O$ was incorporated into both the membrane and the electrodes, it could be operated at 110 °C with continuous power output (Fig. 3.8c), demonstrating that $Ta_2O_5 \cdot nH_2O$ can help to retain water to intermediate temperatures such as 110 °C. For a comparison, similar data were also collected at 60 and 80 °C with the MEA containing the hydrous oxide both in the membrane and the electrodes, and the voltage is pretty steady without fluctuation (Fig. 3.8d).

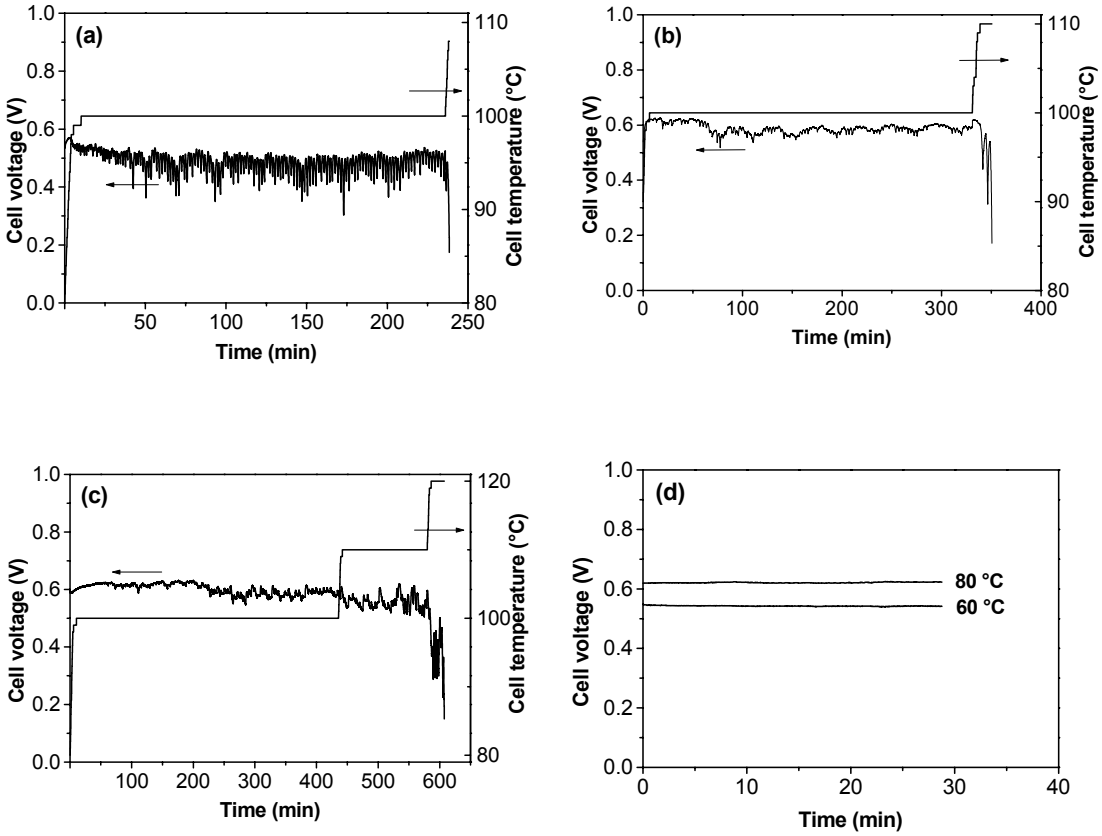

Figure 3.8 Variations of the cell voltage and temperature with time with H_2 fuel for various MEAs: (a) native recast Nafion membrane and unmodified electrodes without $Ta_2O_5 \cdot nH_2O$, (b) Nafion-$Ta_2O_5 \cdot nH_2O$ composite membrane and unmodified electrodes without $Ta_2O_5 \cdot nH_2O$, (c) Nafion-$Ta_2O_5 \cdot nH_2O$ membrane and electrodes with $Ta_2O_5 \cdot nH_2O$, and (d) Nafion-$Ta_2O_5 \cdot nH_2O$ membrane and electrodes with $Ta_2O_5 \cdot nH_2O$ at 60 and 80 °C. The membrane thickness and the current density were kept constant at, respectively, 150 μm and 400 mA/cm^2.

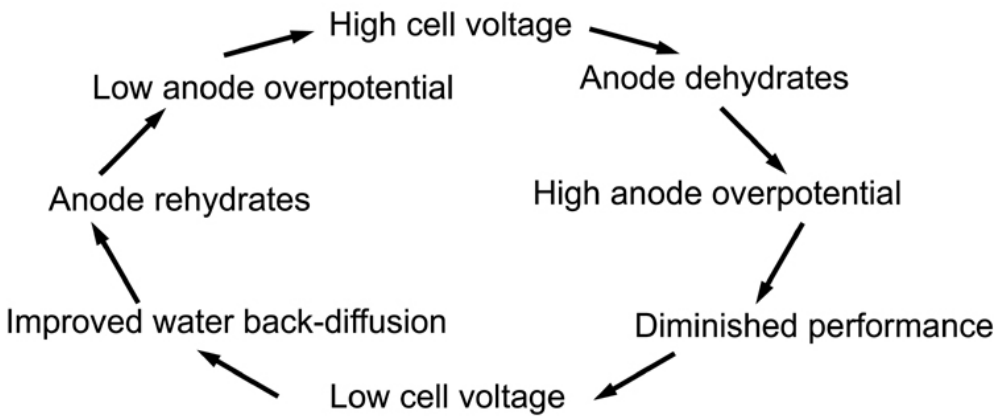

Figure 3.9 Water balance cycle which may cause the observed periodic fluctuations in cell voltage during the operation of a PEMFC at a constant high current under conditions involving dehydration of the MEA.

The observed periodic fluctuations in cell voltage output are believed to be related to the water management issue in the MEA during the cell operation. A possible cyclic scheme that could offer qualitative rationalizations for the cell voltage fluctuations is given in Fig. 3.9. The proposed scheme begins with a cell operating at a constant high current and high cell voltage. A combination of limited water availability at the anode (the humidifier temperature is lower than the cell operating temperature), electro-osmotic drag transporting water from the anode to the cathode due to high current, and insufficient water back-diffusion from the cathode to the anode due to the high thickness of the membrane causes the MEA to dehydrate, especially at the anode side. The dehydration is manifested as an increase in overpotential at the anode, which leads to decreased cell performance and low cell voltage output. With the diminishing of the

cell voltage output level, the water concentration gradient from the cathode to the anode side is increased because the hydration state at the cathode is kept due to the constant high current being delivered by the cell; this facilitates the water back-diffusion from the cathode to the anode. Consequently, the rehydration of the anode side leads to a decrease in the resistance and anode over-potential, and the cell performance improves, which is reflected by an increase in the cell voltage output at the same current. Thus the whole cycle begins again. This sequence of phenomena leads to a fluctuation in the cell voltage.

The results in Fig. 3.8 demonstrated that the incorporation of $Ta_2O_5 \cdot nH_2O$ into both the membrane and the electrodes could alleviate the dehydration of the membrane and the anode. However, the fluctuation in the cell voltage at a fixed current density is still larger at higher temperatures (Figs. 3.8a-c) compared to that at lower temperatures (Fig. 3.8d). Additionally, even the modified MEAs with $Ta_2O_5 \cdot nH_2O$ could not perform well at higher temperatures (120 °C). The relatively thicker membranes (150 μm) used may hinder the back-diffusion of water produced at the cathode, resulting in a drying out of both the membrane and the anode at higher temperatures.

To further improve the water management and power density of the cell, we turned to thin membranes with a thickness of 50 μm and expected an improvement in the water back-diffusion from the cathode to the anode side. The electrochemical performances of these membranes at different temperatures are given in Fig. 3.10. It can be seen that at low temperatures (60 and 80 °C), the performances of the pristine recast membrane are slightly better than those of the composite membranes consisting

of $Ta_2O_5 \cdot nH_2O$, which could be due to the lower proton conductivities of the latter at these temperatures and fully hydrated state as discussed in Section 3.3.2. However, at higher temperatures (100 and 110 °C), the performances of the composite membranes with $Ta_2O_5 \cdot nH_2O$ are better than those of the unmodified Nafion membrane, indicating that the incorporation of the hydrous oxide into the membrane improves the water retention at such humidity-reduced conditions. It can also be noticed that the power density for the composite membrane at 100 °C is close to that at 80 °C, and the value is as high as about 800 mW/cm^2. The voltage stability with time was also monitored for the thin composite membranes consisting of $Ta_2O_5 \cdot nH_2O$ (Fig. 3.11), and it can be seen that the voltage fluctuations are much smaller compared to those for the larger thickness membranes (Fig. 3.8), indicating an improvement in water management mainly due to the enhancement of the water back-diffusion from the cathode to the anode side.

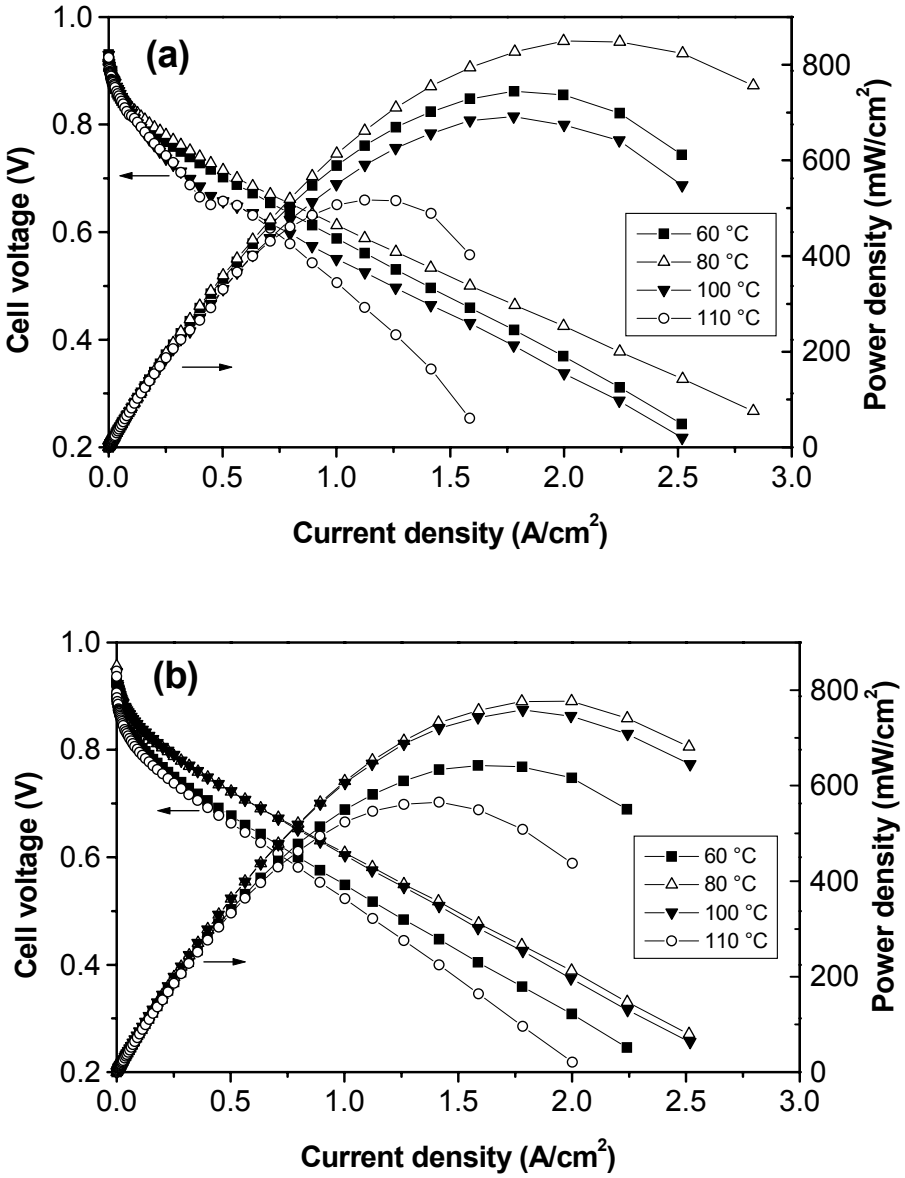

Figure 3.10 Polarization curves and power density variations recorded with H_2 fuel and 50 μm thick membranes: (a) MEA composed of electrodes with $Ta_2O_5 \cdot nH_2O$ and unmodified recast Nafion membrane and (b) MEA composed of electrodes with $Ta_2O_5 \cdot nH_2O$ and Nafion membrane with $Ta_2O_5 \cdot nH_2O$.

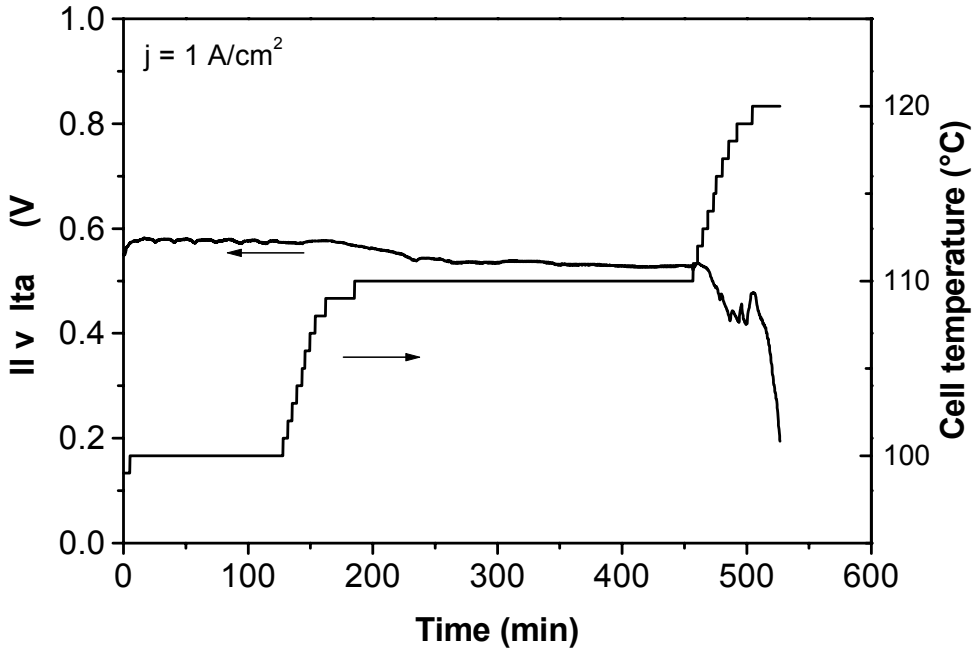

Figure 3.11 Variations of the cell voltage with time at 100 and 110 °C with H_2 fuel for an MEA consisting of 50 μm thick modified Nafion membrane with $Ta_2O_5 \cdot nH_2O$ and electrodes with $Ta_2O_5 \cdot nH_2O$.

3.3.4 Effects of CO Poisoning

To investigate the effect of CO poisoning on the Pt anodes, we have also monitored the voltage evolution with a H_2-CO fuel consisting of 150 ppm CO at a constant current density of 240 mA/cm^2 at 60 °C (Fig. 3.12). Upon applying the H_2 - CO fuel, the voltage initially increases close to a maximum of 0. 5 V in a few minutes, decreases rapidly thereafter to around 0.25 V in about 25 minutes, and then fluctuates around 0.25 V, indicating the completion of the poisoning of the Pt catalyst by CO.

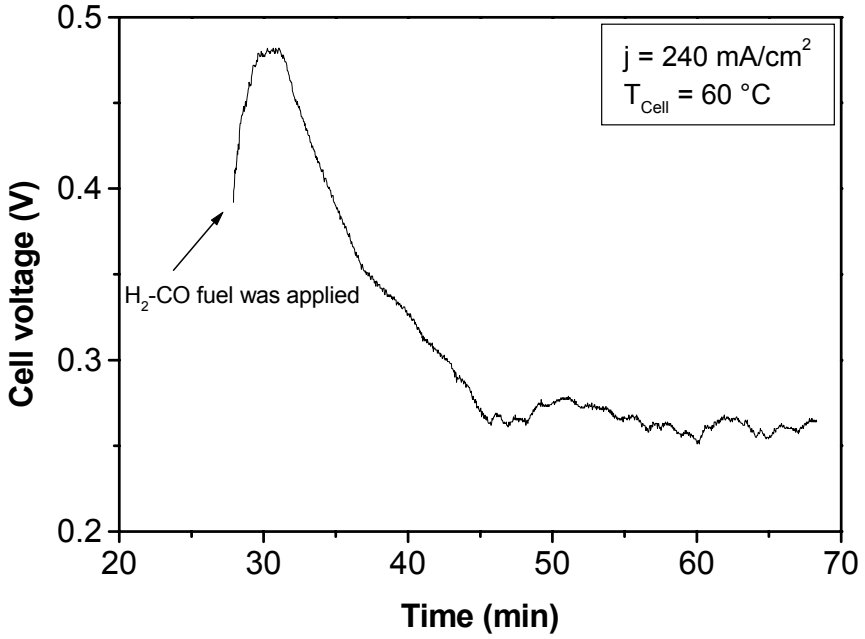

Figure 3.12 Variations of the cell voltage with time at 60 °C and 240 mA/cm^2 upon applying H_2 - CO fuel (150 ppm CO). Both the cathode and anode sides were purged with the inert N_2 gas before applying the fuel and oxidant.

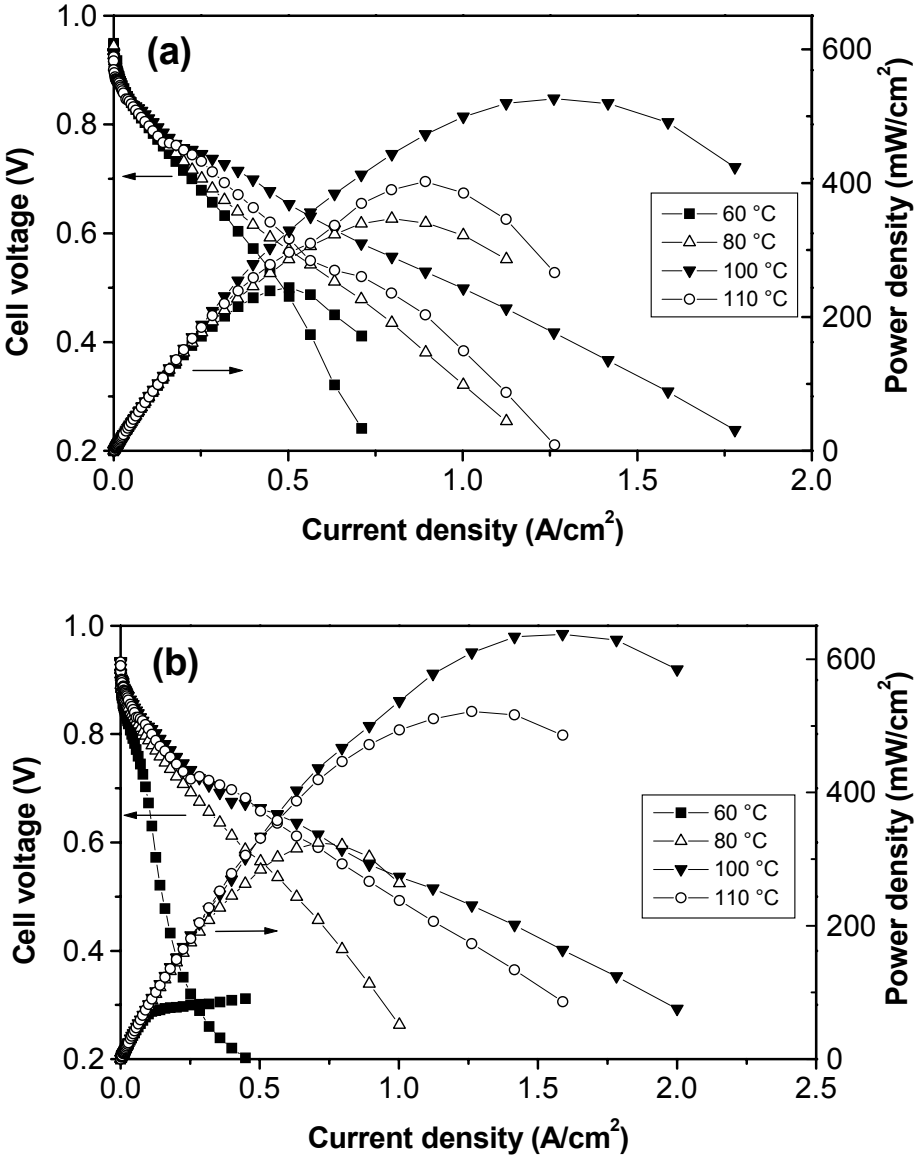

Figure 3.13 Polarization curves and power density variations recorded with H_2-CO fuel (150 ppm CO) and 50 μm thick membranes: (a) MEA composed of electrodes with $Ta_2O_5 \cdot nH_2O$ and unmodified recast Nafion membrane and (b) MEA composed of electrodes with $Ta_2O_5 \cdot nH_2O$ and Nafion membrane with $Ta_2O_5 \cdot nH_2O$.

Figure 3.13 compares the electrochemical performances of the modified MEA consisting of $Ta_2O_5 \cdot nH_2O$ in both the membrane and the electrodes and the MEA consisting of $Ta_2O_5 \cdot nH_2O$ only in the electrodes (not in the membrane) at various temperatures with H_2 - CO fuel. The data reveal that both MEAs show the best performance at 100 °C. This is different from that observed with the pure H_2 fuel, in which the best performance was seen at 80 °C (Fig. 3.10). The difference is attributed to the poisoning of the anode catalysts by CO when the H_2 - CO fuel is used. At low enough temperatures (60 and 80 °C), there is a significant coverage of Pt by CO with the H_2 - CO fuel, which leads to a high anode activation over-potential and very poor cell performance. However, as the temperature increases, the coverage of Pt by CO decreases rapidly, leading to a dramatic improvement in the electrochemical performance with high power density at 100 °C. It should be borne in mind that the decrease in proton conductivity on going from 80 to 100 °C may lead to a decrease in performance (Fig. 3.10). However, in the case of H_2 - CO fuel, the positive effect of temperature in improving the CO tolerance is more profound compared to the adverse effect of the decrease in proton conductivity, and the overall effect leads to an improved electrochemical performance with the maximum performance at 100 °C. Comparing the data in Figs. 3.13a and b, the MEA without $Ta_2O_5 \cdot nH_2O$ in the membrane shows slightly better performance than the modified MEAs with $Ta_2O_5 \cdot nH_2O$ at 60 and 80 °C similar to the results obtained in Fig. 3.10 due to a higher proton conductivity in the former. However, the modified MEA with $Ta_2O_5 \cdot nH_2O$ in

both the membrane and electrodes show better performance than the unmodified MEA at 100 and 110 °C similar to that in Fig. 3.10 due to the ability of the former to retain water at higher temperatures. Nevertheless, the performances at 110 °C are inferior to those at 100 °C for both the unmodified and modified membranes due to the further decrease in proton conductivity.

Electrochemical impedance spectroscopy (EIS) has been demonstrated to be a powerful experimental technique to examine the complexity of the different processes that take place in fuel cells [153,154]. It has also been employed to investigate the CO poisoning effects at temperatures below 100 °C [155-157]. In this study, the EIS experiments were carried out with the modified MEA with $Ta_2O_5 \cdot nH_2O$ in both the membrane and the electrodes to study the process of CO poisoning on the anode Pt catalyst at different temperatures. Figures 3.14 and 3.15 depict the Nyquist plots for the cells operated, respectively, with pure H_2 and H_2 - CO fuels at two different potentials of 0.85 and 0.75 V. It can be seen that all the plots exhibit similar shapes. The high frequency intercept of the semicircle (left) with the real axis is attributed to the ohmic resistance of the membrane, and the values are almost independent of the cell potential. The semicircles, on the other hand, are characteristics of the charge transfer processes taking place at the electrodes, and the diameter of the semicircle can be taken as the charge transfer resistance.

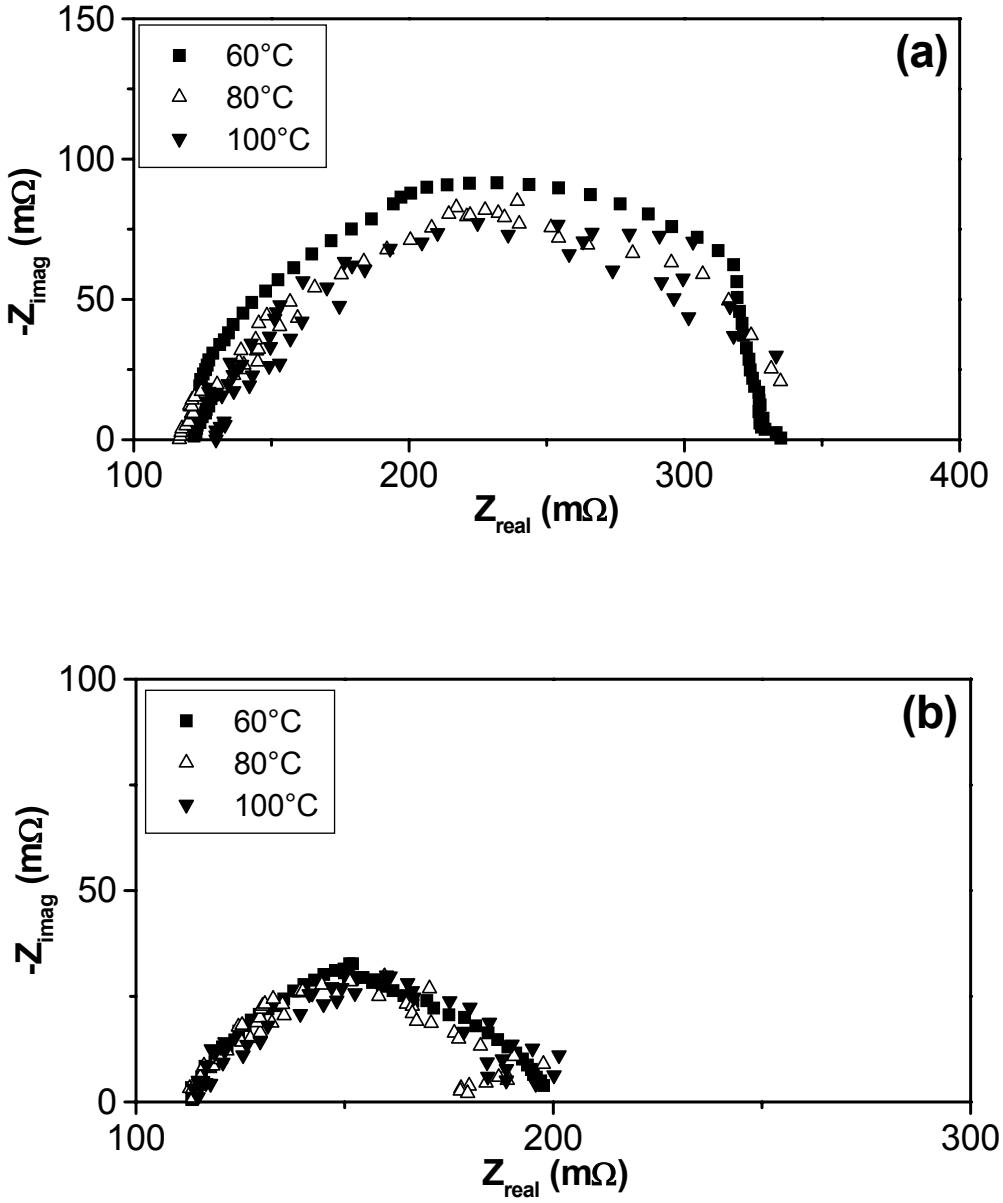

Figure 3.14 Impedance plots recorded at (a) 0.85 and (b) 0.75 V with H_2 fuel and MEA composed of modified Nafion (50 μm thick) membrane with $Ta_2O_5 \cdot nH_2O$ and electrodes with $Ta_2O_5 \cdot nH_2O$.

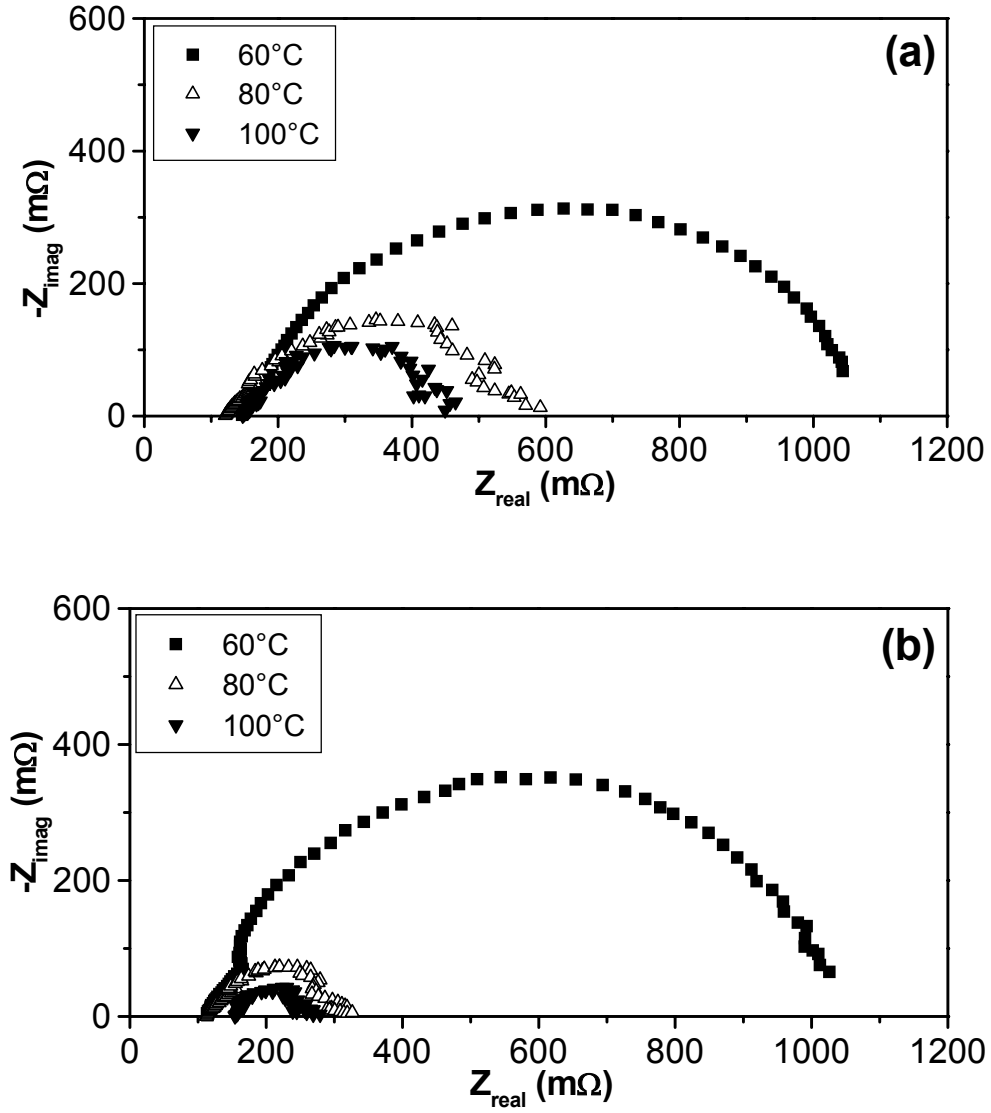

Figure 3.15 Impedance plots recorded at (a) 0.85 and (b) 0.75 V with H_2 - CO fuel (150 ppm CO) and MEA composed of modified Nafion (50 μm thick) membrane with $Ta_2O_5 \cdot nH_2O$ and electrodes with $Ta_2O_5 \cdot nH_2O$.

With the pure H_2 fuel, the main characteristics of the spectra (Fig. 3.14) are determined by the oxygen reduction process at the cathode since the electrochemical reactivity of pure H_2 is extremely high. At a fixed cell potential, the spectra do not change much on varying the cell temperature from 60 to 100 °C, suggesting that the oxygen reduction kinetics is not obviously promoted by temperature, which is in agreement with the observation that the activity of Pt for oxygen reduction reaches a plateau in the low and intermediate temperature ranges after the temperature is increased to around 50 °C [158]. On the other hand, as the potential is decreased from 0.85 to 0.75 V, the semicircle shrinks, indicating a decrease in the charge transfer resistance at the cathode.

In contrast, with the H_2 - CO fuel, the spectra change significantly at a given cell potential on varying the cell temperature from 60 to 100 °C (Fig. 3.15), which could be attributed to changes in the electrocatalytic activity of the anode in presence of CO. At 60 °C and 0.85 V, the diameter of the semicircle (Fig. 3.15a), which represents the charge transfer resistance, is about five times larger than that found with pure H_2 fuel (Fig. 3.14a), demonstrating that the cell behaviors are determined by both the cathodic and anodic impedances in the presence of CO impurities in the fuel. The large anode impedance leads to a drastic increase in the over-potential and decrease in power density in presence of CO. Comparing the data in Figs. 3.15a and b, the spectra at 60 °C do not change much on going from 0.85 to 0.75 V. This is because the poisoning of the anode catalyst by CO at such a low temperature is so severe that the spectra is dominated by the anodic impedance, and the effect of the potential change on cathodic

impedance is negligible compared to the large anodic impedance. However, at a given cell potential, the total impedance drops significantly as the cell temperature is increased from 60 to 100 °C due to the drastic decrease in the coverage of Pt by CO and the anode impedance assuming the cathodic impedance does not change between the two fuels.

All the MEAs in this study were operated from low temperatures to high temperatures discontinuously (shutdown overnight) for five days, about 10 h for each day. No obvious performance degradation was observed during this period, indicating good temperature-cycling for these MEAs below and above 100 °C.

3.3.5 Discussion of the Role of the Hydrous Oxides

As with many other studies of different Nafion/oxide systems in the literature, the results in this work also demonstrate that the incorporation of hydrous oxides into Nafion membrane does improve the hydrophilicity of the membrane and help the membrane possess satisfactory proton conductivity to higher temperatures. All these similar results suggest some common roles of these hydrous oxides in the Nafion membrane. However, only a few studies have been performed on this aspect.

Oxides prepared by low temperature methods are hydrophilic and may have significant amount of -OH groups on the surface, generated by a reaction with the water in the ambient [159]. Based on these facts, a schematic representation of a structural model of hydrous tantalum oxides is shown in Fig. 3.16, which is modified

from that of hydrous tin oxides ($SnO_2 \cdot nH_2O$) proposed by England *et al.* [160]. It can be seen that hydrous tantalum oxide has a partially protonated oxide-hydroxide surface. These –OH groups on the surface may help retain water molecules through hydrogen bonds. There are also some free protons that may transport through either vehicle mechanism (e.g. H_3O^+ and $H_5O_2^+$) or Grotthuss mechanism as shown in Fig. 3.16. It was suggested that only free, i.e., chemically unbound, protons contribute to the ionic transport in both mechanisms. In the hydrous state, although dissociated protons exist in the structure of $Ta_2O_5 \cdot nH_2O$ in the form of H_3O^+, or even $H_5O_2^+$ (see Fig. 3.16), the amount of this kind of protons is still not sufficient enough to have a conductivity comparable to that of hydrated Nafion. However, the -OH groups covered oxide surface can physically adsorb water very easily from the humid environment. When these oxides are introduced into the pores of Nafion membrane, the lattice water and physically absorbed water on the surface could facilitate the dissociation of the protons in $-SO_3H$ groups that are attached to the PTFE backbone of Nafion, helping the membrane to keep the high proton conductivity even at high temperatures.

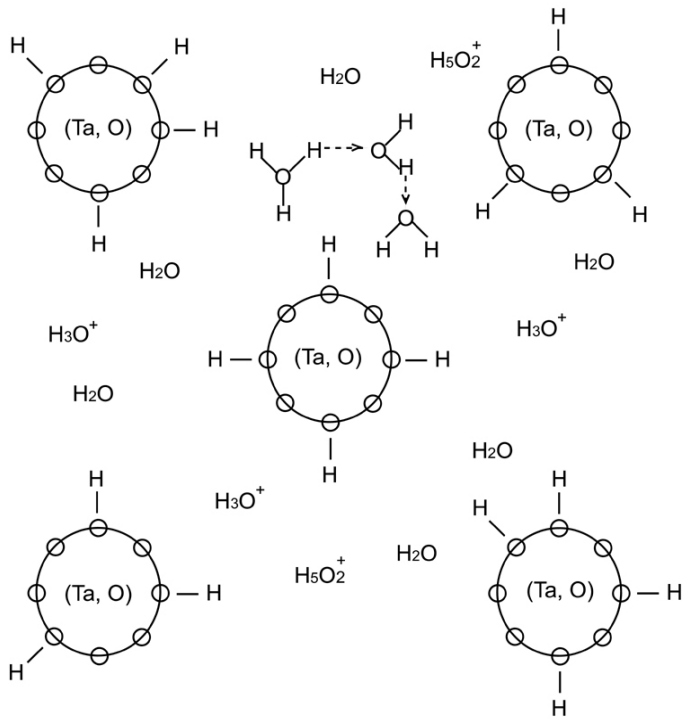

Figure 3.16 Schematic representation of the $Ta_2O_5 \cdot nH_2O$ structure and proton transport involved.

Lvov [161] investigated ZrO_2/water and TiO_2/water systems and found that the concentration of protons in the electrical double layer at the interface can be significantly increased if temperature changes from 25 to 120 °C. This observation could logically explain why the solid oxides are useful for making the composite solid/polymer membrane for high temperature PEMFCs.

3.4 CONCLUSIONS

Hydrous $Ta_2O_5 \cdot nH_2O$ modified MEAs have been investigated in PEMFC in the presence and absence of CO impurities in the fuel. The presence of hydrous $Ta_2O_5 \cdot nH_2O$ in both the membrane as well as the electrodes helps to retain water to elevated temperatures and allows higher operating temperatures, which in turn is beneficial to alleviate the poisoning of the Pt catalysts by the CO impurities in the fuel. The MEAs consisting of $Ta_2O_5 \cdot nH_2O$ show high power densities of around 800 and 650 mW/cm^2 at 100 °C, respectively, with pure H_2 and H_2 - CO (150 ppm CO) fuels. The suppression of CO poisoning on increasing the operating temperature from 60 to 100 °C is indicated by a significant decrease in the charge transfer resistance. This study demonstrates that incorporation of hydrous inorganic oxides that retain water to higher temperatures into the MEAs (membrane and electrodes) could prove to be a viable strategy to develop PEMFC for transportation applications with on-board reforming.

To further increase the operating temperature and improve the proton conductivity of the membranes and the fuel cell performance at high temperatures, the properties, especially the surface properties, of the oxides deserve more fundamental studies. The knowledge will guide the preparation and optimization of the hygroscopic particles. In addition, proton conductive functional groups such as $-SO_3H$ can be tethered to porous oxides such as silica to increase the IEC of the oxides and keep high proton conductivity even at high temperatures.

Chapter 4

Polymer Electrolyte Membranes Based on Sulfonated Poly(etheretherketone) for Direct Methanol Fuel Cells

4.1 INTRODUCTION

To overcome the problems associated with methanol crossover in DMFC, many efforts are being made to develop proton exchange membranes with zero or reduced methanol permeability. As discussed in Section 1.5.1, various approaches can be employed to modify the currently used Nafion membranes to make them less permeable to methanol. However, such modified membranes suffer either a decrease in proton conductivity or deterioration of the mechanical strength. Additionally, these modifications do not address the fact that the high cost of Nafion based membranes is one of the obstacles that prevent the widespread commercialization of PEMFC and DMFC technologies.

These difficulties have promoted the search for alternative membranes based on partially perfluorinated ionomers and hydrocarbon polymers. In this regard, polymers such as polyimide (PI) [66,81,127], polysulfones (PSU) [52,128], and various polyketones (PEKs) [46,132-134] are actively being investigated around the world. As discussed in chapter 1, membranes based on aromatic poly(etheretherketone) (PEEK) were shown to be promising for fuel cell application since they possess good thermal stability and mechanical properties, and the proton conductivity can be controlled by the sulfonation level. Sulfonated poly(etheretherketone) (SPEEK) was shown to have

different swelling behaviors and transport properties than those of Nafion due to the difference in their microstructures. According to Kreuer *et al.* [46,106,162], for a given water content, SPEEK has narrower hydrophilic channels and they are more branched with increased dead-ends compared to that in Nafion. These characteristics of SPEEK may lead to low water/methanol permeation, alleviating the effects of the methanol crossover. However, little information is available on the performance of SPEEK membranes in DMFCs. For a polymer membrane to be successfully used in DMFC, it should have good stability in the fuel cell environment while providing satisfactory performance. In this study, SPEEK membranes are systematically investigated in DMFC, and the optimum membrane processing and fuel cell operating conditions are discussed.

Membranes based on sulfonated hydrocarbon polymers that show lower methanol permeability usually exhibit lower proton conductivity as well compared to Nafion, which may lead to a large cell resistance and poor electrochemical performance. The cell resistance can, however, be reduced to some extent by using thinner membranes in the fuel cell MEAs, but the thinner membranes could potentially lead to poor mechanical strength and long-term stability problems. To overcome these difficulties, we present here a multilayered concept involving a sandwiching of a thin layer of SPEEK membrane with two outer layers of recast Nafion membranes. The thin middle layer of SPEEK is expected to block the methanol permeation effectively without adversely increasing the cell resistance significantly. The multilayered membranes

could thus alleviate the methanol crossover problem while offering good mechanical strength and cell performance.

4.2 EXPERIMENTAL

The SPEEK samples were obtained by direct sulfonation of commercial poly(etheretherketone) (PEEK450 PF, Victrex) at room temperature [133,135]. 15 g of PEEK powders were dissolved in 750 mL of concentrated sulfuric acid (95.9 %, Fisher Scientific), vigorously stirred at room temperature for the desired amount of time, and gradually transferred into a large volume of ice-cold water under mechanical agitation. After settling for several hours, the polymer precipitates formed were filtered, washed thoroughly with distilled water until the pH was neutral, and dried at 100 °C overnight.

The ion exchange capacities (IEC) of SPEEK with various sulfonation time were determined by suspending around 0.5 g of SPEEK in 30 mL of 2 M NaCl solution for 24 h to liberate the H^+ ions and then titrating with 0.1 M NaOH solution using phenolphthalein indicator. The degree of sulfonation could be calculated from the IEC.

The membranes were obtained by casting into a glass plate a N, N-dimethylacetamide (DMAc) (Aldrich Chemical Co. Inc.) solution of the SPEEK polymer (~ 10 % w/v) and drying at 95 °C overnight. For those with low sulfonation level, heating at ~ 50 °C was needed to help the dissolving of the polymer. The thickness of the membrane was controlled by changing the amount of SPEEK polymer in the solution. SPEEK membranes with thickness of about 70, 45, and 25 μm were prepared in this study.

The thermal stabilities of SPEEK, PEEK and Nafion samples were assessed by TGA. Approximately 20 mg samples were heated from 25 to 900 °C at a rate of 5 °C/min under a flowing nitrogen atmosphere.

The liquid uptake measurements of the membrane samples in water and methanol solutions with different concentrations were carried out at various temperatures. Proton conductivities of the membranes at various temperatures and relative humidity were assessed by impedance spectroscopy as described in chapter 2.

To prepare the multilayered membranes, a thin layer of SPEEK membrane with certain sulfonation level was sandwiched between two recast Nafion membranes and hot-pressed at 140 °C for 5 min. For a comparison, multilayered membranes with recast Nafion as the middle layers were also fabricated. For all the membranes, the outer Nafion layers had the same thickness of around 50 μm, but the inner SPEEK or Nafion layers had different thickness.

The anode catalyst was a commercial 40 wt% PtRu (1:1)/Vulcan (E-TEK), whereas the cathode catalyst was either a commercial 20 wt% Pt/Vulcan (E-TEK) or a homemade 40 wt% Pt/Vulcan that was prepared by reducing chloroplatinic acid (H_2PtCl_6) with 0.5 M sodium formate at around 70 °C (see Section 2.1.3). Nafion-impregnated electrodes were prepared from these catalysts. The loading is 3 mg/cm^2 Pt (from the homemade 40 wt% Pt/C) for the cathode, and 4 mg/cm^2 Pt-Ru for the anode. The Nafion loading for both the anode and cathode catalysts is 0.35 mg/cm^2. For multilayered membrane studies, electrodes with 0.6 mg/cm^2 Pt-Ru (anode) and 1.0

mg/cm^2 Pt (from commercial 20 % Pt/C) (cathode) were used, and the Nafion loading in both the anode and cathode was 0.6 mg/cm^2.

The membrane-electrode assembly (MEA) was fabricated by uniaxially hot-pressing the anode and cathode onto a SPEEK membrane at 100 °C for 2 min. For a comparison, a MEA consisting of Nafion 115 was also prepared, which was hot-processed at 130 °C for 2 min. In the DMFC test, 2 M methanol solutions were pre-heated to the cell temperature and pumped through the anode flow-fields.

Methanol permeation properties of the membranes were qualitatively evaluated by the voltammetric method described in Section 2.4.2.

4.3 RESULTS OF SPEEK MEMBRANES AND A COMPARISON WITH NAFION MEMBRANES

4.3.1 Sulfonation of PEEK

The chemical structure of PEEK is shown in Fig. 4.1. It is a thermostable polymer with an aromatic, non-fluorinated backbone. PEEK can be functionalized by sulfonation and the degree of sulfonation (DS) can be controlled by the reaction temperature and time [69,71]. Sulfonation is an electrophilic substitution reaction and the active site for substitution is determined by the electron density of the site. It can be judged that the substitution will preferentially take place in one of the four chemically equivalent positions of the phenyl ring surrounded by two ether groups as specified in Fig. 4.1, which shows the repeat unit of the polymer. Since the electron density of the other two aromatic rings in the repeat unit is relatively low due to the electron-

attracting nature of the neighboring carboxyl group under ordinary sulfonation conditions (e.g., at room temperature) and with the concentrated sulfuric acid used as solvent, there is only one $-SO_3H$ group attached to each of the repeating units. However, at higher temperatures and/or long period of reaction time, the substitution in the other two aromatic rings is also possible. Detailed investigation of the mechanism and kinetics of the sulfonation of poly(etheretherketone) polymer has been conducted by several researchers [69,71,74].

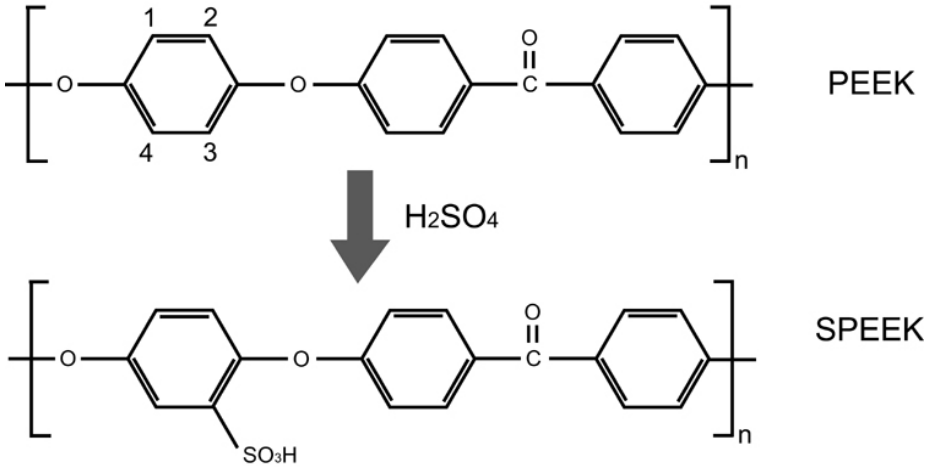

Figure 4.1 Sulfonation of PEEK polymer.

When using the direct sulfonation method, it is difficult to obtain truly random copolymers at sulfonation levels of less than 30 % because dissolution and sulfonation in sulfuric acid occur in a heterogeneous environment due to the increase of the

viscosity of the reactant solutions. Thus, the dissolution process needs to be kept short normally for less than 1 h in order to produce a more random copolymer.

The physical and chemical properties of SPEEK depend on the degree of sulfonation (DS). Sulfonation modifies the chemical character of PEEK, reduces the crystallinity and, consequently affects the solubility. As a result, at DS lower than 30 %, SPEEK is soluble only in strong H_2SO_4. Above 30 % DS, the SPEEK polymers are soluble in hot dimethyformamide (DMF), dimethylacetamide (DMAc) and dimethylsulfoxide (DMSO). Above 40 % DS, they are soluble in the above organic solvents at room temperature. Above 70 % DS they are soluble in methanol and at 100 % sulfonation they are soluble in hot water [31].

4.3.2 Determination of the Ion Exchange Capacity (IEC), Degree of Sulfonation (DS), and the Liquid Uptake

IEC is defined by the number of sulfonic acid groups in an electrolyte; it indicates the ease of ion flow in the film. The unit is the milliequivalent per gram of the dry electrolyte (meq/g). The IECs of SPEEK polymers were determined by a titration method described in section 4.2. In this method, by measuring the amount of the standard NaOH consumed in the titration, the molar quantity of the $-SO_3H$ groups contained in the SPEEK sample could be determined using the following equation:

$$N_{-SO_3H} = (M \cdot V)_{NaOH} \tag{4.1}$$

where M and V are the molar concentration and volume of the consumed standard NaOH solution, respectively. The IEC can thus be obtained as

$$IEC = (N_{-SO_3H} / m_{sample}) \cdot 1000 \quad \text{(meq/g)} \tag{4.2}$$

where m_{sample} is the mass of the dry SPEEK sample.

SPEEK is a copolymer that consists of a PEEK-SO_3H unit and a PEEK unit. The *DS* can thus be defined as

$$DS = N_{PEEK-SO_3H} / (N_{PEEK-SO_3H} + N_{PEEK}) \tag{4.3}$$

where, $N_{PEEK-SO_3H}$ is the molar number of the PEEK-SO_3H unit, and N_{PEEK} is the molar number of the PEEK unit. The molar number (N_1) of the PEEK-SO_3H unit in 1 g SPEEK copolymer is

$$N_1 = 0.001 \cdot IEC \tag{4.4}$$

The molar number (N_2) of the PEEK unit in 1 g sulfonated PEEK copolymer is

$$N_2 = (1 - 0.001 \cdot IEC \cdot M_1) / M_2 \tag{4.5}$$

where $M_1 = 368$ and $M_2 = 288$ are the molecular weights of the PEEK-SO_3H unit and the PEEK unit, respectively. With these and inserting equations (4.4) and (4.5) into equation (4.3), we get

$$DS = 288 \cdot IEC / [1000 - (368 - 288) \cdot IEC] = 288 \cdot IEC / (1000 - 80 \cdot IEC) \tag{4.6}$$

Table 4.1 summarizes the IEC, DS, and % water uptake at 25 and 80 °C for various sulfonation time. For a comparison, the corresponding values for Nafion 115 membrane are also given. The IEC, DS, and water uptake of the SPEEK membranes increase with increasing sulfonation time as expected. At higher degrees of sulfonation, the membranes in fact swell too much and dissolve in water, which limits the level of

sulfonation to around 50 % for the membranes to be useful for fuel cell applications. Therefore, membranes with DS of 44, 46, 54, and 58 % were selected for further fuel cell investigation and these membranes are designated hereafter as, respectively, SPEEK-44, SPEEK-46, SPEEK-54, and SPEEK-58.

Table 4.1. Ion exchange capacity (IEC), degree of sulfonation (DS), proton conductivity (σ), and water uptake of SPEEK membranes obtained with different sulfonation reaction times.

Sulfonation time (h)	IEC (meq./g)	DS (%)	Water uptake (%)[a]	
			25 °C	80 °C
15	0.98	31	-	-
25	1.23	39	-	-
35	1.36	44	1.4	8.6
40	1.42	46	2.4	22.8
45	1.62	54	5.1	140
50	1.74	58	5.3	509.5
65	1.92	65	19.9	dissolved
85	1.95	67	17.4	dissolved
115	2.06	71	18.3	dissolved
135	2.09	72	25.1	dissolved
Nafion 115[b]	0.91	-	18.0	26.7

[a] Membranes could not be prepared for low sulfonation levels due to the limited solubility of the membranes in the N, N- dimethylacetamide solvent.
[b] For a comparison, the data for Nafion are included.

Table 4.2. Comparison of the liquid uptake of SPEEK and Nafion membranes in methanol solution at different temperatures.

Membrane	Methanol Concentration (M)	Liquid Uptake (wt %)			
		25 °C	45 °C	65 °C	80 °C
SPEEK-44	0	1.4	5.8	7.6	8.6
	1	1.3	5.1	7.1	10.0
	2	5.6	5.0	7.2	21.5
	3	3.4	5.0	9.2	34.3
SPEEK-46	0	2.4	8.2	13.1	22.8
	1	1.9	8.1	11.3	68.8
	2	7.5	7.5	15.4	96.3
	3	10.9	10.9	22.3	97.4
SPEEK-54	0	5.1	7.6	9.4	140.0
	1	3.4	6.3	15.3	617.4
	2	5.2	11.5	25.4	727.8
	3	4.1	9.0	42.7	706.9
SPEEK-58	0	5.3	12.3	21.1	509.5
	1	16.2	19.4	27.1	728.0
	2	11.0	15.4	46.9	770.3
	3	8.8	15.0	214.5	802.4
Nafion 115	0	18.0	19.7	24.4	26.7
	1	20.9	22.7	26.7	33.0
	2	22.7	26.4	31.4	37.5
	3	25.7	29.2	34.3	39.6

Table 4.2 compares the % liquid uptake at different temperatures and methanol concentrations for Nafion 115 and the SPEEK membranes with various sulfonation levels. The liquid uptake and swelling generally increase with increasing temperature and methanol concentration, but the temperature effect is more pronounced. The

membranes with high levels of sulfonation (SPEEK-54 and SPEEK-58) in fact experience huge swelling at 80 °C and, therefore, their use is limited to < 80 °C. In contrast, the Nafion membranes experience huge swelling at much higher temperatures of around 140 °C [46].

4.3.3 Thermal Stability: TGA Studies

The TGA curves of pure and sulfonated PEEK are shown in Fig. 4.2. Since PEEK is a temperature resistant polymer, the onset of weight loss for this polymer, which is obviously due to the main chain decomposition, starts at about 530 °C. For the SPEEK membrane, except for the weight loss below 100 °C related to the desorption of water bonded to the sulfonic acid groups, there are two other weight loss steps, which are reflected by the broad peaks in the DTG curves in separate temperature ranges. The first weight loss corresponds to the sulfonic acid decomposition while the second step is due to the main chain decomposition. Sulfonated samples show lower decomposition temperatures compared to unsulfonated PEEK. This difference could be due to the enhancement of the irregularity of the PEEK structure because of the introduction of the $-SO_3H$ groups. Comparing the DTG curves of SPEEK-46 and SPEEK-72, it can be seen that both the desulfonaiton and main chain decomposition temperatures shift to lower values with increasing sulfonation level, indicating that the instability increases at higher sulfonation levels (e.g. SPEEK-72). Nevertheless, SPEEK membranes with DS of ~ 50 % are stable up to 200 °C, which is high enough for fuel cell applications.

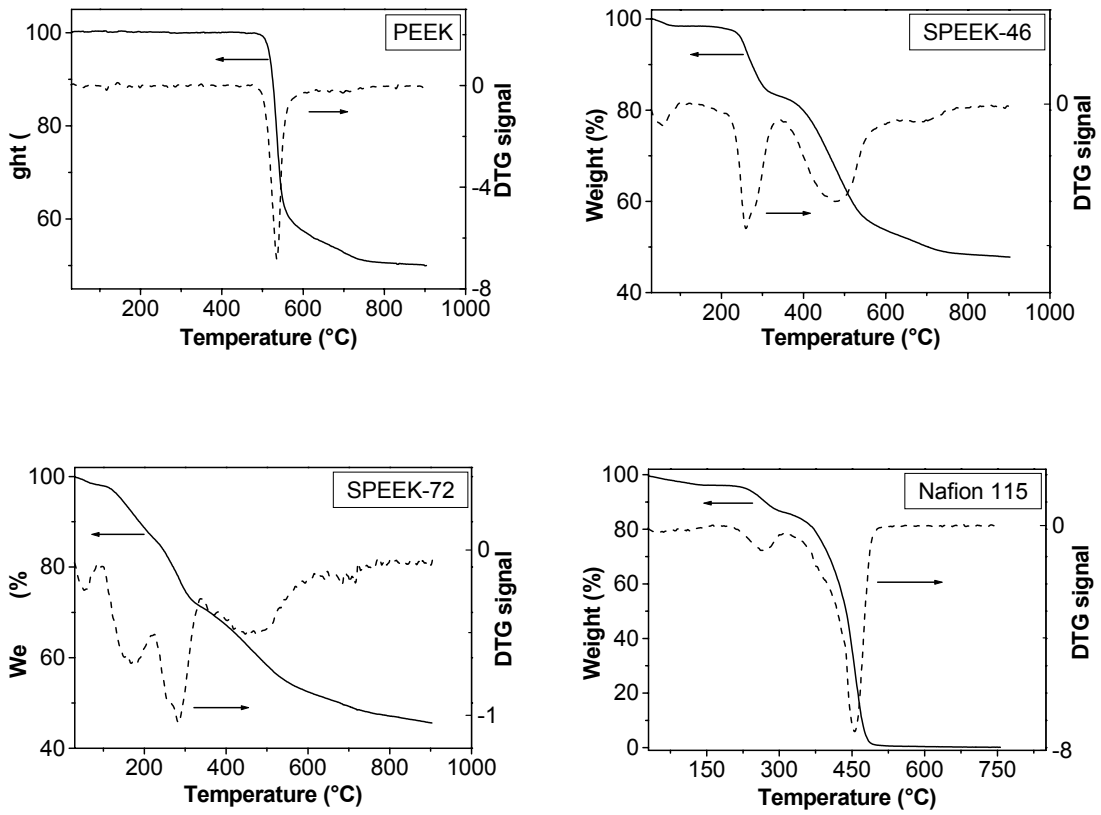

Figure 4.2 Thermogravimetric analysis of PEEK, SPEEK, and Nafion in flowing N_2 atmosphere at a heating rate of 5 °C/min.

4.3.4 Proton Conductivity

The impedance measurements of the Nafion and SPEEK membranes were carried out at 80 °C and various relative humidities (20 - 100 %). While the Nafion 115 membrane has an impedance spectrum similar to that of the $Ta_2O_5 \cdot nH_2O$ modified composite Nafion membrane (Fig. 3.6), SPEEK membranes have different impedance diagrams, especially at low relative humidity. Typical Nyquist plots of SPEEK membranes at various relative humidities are shown in Fig. 4.3. The difference

between the impedance spectra of Nafion and SPEEK membranes is possibly due to the different microstructure evolution with relative humidity, and more details will be discussed in chapter 5.

The proton conductivities calculated from the impedance values at various relative humidities are shown in Fig. 4.4. The conductivity increases with increasing relative humidity as expected for both the SPEEK and Nafion membranes. Generally, the proton conductivity of SPEEK membranes increases with the increasing sulfonation level. However, at high relative humidity (e.g. 100 %), the conductivity of SPEEK-72 is lower than that of SPEEK-58 and similar to that of SPEEK-54. The possible reason for this interesting phenomenon is that SPEEK-72 may partially dissolve at 80 °C and 100 % humidity during the period of stabilizing the system, which usually needs several hours. This indicates that SPEEK membranes with very high sulfonation level are not suitable for practical use in fuel cell. From Fig. 4.4, it can also be seen that the conductivity values of the SPEEK membranes are generally lower than those of Nafion membrane at each relative humidity in spite of the higher IEC for SPEEK membranes. This behavior could be explained by considering the greater hydrophobicity and chain flexibility of the Nafion backbone compared to the more rigid SPEEK. In Nafion membrane, sulfonic acid-water clusters with higher $-SO_3H$ densities can be easily formed and connected with each other, providing continuous pathways for proton conduction. Moreover, it is known that Nafion is a solid superacid [163,164] that has acid strength greater than that of 100 % H_2SO_4. Its superacidity is attributed to the electron-withdrawing effect of the perfluorocarbon chain acting on the sulfonic acid

group, which favors proton mobility. On the other hand, in SPEEK membranes, the hydrophilic/hydrophobic difference is smaller (the backbone is less hydrophobic, and the sulfonic acid groups is less acidic), the distance between the $-SO_3H$ groups is larger, and the PEEK backbone is less flexible. All these characteristics lead to unfavorable proton conduction, especially at low relative humidity.

With the increase of the relative humidity, the proton conductivity difference between Nafion and SPEEK membranes decreases due to the increased hydration of SPEEK membranes while the Nafion membrane may have approached the saturation state. More discussions about the different transport properties of Nafion and SPEEK membranes will be presented in chapter 5 by relating them to the different evolutions of microstructure and ionic clusters with humidity and temperature.

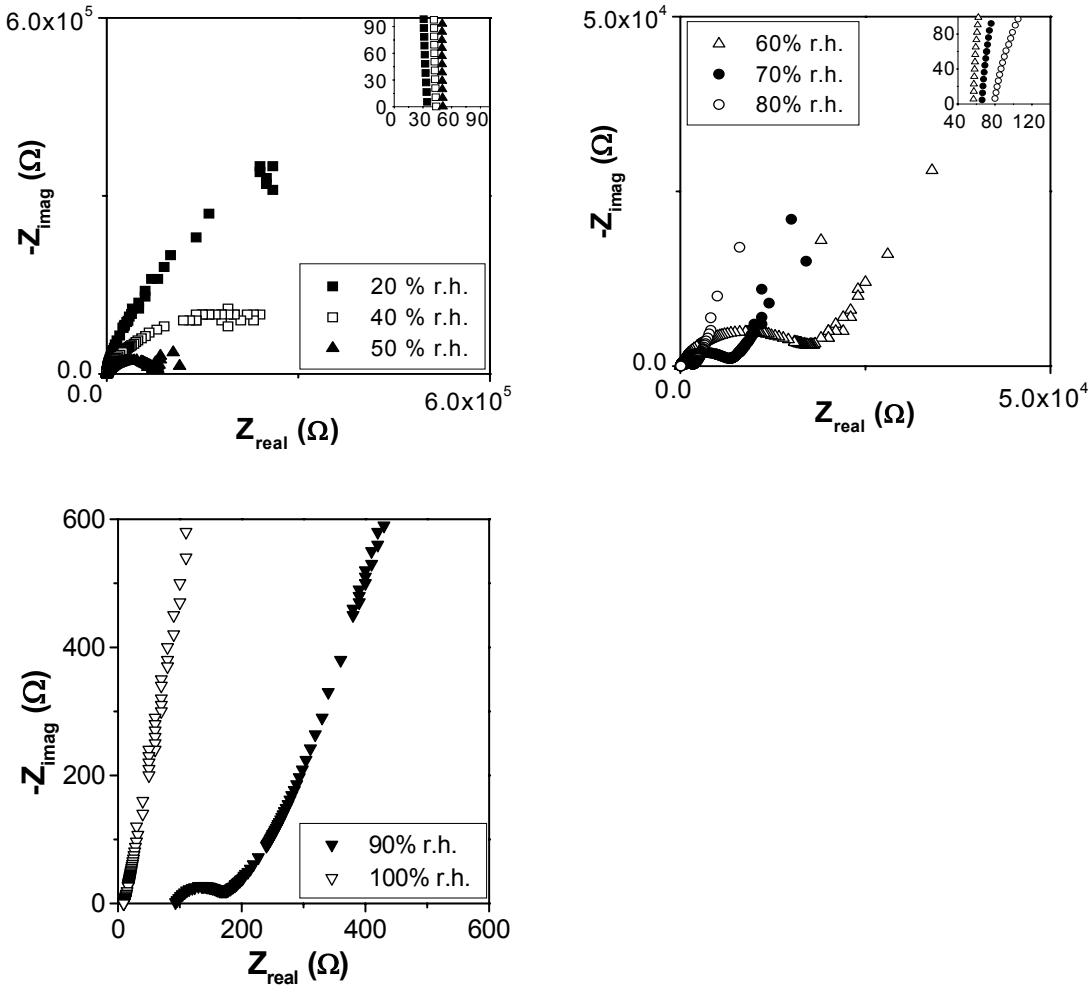

Figure 4.3 Impedance spectra of SPEEK-44 membrane at 80 °C and various relative humidities.

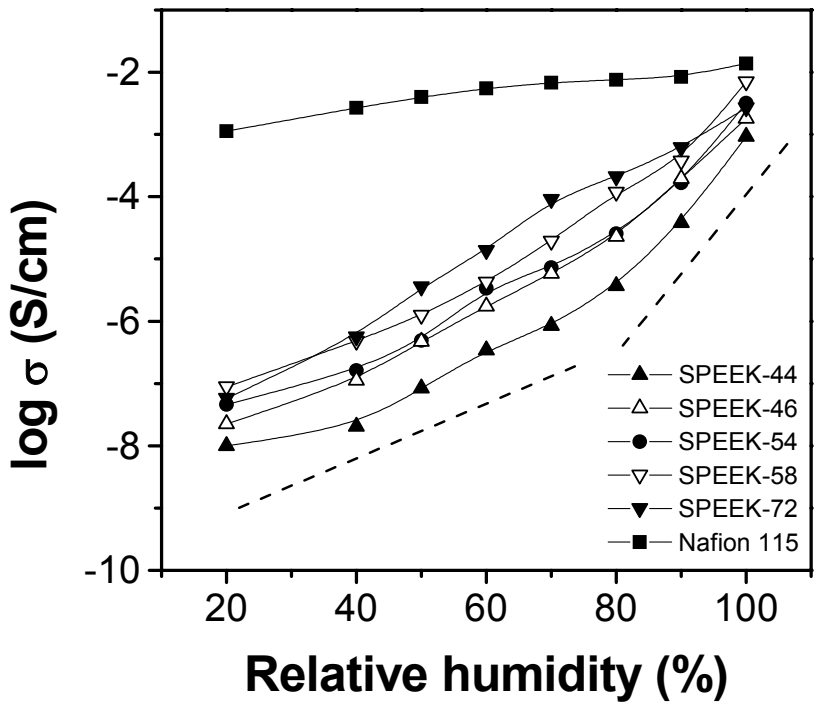

Figure 4.4 Arrhenius plots of the variations of proton conductivity of Nafion and SPEEK membranes with relative humidity at 80 °C.

4.3.5 DMFC Tests and Methanol Crossover Evaluation

Figure 4.5 compares the performances of the SPEEK and Nafion membranes in DMFC at 65 and 80 °C. The polarization loss of the SPEEK membranes decreases with increasing degree of sulfonation, and SPEEK-54 exhibits better performance than Nafion 115 despite a lower proton conductivity. The better performance of SPEEK-54 is due to lower methanol crossover as indicated by a lower methanol crossover limiting current density in Fig. 4.6. As can be seen, the electro-oxidation current of methanol

reaches a transport-controlled limiting value at higher applied potentials. Although the thickness of the SPEEK membranes (~ 70 μm) is less than that of Nafion (~ 125 μm), the measured limiting crossover current density is less than half of that of Nafion, indicating a much lower methanol permeability.

Although all the SPEEK membranes given in Fig. 4.5 operated discontinuously (shutdown overnight) for at least two days at 65 °C, both SPEEK-46 and SPEEK-54 failed within a few hours on increasing the temperature to 80 °C and a scission was observed at the line of overlap with the electrodes. This finding is similar to that reported for SPEEK membranes in PEMFC at 100 °C [57]. However, no failure was observed for SPEEK-44 at 80 °C for two days, but its performance was inferior due to a low level of sulfonation.

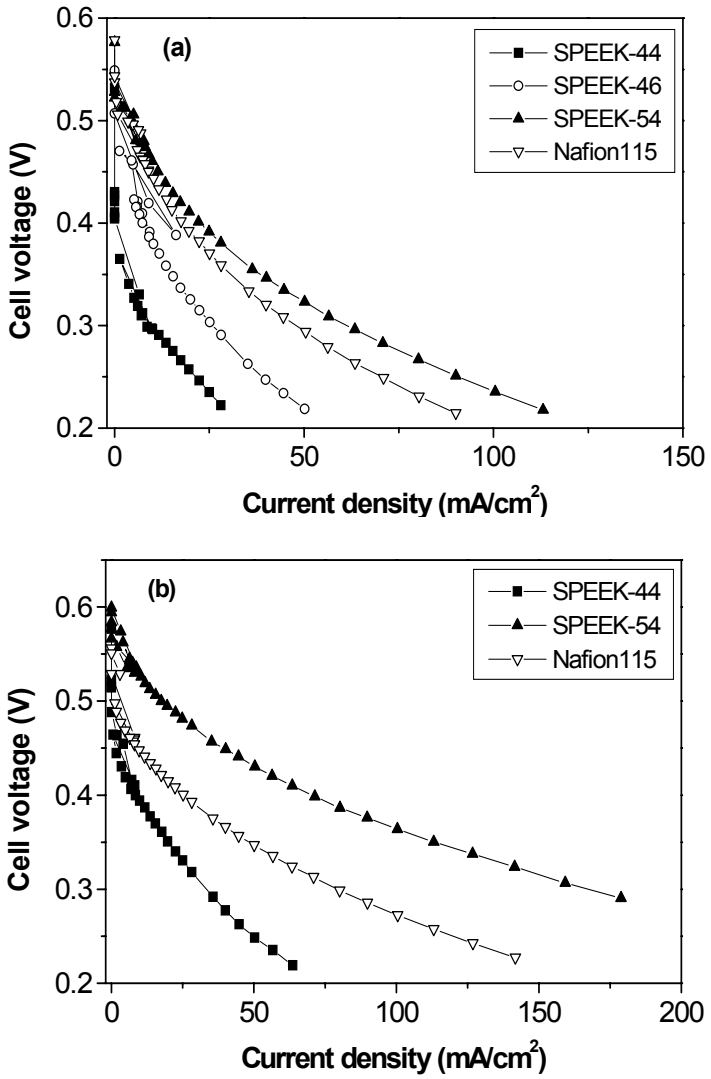

Figure 4.5 Comparison of the polarization characteristics of the SPEEK membranes with that of Nafion in DMFC: (a) 65 °C and (b) 80 °C. The data were collected with a methanol flow rate of 2.5 mL/min at the anode and a O_2 flow rate of 600 mL/m with a pressure of 40 psi at the cathode and the humidifier temperature for O_2 was same as the cell temperature. (Anode: 4 mg/cm^2 PtRu, Cathode: 3 mg/cm^2 Pt).

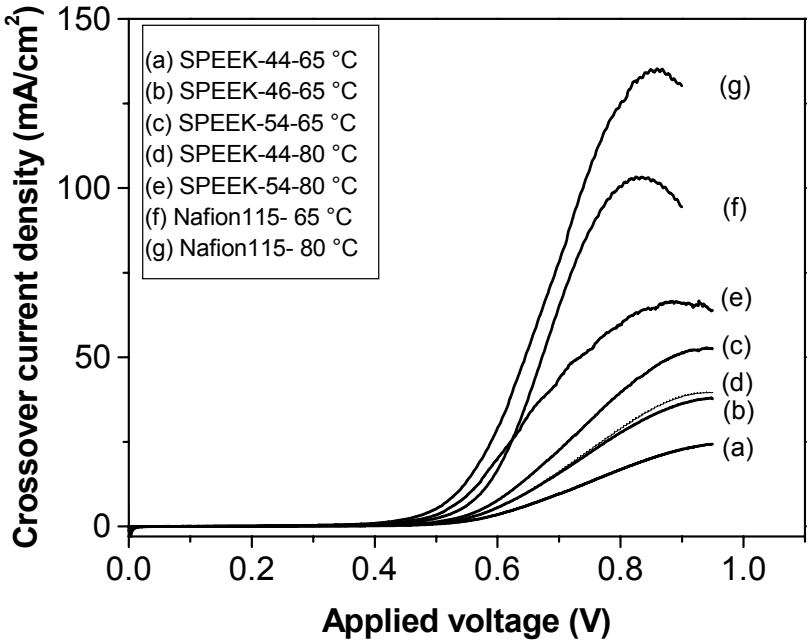

Figure 4.6 Comparison of the variations of methanol crossover current density for SPEEK and Nafion membranes at different temperatures. The data were collected with a methanol flow rate of 2.5 mL/min at the anode and a N_2 flow rate of 600 mL/min with a pressure of 40 psi at the cathode. (Anode: 4 mg/cm^2 PtRu, Cathode: 3 mg/cm^2 Pt). The applied potential step is 1 mV/s.

It should be noted that the electro-oxidation of the crossed-over methanol at the cathode will produce protons and the migration of protons from the cathode to the anode via the membrane may carry some crossed over methanol back from the cathode to the anode (electro-osmotic drag of fluid by the protonic current). This will lead to a lower measured value of the limiting current density at the cathode by the voltammetric method, and therefore, it needs to be corrected to obtain the actual methanol crossover flux.

According to the mathematical model developed by Ren *et al.* [144] for Nafion membranes, the actual methanol crossover current density at open circuit is around 30 % higher than the measured value at 65 or 80 °C with 2 M methanol solution fed into the anode. The % liquid uptake in 2 M methanol solution for SPEEK membranes at 65 °C is lower or similar to that of Nafion (Table 4.2), and under these conditions, the SPEEK membranes are known to have lower electro-osmotic drag coefficients than Nafion [46]. Therefore, the difference between the measured and actual limiting crossover current density values should be smaller (< 30 %) in the case of SPEEK membranes compared to that with the Nafion membranes. This implies that the difference between the actual methanol crossover current densities of SPEEK and Nafion might be even larger than that seen in Fig. 4.6. However, the % liquid uptake for SPEEK-54 at 80 °C is large (Table 4.2), and it is possible that both the methanol concentration flux from the anode to the cathode and the electro-osmotic drag flux in the opposite direction may be large, resulting in a smaller measured limiting current value in Fig. 4.6.

4.4 MULTILAYERED MEMBRANES

Multilayered membranes with SPEEK-44, SPEEK-54 and native recast Nafion as the middle layers and two Nafion outer layers were fabricated, and these multilayered membranes are designated, respectively, as, N-S44-N, N-S54-N and N-N-N. Two sets of multilayered membranes with a total thickness of about 135 μm and 115 μm were fabricated and the thickness values are given in parenthesis in the membrane designation indicated in Table 4.3.

Table 4.3 Multilayered membranes and their thickness.

Layer Sequence in the multilayered membrane	Total thickness (μm)	Middle layer thickness (μm)	Membrane designation
Nafion-Nafion-Nafion	135	50	N-N-N(135)
Nafion-SPEEK-54-Nafion	135	45	N-S54-N(135)
Nafion-SPEEK-44-Nafion	135	45	N-S44-N(135)
Nafion-Nafion-Nafion	115	30	N-N-N(115)
Nafion-SPEEK-54-Nafion	115	25	N-S54-N(115)
Nafion-SPEEK-44-Nafion	115	25	N-S44-N(115)

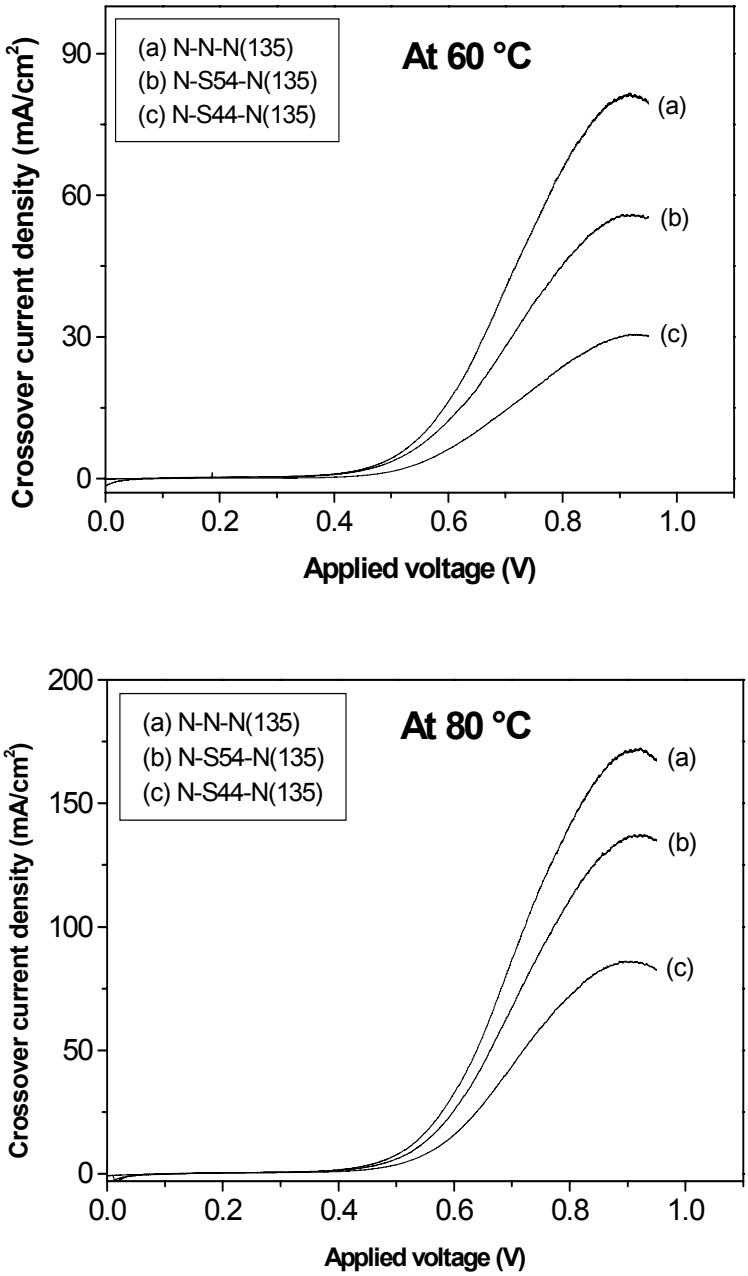

Figure 4.7 Comparison of the variations of methanol crossover current density for the multilayered membranes with a thickness of 135 μm at 60 and 80 °C. The data were collected with a methanol solution (2 M) flow rate of 8 mL/min at the anode and a N_2 flow rate of 600 mL/min with a pressure of 15 psi at the cathode. (Anode catalyst: 0.6 mg/cm^2 PtRu, cathode: 1 mg/cm^2 Pt). The applied potential step is 1 mV/s.

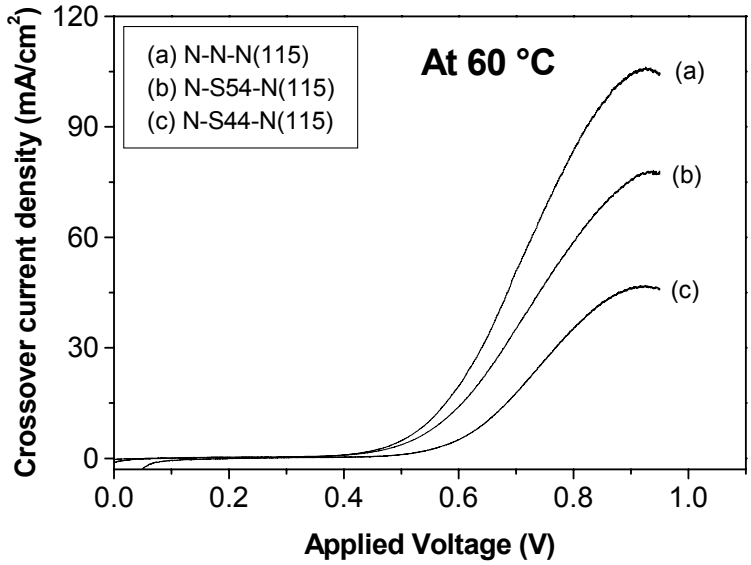

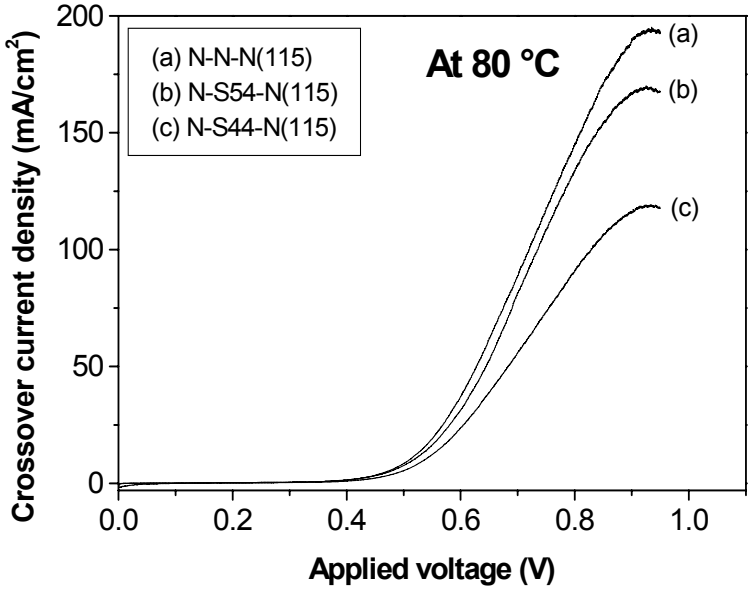

Figure 4.8. Comparison of the variations of methanol crossover current density for the multilayered membranes with a thickness of 115 μm at 60 and 80 °C. The data were collected with a methanol solution (2 M) flow rate of 8 mL/min at the anode and a N_2 flow rate of 600 mL/min with a pressure of 15 psi at the cathode. (Anode catalyst: 0.6 mg/cm^2 PtRu, cathode: 1 mg/cm^2 Pt). The applied potential step is 1 mV/s.

Figures 4.7 and 4.8 compare the current densities corresponding to the electro-oxidation of the crossed-over methanol that is taking place at the Pt/membrane interface of the cathode side of the membrane-electrode assembly (MEA) in DMFC. The membranes designated as N-S44-N(135) and N-S44-N(115) in Table 4.3 exhibit the lowest limiting current density both at 60 and 80 °C, while the membranes designated as N-N-N(135) and N-N-N(115) show the highest limiting current density, indicating the highest methanol permeation flux. Additionally, the N-S44-N(135) membrane with a higher thickness (45 μm) for the middle SPEEK-44 layer exhibits a lower limiting current density than the N-S44-N(115) membrane with a lower thickness (25 μm) for the middle SPEEK-44 layer. The N-S44-N(135) and N-S44-N(115) membranes exhibit, respectively, up to 51 and 37 % reduction in methanol permeation flux at 80 °C compared to the corresponding N-N-N(135) and N-N-N(115) membranes. These observations reveal that the middle SPEEK-44 layer is effective in suppressing the methanol crossover. However, when the sulfonation level is as high as in SPEEK-54 and the temperature is high (80 °C), the liquid uptake is so large that the methanol permeation becomes larger and consequently the methanol blocking effect is limited as seen in Figs. 4.7 and 4.8.

Assuming the activities of the catalysts to be the same for all the MEAs, the open-circuit voltage (OCV) value would be expected to decrease as the methanol crossover increases. In this study, the OCV values were taken from the stable potential values measured after switching the cell from the full current load to open circuit for about 10 min. A typical OCV change with time is shown in Fig. 4.9. It can be seen that after the

load is removed, the cell voltage increases greatly and reaches a peak in several seconds. Rather than stabilizing at this voltage, it declines quite rapidly, and approaches a stabilized OCV after several minutes. This behavior is identified as the influence of different mixed potentials at the cathode, due to varying methanol crossover flow densities [165,166].

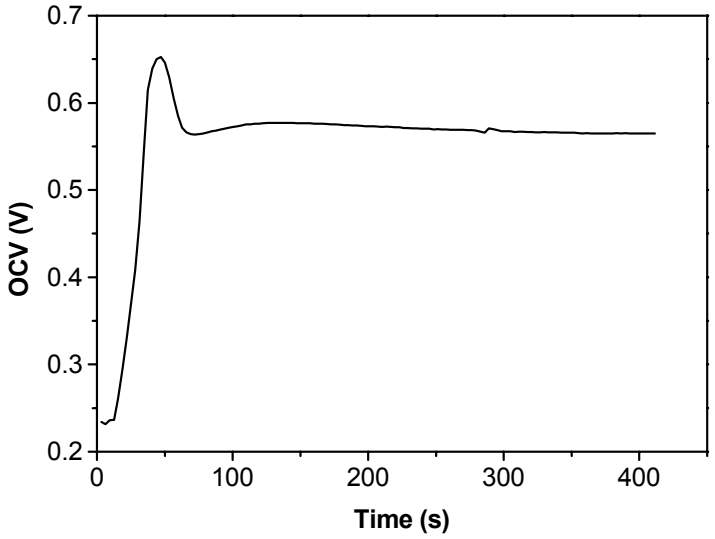

Figure 4.9 Cell voltage variation of MEA with N-S54-N(135) multilayered membrane after the cell is changed from the full current load to open circuit . T_{cell} = 60 °C; anode: 2.0 M methanol, 8 mL/min; cathode: oxygen flow rate = 600 mL/min, P = 15 psi.

The OCV values for the various multilayered membranes are given in Table 4.4; the differences between the OCV values measured at 60 and 80 °C are also included. The membranes with a middle SPEEK layer exhibit higher OCV compared to that with a middle Nafion layer, indicating a less methanol crossover for the former. Additionally, the OCV values increase with increasing temperature due to the enhanced

activity of the catalysts. However, the increase in OCV on going from 60 to 80 °C is much smaller for the N-S54-N(135) and N-S54-N(115) membranes compared to that for the other membranes (Table 4.4). This is because the increase in OCV caused by the enhanced catalytic activity may be partly countered by the negative effect caused by a higher methanol crossover at 80 °C. The methanol permeation for SPEEK-54 is smaller than that for Nafion at 60 °C, but SPEEK-54 has a much higher liquid uptake at 80 °C, which may lead to a methanol crossover value close to that for Nafion. This conclusion is also supported by the close OCV values of N-N-N and N-S54-N membranes at 80 °C.

Table 4.4 Comparison of the open-circuit voltages (OCV) of the MEAs fabricated with the various multilayered membranes.

Membrane	OCV (V)		$OCV_{80\,^{o}C}$ - $OCV_{60\,^{o}C}$ (mV)
	60 °C	80 °C	
N-N-N(135)	0.511	0.556	45
N-S54-N(135)	0.565	0.571	6
N-S44-N(135	0.576	0.616	40
N-N-N(115)	0.502	0.539	37
N-S54-N(115)	0.546	0.550	4
N-S44-N(115)	0.554	0.590	36

Figure 4.10 compares the performance of the MEAs fabricated with the various multilayered membranes in DMFC at 60 and 80 °C. With a total thickness of 135 μm and a SPEEK layer thickness of 45 μm, both the N-S54-N(135) and N-S44-N(135) membranes exhibit larger polarization losses than the N-N-N(135) membrane (Fig.

4.10a). However, with a total thickness of 115 μm and a SPEEK layer thickness of 25 μm, all the three membranes exhibit similar polarization behaviors at 80 °C (Fig. 4.10b). At 60 °C, the N-S54-N(115) membrane exhibits lower polarization while the N-S44-N(115) exhibits larger polarization than the N-N-N(115) membrane. The data suggest that the higher polarization losses of the N-S54-N(135) and N-S44-N(135) membranes compared to the N-N-N(135) membrane in Fig. 4.10a could be due to a higher cell resistance arising from the thicker SPEEK layers (45 μm). The comparable performances of the N-S54-N(115) and N-S44-N(115) membranes to that of N-N-N(115) in Fig. 4.10b despite a higher cell resistance arising from a lower conductivity of SPEEK is due to the suppression of the methanol crossover by the thin middle SPEEK layer.

All these MEAs with multilayered membranes were operated discontinuously (shutdown overnight) for two days at 60 °C, and then for another two days at 80 °C. There was no failure during these periods of tests, and no damage of the membrane was observed, indicating that the thin middle SPEEK layer is well protected by the outer recast Nafion layers. However, while the N-N-N membranes remained as a single integral film after the DMFC operation, the layers in both the N-S44-N and N-S54-N membranes were found to separate from each other which may be due to the poor interlayer bonding achieved by hot pressing. The delamination may lead to additional contact resistance at the interfaces between the three layers and consequent performance losses. Development of procedures that can chemically bond the different layers to an integral single film could lead to further improvement in cell performance.

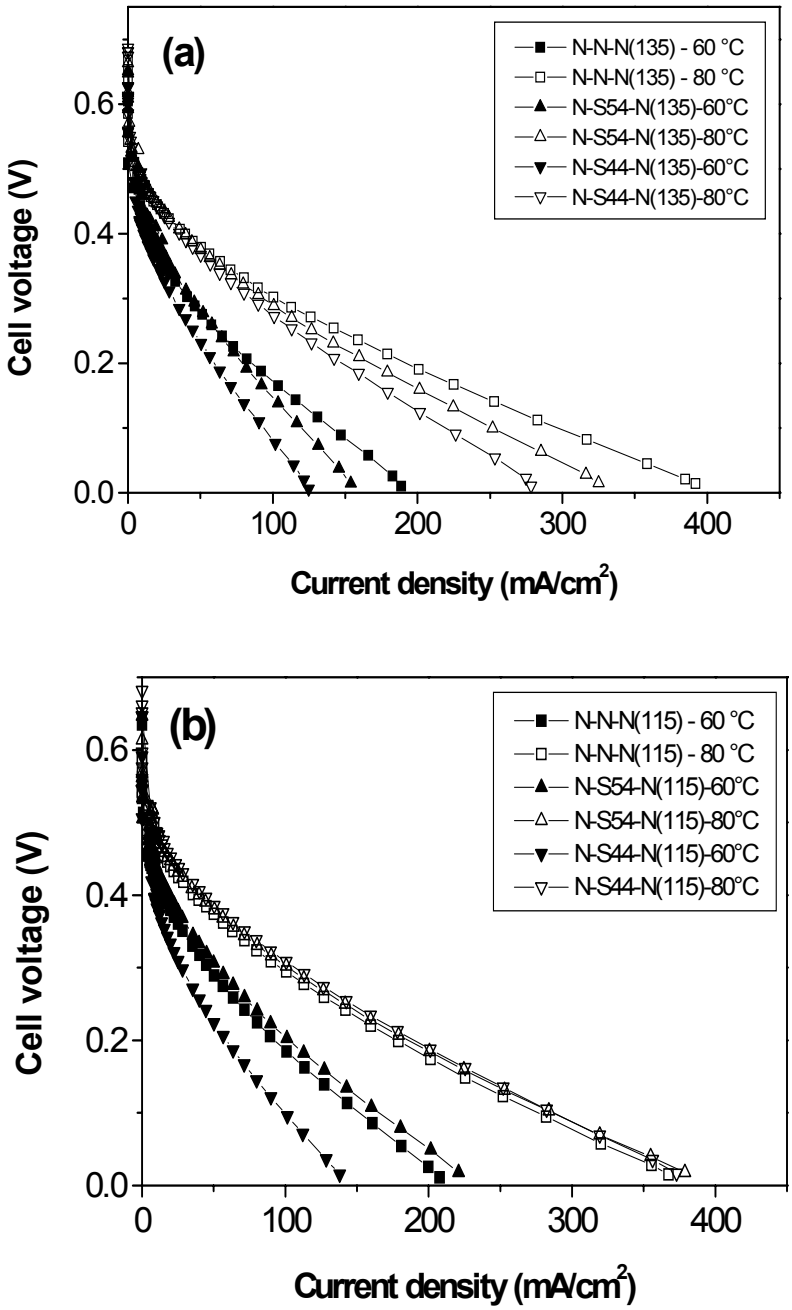

Figure 4.10 Comparison of the polarization characteristics of the multilayered membranes with a thickness of (a) 135 μm and (b) 115 μm at 60 and 80 °C. The data were collected with a methanol solution (2 M) flow rate of 8 mL/min at the anode and a N_2 flow rate of 600 mL/min with a pressure of 15 psi at the cathode. (Anode catalyst: 0.6 mg/cm^2 PtRu, cathode: 1 mg/cm^2 Pt).

4.5 CONCLUSIONS

The electrochemical performances of SPEEK membranes with different degrees of sulfonation have been investigated in DMFC. SPEEK membranes with a degree of sulfonation of around 50 % exhibit performances comparable or exceeding that of Nafion due to lower methanol crossover, but the operating temperature needs to be limited to < 65 °C. Membranes with high degrees of sulfonation experience huge swelling at higher temperatures (80 °C) and undergo failure. The lower cost and suppressed methanol crossover compared to that of Nafion make the SPEEK membranes promising alternatives for DMFC. However, further work is needed to fully assess the long-term stability in the DMFC environment.

A multilayered membrane concept was proposed and demonstrated for alleviating the effects of methanol crossover in DMFC. Multilayered membranes containing a thin inner layer of SPEEK polymer as a barrier and two outer Nafion layers are found to significantly reduce the methanol crossover in DMFC compared to plain Nafion membrane. Inner SPEEK layers with a sulfonation level of 44 % and a thickness of 25 μm are found to offer electrochemical performance comparable to that of Nafion despite a lower proton conductivity due to a 37 % reduction in methanol crossover compared to the native N-N-N membrane. The middle thin layer SPEEK membrane is well protected by the outer Nafion layers, leading to good mechanical property. We believe that this multilayered approach to membrane fabrication is a promising strategy to circumvent the methanol crossover problems in DMFC. Investigations to chemically bond the different layers need to be conducted in order to solve the delamination

problem and to improve further the DMFC performance. After obtaining integral multiayered membrane, the optimization of the sulfonation level and thickness of middle layer SPEEK membrane could further enhance the fuel cell performance.

Chapter 5

Comparison of the *In-situ* Small Angle X-ray Scattering and Impedance Spectroscopic Studies of Sulfonated Poly(etheretherketone) and Nafion Membranes for Direct Methanol Fuel Cells

5.1 INTRODUCTION

In chapter 4, we have demonstrated that membranes based on sulfonated poly(etheretherketone) (SPEEK) with sulfonation levels of around 50 % showed low methanol permeability and electrochemical cell performance comparable to that of Nafion membrane. However, many of these different performance features of the two kinds of polymer membranes are not well understood mainly due to the complexity of the membrane structures arising from the phase separation when hydrated.

Nafion membrane has the following chemical structure

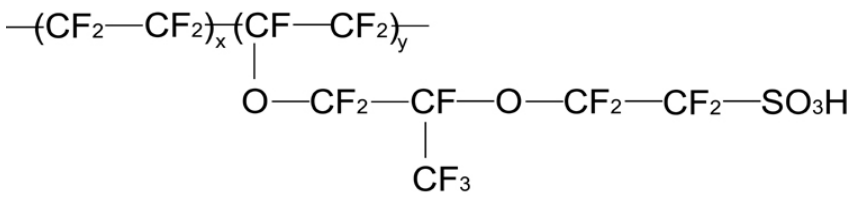

in which the values of x and y can be varied to give materials with a range of equivalent weights (900 – 1400), and the material with an equivalent weight of 1100 is the most common. Nafion consists of an extremely hydrophobic perfluorinated backbone and highly hydrophilic terminal sulfonic acid functional groups ($-SO_3H$)

attached to the backbone. The unique properties of Nafion membranes are believed to be closely related to the microscopic phase separation of the ionic parts (-SO_3H groups) from the fluorocarbon matrix. While the polymer backbone provides good strength for the Nafion membrane, the aggregation of the sulfonic acid groups leads to high proton conductivity, especially when the membrane is in the hydrated state.

The clustering of the ionic groups in the low dielectric constant polymer matrix is usually indicated by the existence of a scattering maximum, which is often called "ionomer peak", in small angle x-ray scattering (SAXS) or small angle neutron scattering (SANS) [7,167-170]. The scattered intensity, I(q), oscillates with increasing wave vector

$$q = \frac{4\pi}{\lambda} \sin\theta \tag{5.1}$$

where λ is the wavelength and 2θ is the scattering angle. The Bragg spacing d is related to q as

$$d = 2\pi / q \tag{5.2}$$

The origin of the scattering maximum has been extensively studied, but it is still a subject of controversy. Since 1970s, various models have been proposed to interpret the SAXS observations and generally they can be divided into (i) intraparticle models [171,172] and (ii) interparticle models [173-175]. The intraparticle models attribute the "ionomer peak" to the interference within the ionic cluster, implying that the scattering maximum is related to the internal structure of the cluster. On the other hand, the interparticle models attribute the "ionomer peak" to the interference between different

ionic clusters, implying that the Bragg spacing obtained from equation 5.2 refers to the center-to-center distance between two clusters. Although the interparticle models are now commonly being accepted, the origin of the ionomer peak is not fully resolved.

From the molecular structure of SPEEK membrane (Fig. 4.1), it can be seen that the sulfonic acid groups $-SO_3H$ are attached to the main chain of PEEK polymer, which has high rigidity. This may lead to different microstructural characteristics from that of Nafion, in which the $-SO_3H$ groups are attached to the flexible side chains of the PTFE backbone. These different microstructural characteristics such as the size, shape and distribution of the ionic clusters can be studied by small angle techniques.

Generally, SAXS studies of hydrated ionomer membranes use Kapton (polyimide film from DuPont) windows to enclose the samples and keep the water content constant during the measurements. However, it is hard to totally avoid the environmental fluctuations during the long period of SAXS data collection. For those polymer membranes to be used in liquid DMFC, it is highly desirable to obtain the structural information of the electrolyte membranes at conditions close to that in practical fuel cells. Accordingly, we equilibrate the SPEEK membranes with different sulfonation levels in methanol solution at various temperatures and present in this chapter a systematic *in-situ* SAXS investigation of the SPEEK membranes. The relationships between the Bragg spacing and the transport of proton and methanol in the SPEEK membranes are discussed and the data are compared with those of Nafion.

5.2 EXPERIMENTAL

The details of the sulfonation of poly(etheretherketone) (PEEK) polymer (PEEK450 PF, Victrex) and the preparation of the SPEEK membranes have been given in Section 4.2. SPEEK-44, SPEEK-46, SPEEK-54, SPEEK-58, and SPEEK-72 membranes are used in this study. For the comparative study, Nafion 115 membranes were used. To prepare SPEEK membranes with different counter ions, the sulfonated polymers were immersed under stirring for 20 h in excess (1.5 times) 0.1 M NaOH or 0.1 M CsCl solution, washed thoroughly with deionized water, and dried at around 100 °C overnight. The samples with various levels of sulfonation and the Na^+ or Cs^+ counter ions are designated hereafter as, for example, SPEEK-54-Na, SPEEK-44-Cs, SPEEK-54-Cs, and SPEEK-58-Cs.

The SAXS experiments were carried out by placing the sample cell in the path of the X-ray beam. The 1.54 Å Cu-K_α X-rays were generated by a rotating copper-anode generator source (Bruker Nonius). The scattering was detected by a multiwire gas-filled 2D detector (Molecular Metrology, Inc.). The experiments were typically carried out at room temperature for a duration of 90 min.

Membranes were equilibrated in 2 M methanol solution at various temperatures for 24 h before conducting the SAXS experiments. To avoid evaporation of the liquid absorbed on the membranes, the samples were embedded in 2 M methanol solution in stainless steel sample holders, and the sample cells were sealed with Kapton films. From our experience and the literature [176], it was observed that both the SPEEK and

Nafion membranes exhibit a swelling memory, viz. liquid uptakes obtained at high temperatures remain to room temperature as long as the membranes were kept in the same solution. This ensures the retention of the particular swelling state of the membranes at each temperature and the collection of *in-situ* SAXS data.

5.3 RESULTS AND DISCUSSION

5.3.1 SAXS Profiles in Dry States

The room temperature SAXS spectra of the dry SPEEK and Nafion membranes (pre-dried at 100 °C in vacuum overnight followed by equilibrating in ambient atmosphere) are compared in Fig. 5.1. It can be seen that in the dry states, no ionomer peaks are observed for SPEEK-44, SPEEK-54, SPEEK 58, and SPEEK-72 membranes whereas a scattering maximum with a q value of 1.93 nm^{-1} is obtained for the Nafion 115 membrane. There are two possibilities for the absence of the ionomer peaks for the SPEEK membranes in the dry states. One is that the ionic clusters do exist, but the electron density contrast between the clusters and the PEEK polymer phase is too small to produce any pronounced SAXS peak structure. The other possibility is that the -SO_3H groups are only statistically attached to the main chains of PEEK and no ionic clusters are formed in the dry states by considering the very rigid property of the PEEK backbone to which the -SO_3H groups are attached [177]; the rigidity of PEEK may not provide enough free volume and flexibility for the clustering of the -SO_3H groups.

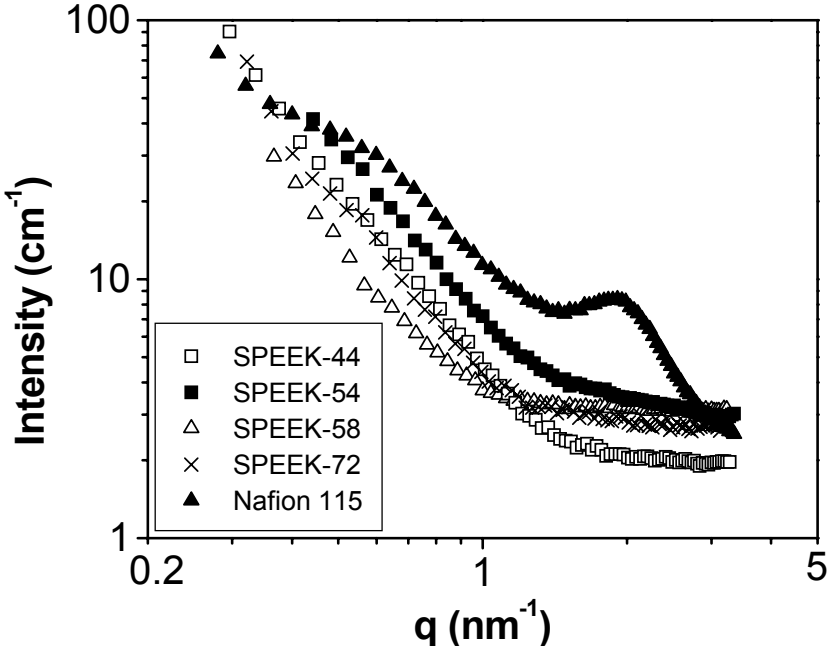

Figure 5.1 Comparison of the SAXS profiles of dry Nafion and SPEEK membranes.

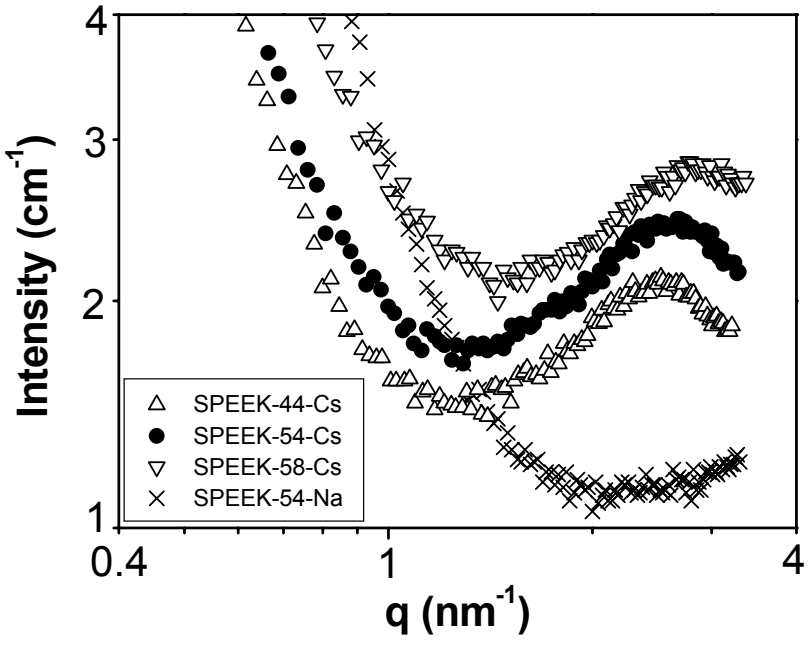

Figure 5.2 Comparison of the SAXS profiles of sodium and cesium neutralized SPEEK membranes.

To clarify this point, SAXS experiments were carried out on the sodium neutralized SPEEK-54 and cesium neutralized SPEEK-44, SPEEK-54 and SPEEK-58 membranes in the dry states. These metal ions are expected to enhance the electron density contrast between the hydrocarbon polymer matrix and the ionic clusters, if they exist. The SAXS profiles of the sodium and cesium neutralized membranes are shown in Fig. 5.2. While the sodium neutralized SPEEK-54 membranes do not exhibit any obvious peak structure, the three cesium neutralized membranes show broad peaks with q values of around 2.7 nm^{-1}. The results indicate that ionic clusters do exist in dry SPEEK membranes, but the cluster size may be small with a small number of ionic $-SO_3H$ groups in each cluster and a small characteristic separation of about 2.3 nm between the clusters. The smaller cluster size is due to the fact that only the closely spaced $-SO_3H$ groups can get clustered due to the high rigidity of the PEEK backbone to which the $-SO_3H$ groups are attached and the smaller free volume. The rigidity of the backbone prevents further structural rearrangement that can lead to larger clusters composed of more ionic groups. On the other hand, in the case of Nafion membrane, the sulfonic acid groups are attached to the PTFE side chains, which due to their high flexibility can provide enough free volume for the ionic groups to cluster easily.

It can also be seen from Fig. 5.2 that the ionomer peak shifts to slightly higher q value as the sulfonation level in the cesium neutralized membranes increases from 44 to 58 %. This observation indicates that the Bragg distance d (see eqn. 5.2) decreases with increasing sulfonation level, suggesting an interparticle origin for the ionomer

peak. With increasing sulfonation level, the number of ionic clusters increases, resulting in a smaller center-to-center cluster distance (Bragg spacing).

5.3.2 Influence of Sulfonation Level on SAXS Profile

Figure 5.3 compares the SAXS profiles recorded after equilibrating the SPEEK and Nafion membranes in 2 M methanol solution at various temperatures. Comparison of the data to that in Fig. 5.1 indicates that ionomer peaks start to appear for the SPEEK membranes on equilibrating in methanol solution. Generally, at each temperature, the scattering maximum shifts toward smaller q values and the intensity of the peak increases as the sulfonation level increases, especially at higher temperatures (≥ 60 °C). This trend is different from that obtained for dry membranes in Fig. 5.2, indicating that microstructural reorganization may be involved upon absorbing methanol/water. In other words, two or more small clusters (clusters composed of small number of ionic groups are called multiplets according to Eisenberg [178]) may combine to form larger clusters containing a larger number of $-SO_3H$ ionic groups. While the starting of the structural rearrangement is obvious at lower temperatures for the SPEEK membranes with high sulfonation levels, it becomes obvious only at higher temperatures in the case of membranes with low sulfonation levels. In fact, a careful look at the spectra at a low temperature of 40 °C (Fig. 5.4) reveal that SPEEK-44 and SPEEK-54 with a low level of sulfonation show characteristics similar to those of cesium neutralized dry SPEEK-44 and SPEEK-54 membranes. SPEEK-54 exhibits a smaller Bragg distance (center-to-

center distance of clusters) compared to SPEEK-44, indicating that not too much structural rearrangement and/or cluster combination are involved for these two membranes at low temperatures and the structural characteristics in the dry states are preserved.

It can be seen from Fig. 5.3d that the scattering maximum has disappeared for the SPEEK-58 membrane at 70 °C. This could possibly be due to the solvation of the ions by methanol/water and a weakening of the attraction between the ions to a point where the cluster would fall apart. Thus the ionic scattering maximum for the ionomers is destroyed upon saturating the SPEEK samples with methanol solution. In contrast, the clusters of the Nafion membranes never fall apart, and the ionic peak is preserved even at high water contents and high temperatures [179]. These comparisons indicate the advantages of the Nafion membranes over other hydrocarbon based polymer membranes from a thermal stability point of view. In fact, for Nafion membrane, the huge swelling starts only when the temperature is increased to 140 °C, which is much higher than the typical operating temperatures of conventional PEMFC and DMFC.

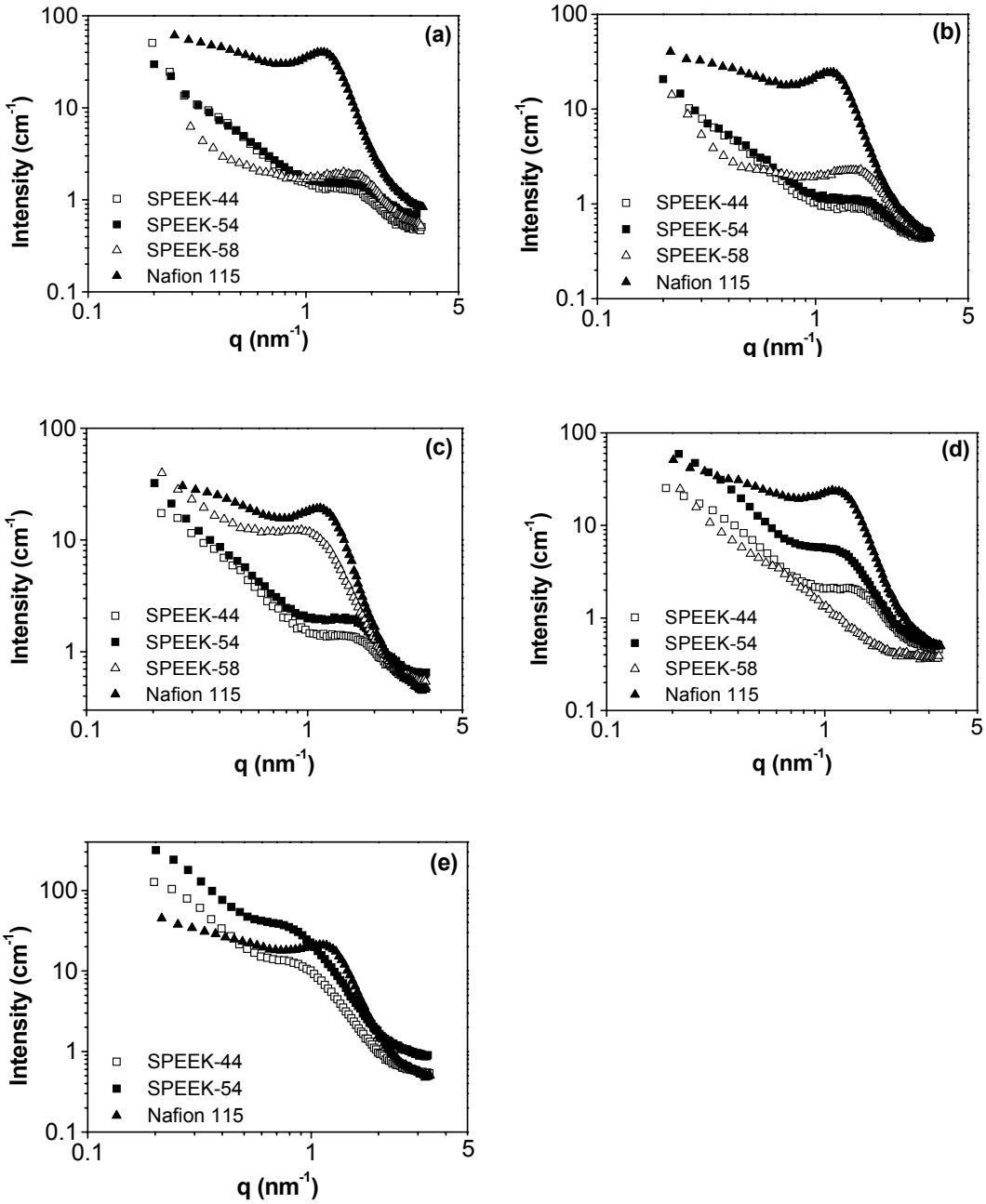

Figure 5.3 Comparison of the SAXS profiles of SPEEK and Nafion membranes after equilibrating in 2 M methanol solution at (a) 40 °C, (b) 50 °C, (c) 60 °C, (d) 70 °C, and (e) 80 °C.

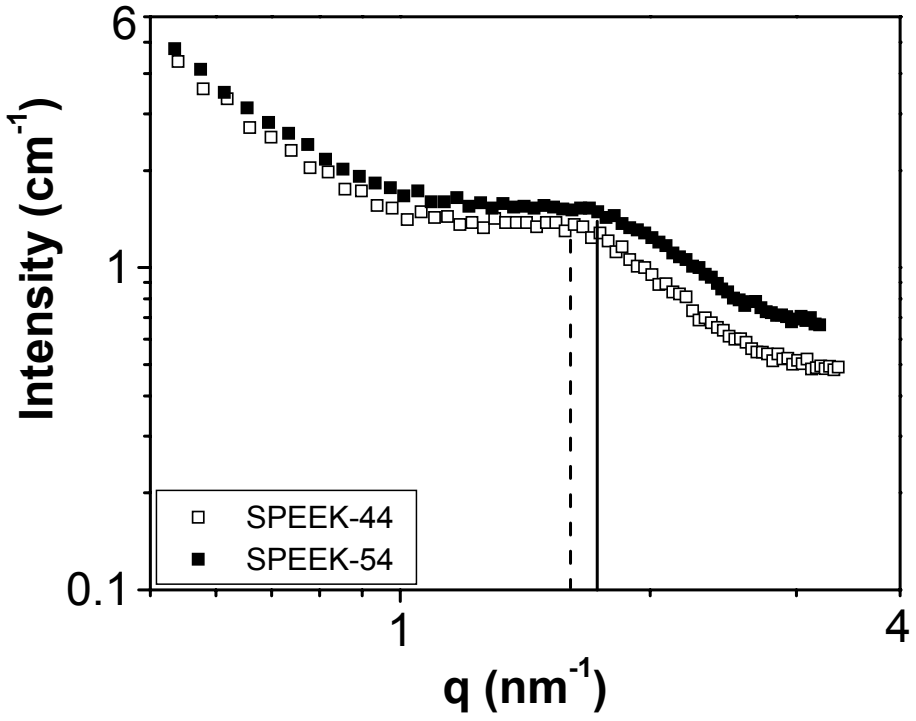

Figure 5.4 Comparison of the SAXS profiles of SPEEK-44 and SPEEK-54 membranes after equilibrating in 2 M methanol solution at 40 ° C.

5.3.3 Influence of Temperature on Bragg Spacing

To investigate how the ionic clusters in the membrane develop with temperature in methanol solution, the Bragg spacing calculated from the q values of the ionomer peaks in the SAXS profiles is plotted in Fig. 5.5 against the equilibrating temperature. It can be seen that the Bragg spacing hardly changes with temperature in the case of SPEEK membranes with low sulfonation levels (SPEEK-44 and SPEEK-54) at low temperatures (40 - 60 °C). However, it increases significantly on increasing the temperature above 60 °C.

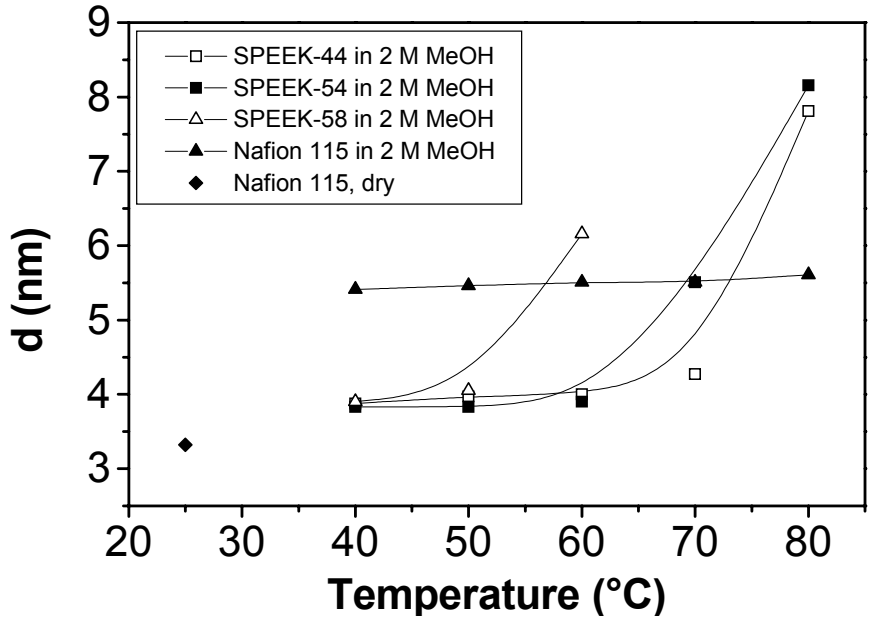

Figure 5.5 Variation of Bragg distance d with the equilibrating temperature in 2 M methanol solution of SPEEK and Nafion membranes.

The interparticle model can be employed to understand the existence of the two temperature regions (for example, 40 - 60 °C and > 60 °C for low sulfonation levels of 44 and 54 %) in Fig. 5.5. According to this model, the Bragg spacing is a measure of the center-to-center distance in the ionic clusters. On going from the dry state to the state of being equilibrated in 2 M methanol solution at 40 °C, we may assume that a first stage of cluster combination occurs. In this stage, the first absorbed water/methanol may cause several neighboring small clusters to aggregate to slightly bigger clusters. After this stage, as the temperature is increased from 40 to 60 °C, which is in the low temperature range, most of the liquid is located around the ionic clusters and the size of the cluster increases while the increase in the center-to-center

distance between the clusters is relatively smaller. However, as the temperature is increased further (> 60 °C), a percolation limit is reached, leading to a reorganization of the clusters to give larger clusters. In addition, methanol may penetrate into the organic part and plasticize the polymer chain, increasing the flexibility of the polymer backbone and facilitating the reorganization of the clusters. Adjacent clusters may combine to form even larger ones and the number of $-SO_3H$ groups per cluster increases in order to keep the specific surface constant and consequently the total number of clusters decreases [179].

On the other hand, different observations are made with the Nafion membranes. On going from the dry state to the state at 40 °C in methanol solution, the Bragg distance increases from 3.25 to 5.51 nm; after that, the Bragg distance hardly changes upon increasing the equilibrating temperature up to 80 °C. These results suggest that the growth and combination of ionic clusters are almost completed on equilibrating with 2 M methanol solution at 40 °C due to the high flexibility of the side chains to which the sulfonic acid groups are attached.

5.3.4 Impedance Spectroscopic Studies

Gieke's cluster network model [167] has been accepted widely to interpret the distribution of the ionic clusters and the high ionic conductivity associated with the phase-separation structure in Nafion membranes. According to this model, the aqueous clusters are connected by narrow channels, and the sizes of the clusters and channels

may vary with the water content in the membrane. Based on this model and the absolute rate theory, Pourcelly *et al.* [150] proposed that the energy barrier to be overcome between two adjacent sites in a cluster is lower than that between two sites on each side of the channel. Consequently, an accumulation of ions on each side of the channel gives rise to capacitance currents. Therefore, the impedance of the membrane can be regarded as a pure resistor associated with the proton conduction inside the cluster, in series with the impedance (resistance in parallel with a capacitance) of the channel. This model is confirmed by the fact that the impedance of the membrane phase has a non-zero value at infinite frequency. However, no details are available on how the non-zero values at infinite frequency change with the degree of swelling.

We adopt here the Pourcelly model to analyze the impedance data obtained at various relative humidity values for both the Nafion and SPEEK membranes. The impedance data of Nafion, SPEEK-54, and SPEEK-58 membranes are given, respectively, in Figs. 5.6, 5.7 and 5.8; SPEEK-44 membrane exhibits impedance plots (Fig. 4.3) similar to those in Fig. 5.7 and 5.8. It can be seen from Fig. 5.6 that the impedance diagram of the Nafion membrane is a slanted line at each relative humidity. Impedance diagrams with this kind of shape correspond to that of a pure resistor when blocking electrodes are used for the impedance measurement, indicating that the energy barrier for the elementary jump of protons in the clusters is same as that in the channels. The intercept value of the slanted line with the real axis can be taken as the resistance of the membrane. It can be seen that the intercept shifts to smaller values with increasing relative humidity, indicating a decrease in the membrane resistance.

The results reveal that Nafion membrane can absorb water from the environment easily and form a homogeneous continuous pathway for proton conduction [150].

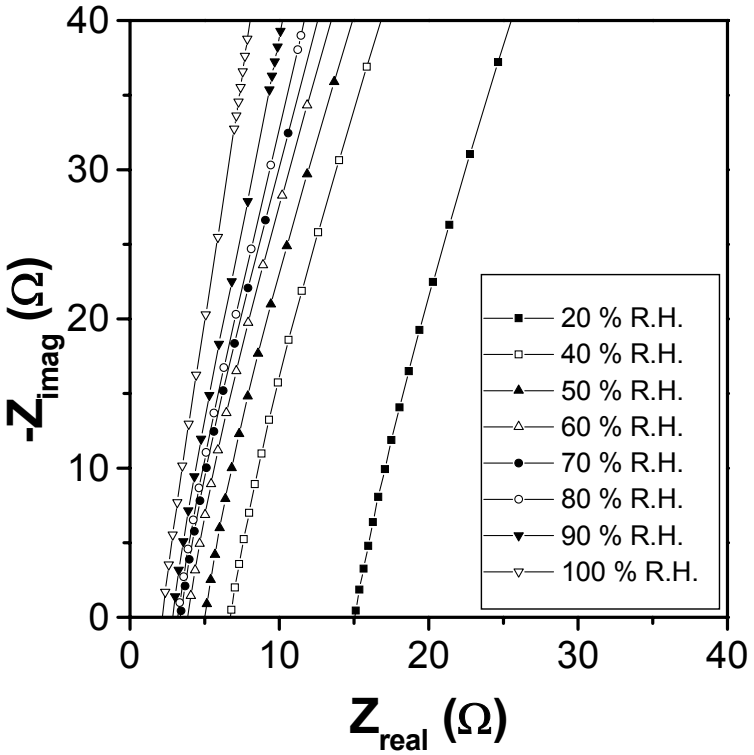

Figure 5.6 Impedance diagrams of the Nafion 115 membrane at 80 °C and various relative humidities.

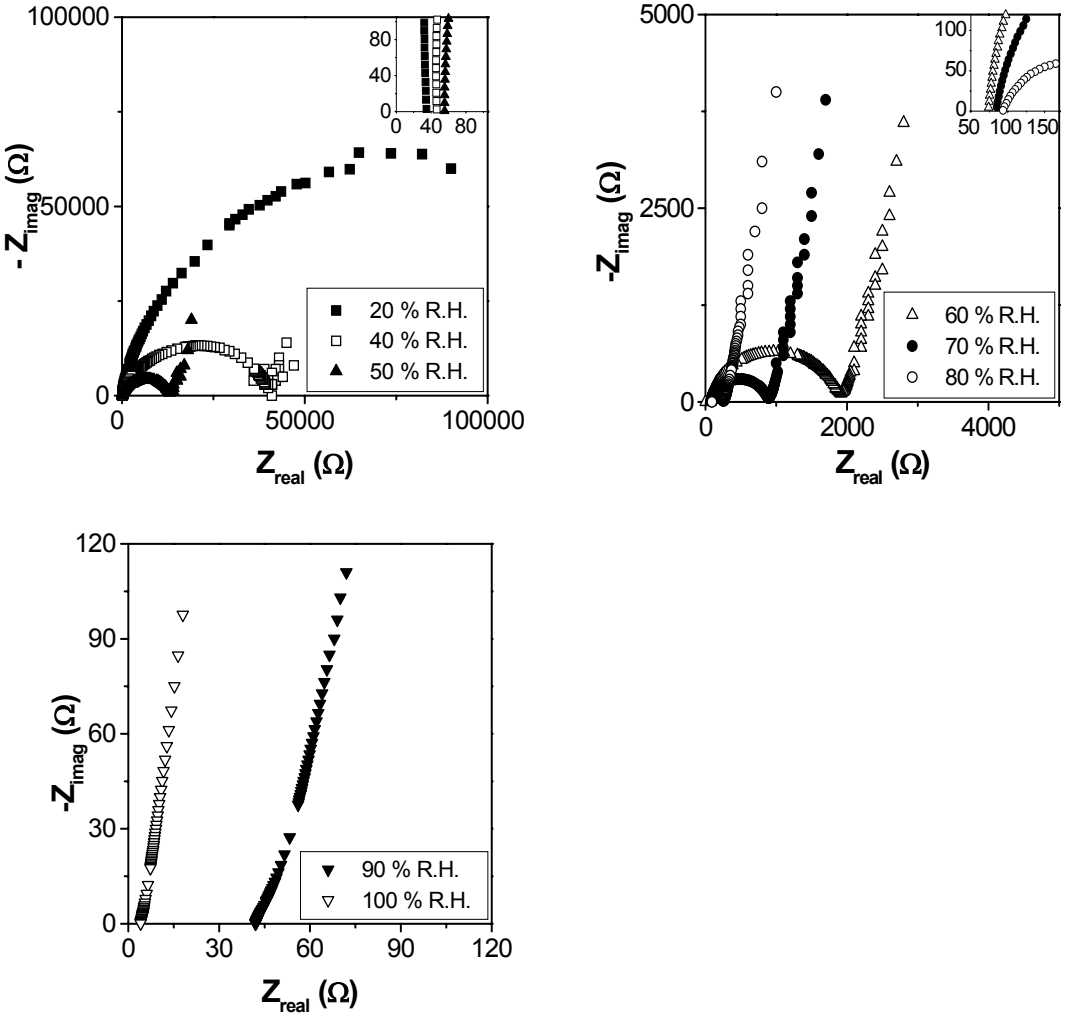

Figure 5.7 Impedance diagrams of the SPEEK-54 membrane at 80 °C and various relative humidities.

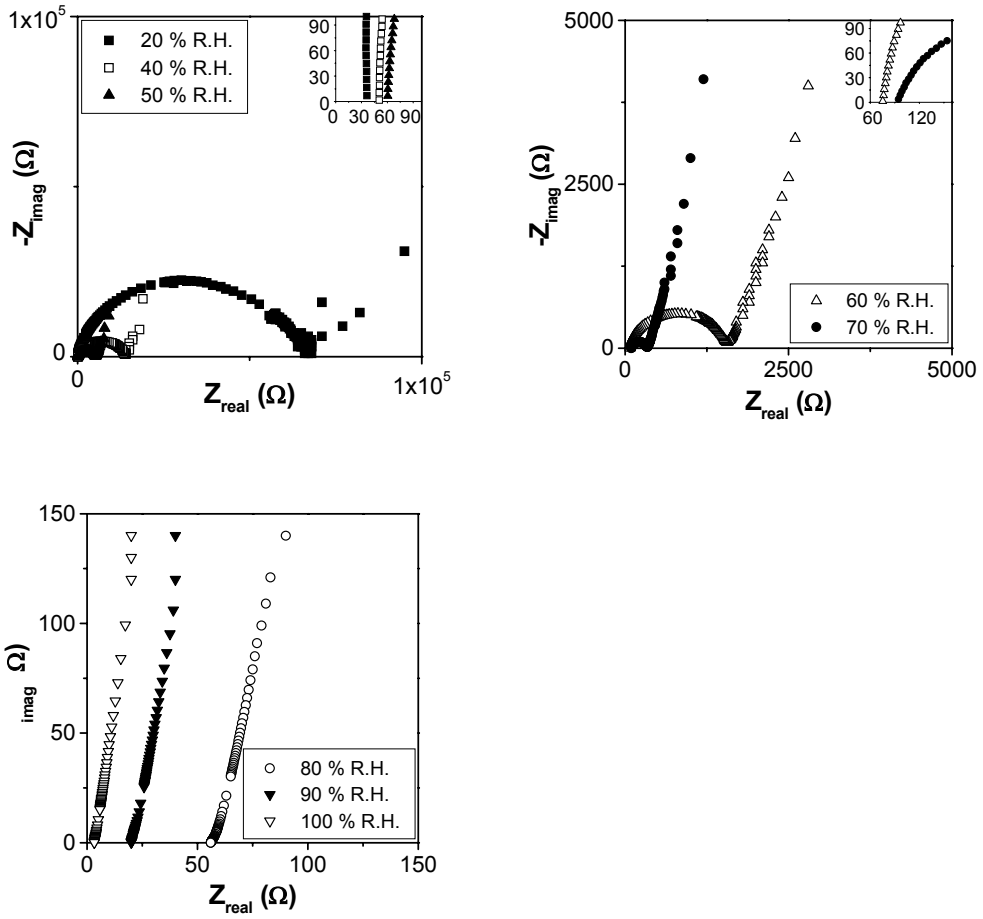

Figure 5.8 Impedance diagrams of the SPEEK-58 membrane at 80 °C and various relative humidities.

On the other hand, the impedance diagram of the SPEEK membranes (Fig. 4.3, Fig. 5.7 and Fig. 5.8) at low relative humidity includes a semicircle with two intercepts with the real axis. It can be observed that the intercept value at high frequency (the intercept on the left side of the semicircle) is not zero. This high frequency intercept value can be regarded as the resistance of the clusters ($R_{cluster}$), while the diameter of the semicircle can be taken as the resistance of the channels ($R_{channel}$) that connect the adjacent clusters. With increasing relative humidity, the diameter of the semicircle shrinks, indicating that the energy barrier for proton conduction in the channels decreases. It can also be observed that the non-zero intercept at high frequency shifts to higher values with increasing relative humidity, indicating an increase in the total resistance of the clusters. A paradox seems to exist since an increasing relative humidity would be expected to enhance the water adsorption and decrease the energy barrier in the clusters. The observed behavior may be explained by considering the evolution of the cluster network upon swelling. With an increase in the relative humidity, the channel that connects two adjacent clusters becomes wider and shorter, leading to a decrease in the impedance of the channel as indicated by the shrinkage of the semicircle. The clusters also absorb more water with increasing humidity and the energy barrier for proton conduction is lowered, but the expansion of the clusters may lead to an increase in both the cluster size and the total length the protons have to transport in the clusters. Consequently, it appears to lead to an increase in the total resistance of the clusters.

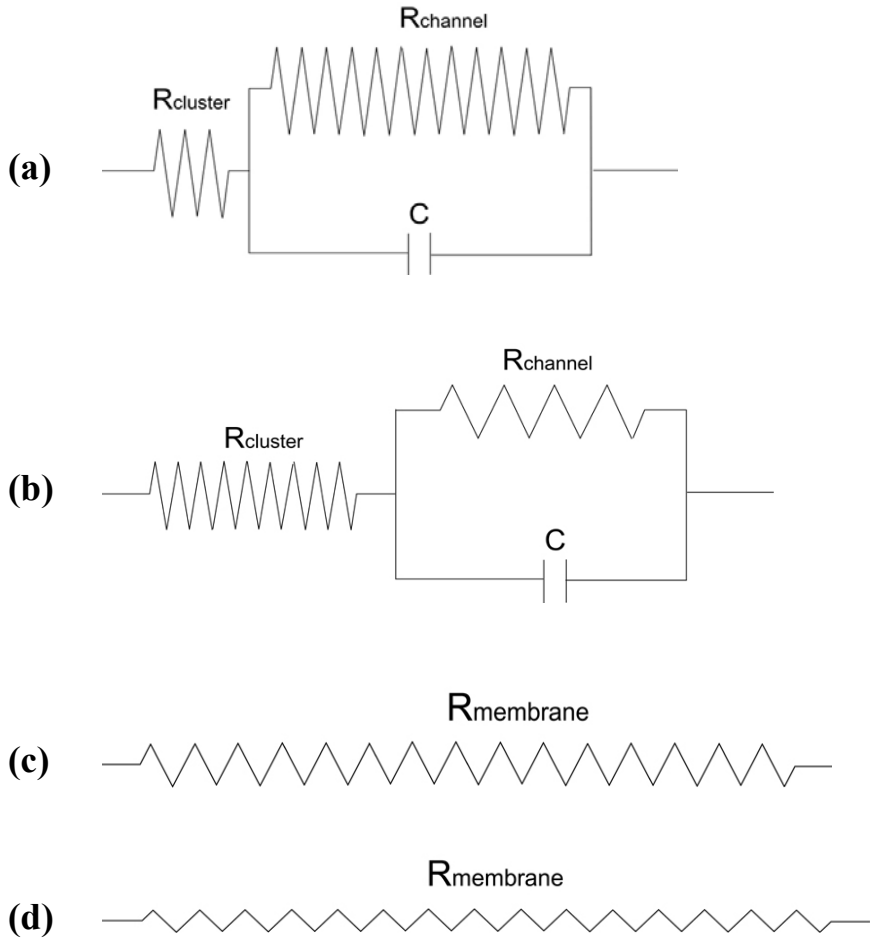

Figure 5.9 Equivalent circuits, indicating the evolution of the cluster networks in the SPEEK-54 membranes with relative humidity at 80 °C: (a) 20 % R.H., (b) 70 % R.H., (c) 90 % R. H., and (d) 100 % R.H.. $R_{cluster}$, $R_{channel}$, and $R_{membrane}$ refer to the resistance of, respectively, the cluster, channel, and membrane.

The evolution of the cluster structures with relative humidity can be represented by the corresponding equivalent circuits as shown in Fig. 5.9 for SPEEK-54 membrane. The height of the resistor corresponds to the energy barrier for the elementary jump of the protons and the number of barriers schematically indicates the total length the protons have to transport through the clusters or channels. At low relative humidity (e.g. 20 % R.H.), the size of the clusters is small, while the channels are narrow and long. Because of the lack of adequate water at low R. H., the energy barriers are high in both the clusters and channels. When the relative humidity is increased to 70 %, more water is absorbed by the membrane and the clusters expand. Consequently, the channels become wider and shorter, leading to a decrease in the energy barriers for proton conduction in both the clusters and the channels. When the relative humidity is increased to 90 %, the energy barriers become the same in the clusters and the channels, leading to a diminishing of the capacitance. Consequently, the membrane becomes a homogeneous environment for proton conduction with the same energy barrier throughout the membrane. Further increase in the relative humidity to 100 % simply lowers the average energy barrier for proton conduction without significant morphological change. However, it should be borne in mind that the discussion here is limited to a state before any dissolving of the membrane starts.

The proton conductivities calculated from the impedance values have been given in Fig. 4.4 as a function of the relative humidity. The proton conductivities of the SPEEK membranes in Fig. 4.4 can be divided into two regions: (i) a region of relatively slow increase in proton conductivity with relative humidity (< 80 % R.H.) and (ii) a region

of relatively faster increase in the proton conductivity with relative humidity (> 80 % R.H.). These two regions are distinguished in Fig. 4.4 by the two dashed lines with different slopes. In the region with R.H. < 80 %, the amount of absorbed water is small and most of the water is located around the ionic clusters, which are not well connected. On the other hand, in the region with R.H. > 80 %, more water is absorbed and the clusters grow and become well connected to each other, increasing the mobility of the protons. In contrast, the proton conductivity of the Nafion membrane increases monotonically in a linear manner with increasing relative humidity, indicating that no significant change in morphology or cluster structure is involved upon swelling.

5.3.5 Relationship between SAXS and Fuel Cell Performance Data

We have shown in chapter 4 that the SPEEK membranes with a sulfonation level of around 50 % exhibit much lower methanol permeability than Nafion and an electrochemical performance comparable to that of Nafion 115 in DMFC, but the operating temperature has to be limited to 65 °C. These results are consistent with the SAXS structural evolution data presented in this chapter for the SPEEK and Nafion membranes. At T < 60 °C, the ionic clusters in SPEEK membranes with low sulfonation levels such as SPEEK-44 and SPEEK-54 are not well connected. So there is no continuous pathway for methanol/water transport through the membrane, leading to lower measured methanol permeability. Also, it can be seen from Fig. 5.5 that below 70 °C, SPEEK-44 and SPEEK-54 have a smaller center-to-center distance between

clusters and smaller cluster sizes. This implies that the membrane can only provide very narrow pathways for methanol/water transportation. The performance loss due to the lower proton conductivity of the SPEEK membranes at these conditions is partly compensated by the advantage gained through the alleviated methanol crossover. On the other hand, continuous pathways for methanol/water permeation can be easily formed in the case of Nafion membranes in contact with the methanol/water solution, leading to high methanol permeability in DMFC. However, other features such as the acidity of the $-SO_3H$ groups and the electro-osmotic drag coefficients in different membranes may also affect their use in DMFC as discussed by Kreuer [46]. It should be noted that the long-term stability of hydrocarbon based polymers such as SPEEK needs to be investigated because methanol may penetrate into the polymer backbone slowly [180,181], leading to further reorganization of the cluster structure and creation of continuous and wide pathways for methanol/water permeation through the membrane.

5.4 CONCLUSIONS

A comparison of the SAXS and impedance spectroscopic data of the Nafion and SPEEK membranes have provided important insight regarding their structural features, especially the evolution of clusters. The differences in the structural features are reflected in the differences in the flexibility of their structures. With a sulfonation level of around 50 %, the SPEEK membranes have narrower pathways for methanol/water

permeation at T < 70 °C, resulting in low methanol permeability. In contrast, wide channels are easily formed in Nafion membranes even at low temperatures, which facilitates the transportation of methanol/water and thereby leads to serious methanol crossover problems in DMFC. With a careful control of the processing and operating conditions, the hydrocarbon polymers such as SPEEK may evolve as a promising alternate for the Nafion membranes in DMFC.

Chapter 6

Dry Proton Conductor $CsHSO_4$ and Its Stability in Hydrogen Atmosphere

6.1 INTRODUCTION

Nafion and sulfonated poly(etheretherketone) based membranes discussed in chapters 3 and 4 both are polymeric materials and they need to be well hydrated to conduct protons. For a PEMFC to function properly, the reactant gases are usually humidified prior to entry into the cell through external humidification subsystem. However, operating PEMFC without external humidification system is beneficial for reducing the weight and cost of the system significantly. Also, it would facilitate the water and thermal management in the cell. Therefore, there will be enormous interest if we could find some proton conductors that can offer high proton conductivity in the absence of water at high temperatures (say around 150 °C) since the catalyst poisoning problem would be significantly alleviated, the complex gas-humidification subsystem would be eliminated, and the design of the fuel cell system would be significantly simplified. In this regard, one attractive approach is to explore dry inorganic proton conductors such as solid acid cesium hydrogen sulfate ($CsHSO_4$).

Solid acids are compounds, such as $KHSO_4$ and $CsHSO_4$, whose chemistry and properties lie between those of a normal acid such as H_2SO_4 and a normal salt such as K_2SO_4 [19]. They usually consist of oxo-anions XO_4^{2-} (X = S, Se, P, or As), which are

linked together by hydrogen bonds. Within this category, the $MHXO_4$ and $M_3H(XO_4)_2$ compounds (M = Cs, NH_4, Rb, and X = S or Se) are known to undergo a "superprotonic" phase transition by a sharp increase in the protonic conductivity up to 10^{-2} S/cm. A key feature of the proton transport process in the compounds is that it does not require humid atmosphere.

$CsHSO_4$ was the first solid acid compound found to undergo the superprotonic transition at 414 K and a very high protonic conductivity between 10^{-3} - 10^{-2} S/cm was obtained above this temperature. The properties and structures of $CsHSO_4$ have been extensively investigated by those who have been intrigued by the remarkable superprotonic transition of this compound.

On heating a freshly prepared $CsHSO_4$ crystal, the room temperature phase III goes to phase II at around 349 K (76 °C) and to phase I at 414 K (141 °C). The structures of these three phases of $CsHSO_4$ projected on the *a* axis are shown in Fig. 6.1.

Both accurate X-ray studies and neutron scattering results indicate that phase III is monoclinic with $p2_1/c$ space group and Z = 4. A projection of the crystal structure along the *a* axis is shown in Fig. 6.1a, in which the zig-zag chains of the hydrogen bonds along the *b* axis of the crystal linking SO_4 tetrahedra can be clearly seen.

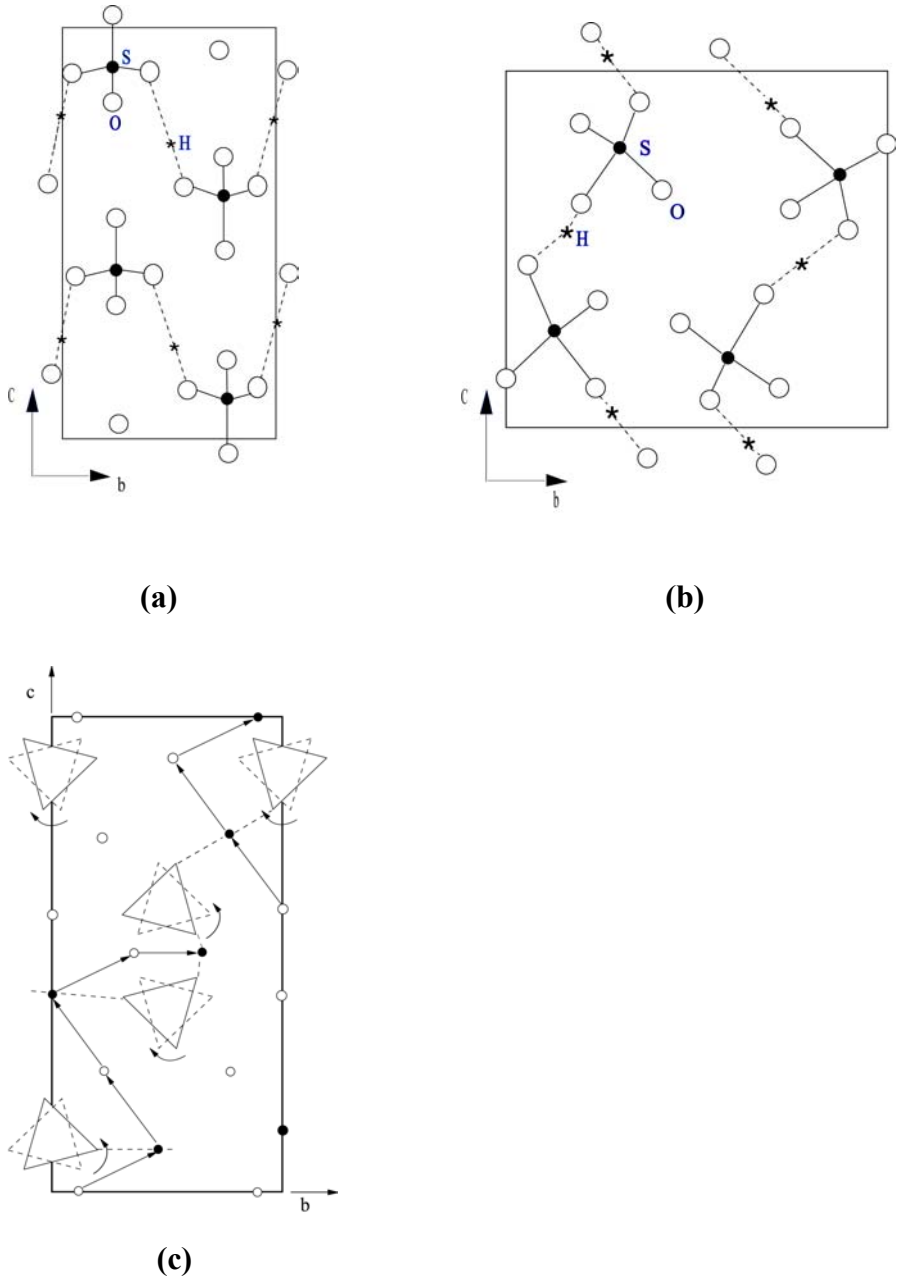

Figure 6.1 Structures of $CsHSO_4$: (a) Phase III ($p2_1/c$), (b) Phase II ($p2_1/c$), and (c) Phase I ($I4_1/amd$) [182].

The transition temperature from phase III to phase II is well defined for a single crystal which is 349 K, but for powdered samples it strongly depends on external conditions such as pressure and humidity. Phase II is also monoclinic ($p2_1/C$, Z = 4). However, the unit cell parameters are different from phase III, resulting in a smaller unit cell volume. The projection of the phase II crystal structure along the *a* axis is shown in Fig. 6.1b. The hydrogen bonds again form zig-zag chains but now along the *c* axis.

At about 414 K, phase II of $CsHSO_4$ undergoes a rather spectacular phase transition into a highly symmetrical "plastic phase" (phase I), which shows high proton conductivity. This phase is still a solid, with long-range order, but locally there is a tremendous dynamic reorientational disorder of the SO_4 tetrahedra with extended vibrations of both cesium and sulfate. Several models have been proposed for the structure of phase I, and the most reliable data were obtained using high resolution neutron powder diffraction [183]. The crystal structure of phase I obtained in that work is shown in Fig. 6.1c projected along the *a* axis, which is tetragonal ($I4_1/amd$). The key feature of Phase I is that in contrast to the lower temperature phases II and III, each SO_4 tetrahedra in Phase I can adopt not one but four crystallographically equivalent orientations. As a result, the number of possible proton positions in the unit cell becomes larger than the number of protons. The hydrogen-bond network becomes dynamically disordered, allowing protons to move through the lattice by jumping to unfilled positions. One of the possible routes for proton migration is shown in Fig. 6.1c (straight arrows). Proton jumps are associated with reorientations of SO_4 tetrahedra,

shown by curved arrows. Therefore, without doubt, Grotthuss mechanism dominates the proton conduction process in the phase I $CsHSO_4$, and no water is needed as the proton carrier.

Despite the remarkable properties of $CsHSO_4$, not much attention was paid to use it for practical applications such as fuel cells due to its solubility in water and the difficulties to fabricate thin membranes with this material. Recently, Haile *et al.* [34,113] reported the first examination of $CsHSO_4$ for PEMFC applications. They made a fuel cell by sandwiching the solid acid pellet between two electrode layers made from $CsHSO_4$ mixed with platinum and carbon. The entire fuel cell was compressed to provide good contact between the electrolyte and electrode layers. They indicated that $CsHSO_4$ electrolyte was not attacked by the water generated at the cathode side due to the high operating temperature (160 °C), while observed a quick drop in the fuel cell voltage with increasing current density and attributed it to high the resistance of the relatively thick electrolyte (1.5 mm) and the rate-limited gas flow through the electrode. They also found a very small weight loss of 0.03 wt % when $CsHSO_4$ was heated at 160 °C in H_2 atmosphere. Yang *et al.* [43] incorporated $CsHSO_4$ onto a porous glass and found no appreciable current when it was used as a membrane in PEMFC. Although the reason for this behavior was not investigated extensively, they suggested that it could be due to the chemical incompatibilities of $CsHSO_4$ with the fuel cell environment.

However, no data are available on the chemical stability of $CsHSO_4$ in the fuel cell environment in presence of the fuel (hydrogen) and the electrocatalyst (platinum). In

order for a material to be used as electrolyte in practical fuel cells, it should exhibit good chemical stability in presence of the fuel and the electrocatalyst. With an objective to assess its suitability for fuel cell applications, we present here an investigation of the chemical stability of $CsHSO_4$ in hydrogen atmosphere in the presence of platinized carbon (Pt/C) catalysts. Additionally, appropriate processing procedures need to be developed to fabricate thin membranes with this ceramic conductor $CsHSO_4$ in order for it to be suitable for fuel cell applications. Haile *et al.* [34,113] presented conductivity and fuel cell data only with relatively thick pellets made either with $CsHSO_4$ alone (1.5 mm thick) or by hot pressing $CsHSO_4$ and poly(vinylidene fluoride) (PVDF) to give a composite (~ 0.5 mm thick). We present here the fabrication of thin membranes of ~ 80 μm thick by casting a slurry of $CsHSO_4$ and polymers such as PVDF and sulfonated poly(etheretherketone) membrane with 54 % sulfonation level (SPEEK-54) and their proton conductivity data.

6.2 EXPERIMENTAL

$CsHSO_4$ was synthesized by following a procedure described in the literature [113]. Cs_2SO_4 was first dissolved in dilute sulfuric acid solution so that the molar ratio of Cs_2SO_4 : H_2SO_4 : H_2O was 1 : 2 : 12. After a complete dissolution of Cs_2SO_4, ethanol was added to the solution to precipitate $CsHSO_4$, which was then filtered, dried at 100 °C overnight, and stored in a vacuum desiccator before further characterization.

Composite membranes consisting of different amounts of $CsHSO_4$ (50 - 80 vol%) were prepared by mixing with PVDF 2801-00 (ELF-Autochem). The densities of PVDF and prepared $CsHSO_4$ were measured by an Accupyc 1330 Micromeritics equipment, and the obtained values were 1.82 g/cm^3 and 3.36 g/cm^3, respectively. Appropriate amount of $CsHSO_4$ was added to a solution of PVDF in acetone, that was prepared at 40 °C, and the mixture was ball milled using zirconia media for 24 h. The slurry obtained was then cast onto a glass plate using a Doctor Blade to obtain thin membranes, which were then dried in air to a thickness of around 80 μm. The composite membranes thus prepared were found to be soft and weak for compositions having > 80 vol % $CsHSO_4$, and therefore the $CsHSO_4$ content in the membrane was restricted to 50 - 80 vol %. When SPEEK-54 was used as the polymer matrix, N, N - dimethylacetamide (DMAc) was used as the solvent. Membranes with a composition of 80 wt % $CsHSO_4$ - 20 wt % SPEEK-54 were prepared.

Proton conductivity measurements were carried out by impedance spectroscopy in the temperature range of 80 - 170 °C. The sample was equilibrated at each temperature for 1 h before collecting the impedance data.

Chemical stability of $CsHSO_4$ was investigated by heating a 3:1 mixture consisting of 300 mg of $CsHSO_4$ and 100 mg of Pt/C electrocatalyst (20 wt% Pt on carbon, E-TEK) at 150 °C in a flowing H_2 atmosphere for 48 h. The weight change during the heat treatment was assessed by weighing the mixture before and after heating. For a comparison, similar experiments were also carried out with $CsHSO_4$ alone and the Pt/C electrocatalyst alone in H_2 atmosphere (Table 6.1). The Pt/C catalyst was found to be

reactive with air on removal from the H_2 atmosphere. To avoid this difficulty, the H_2 atmosphere was replaced with a flowing argon atmosphere for 1 h after the furnace cooled to room temperature before removing the samples from the furnace during the above three experiments. Additionally, another set of similar experiments was carried out by heating the samples in air instead of H_2 (Table 6.1). Structural characterization and the measurement of superionic transitions of $CsHSO_4$ before and after heating were carried out, respectively, by X-ray powder diffraction and a Perkin-Elmer series 7 differential scanning calorimeter (DSC). The DSC experiments were carried out with around 10 mg of sample in N_2 atmosphere at a heating rate of 10 °C/min.

Table 6.1 Comparison of the weight losses experienced by $CsHSO_4$, Pt/C, and $CsHSO_4$-Pt/C mixture on heating at 150 °C for 48 h.

Material	Heating atmosphere	Weight loss (%)
$CsHSO_4$	H_2	2.6
$CsHSO_4$	Air	0.83
Pt/C	H_2	2.8
Pt/C	Air	3
$CsHSO_4$ + Pt/C (3:1 weight ratio)	H_2	12.7[a]
$CsHSO_4$ + Pt/C (3:1 weight ratio)	Air	1.9

[a] This value corresponds to a weight loss of 16% for $CsHSO_4$ alone, assuming the Pt/C catalyst experiences identical weight losses in the presence and absence of $CsHSO_4$.

6.3 RESULTS AND DISSCUSION

6.3.1 Characterizations of $CsHSO_4$ and PVDF/CsHSO4 Composite Membranes

The X-ray diffraction pattern given in Fig. 6.2a confirms the formation and purity of $CsHSO_4$. All the reflections in Fig. 6.2a match with that reported for $CsHSO_4$ (Phase II) in JCPDS card No. 47-1724. Furthermore, the DSC plot shown in Fig. 6.3a confirms the superprotonic transition from phase II to phase I at around 141 °C and the melting of $CsHSO_4$ around 212 °C [19]. The enthalpy for the superprotonic transition measured here for pure $CsHSO_4$ (Fig. 6.3a) is 24.6 J/g, which is very close to the value reported in the literature [113,184].

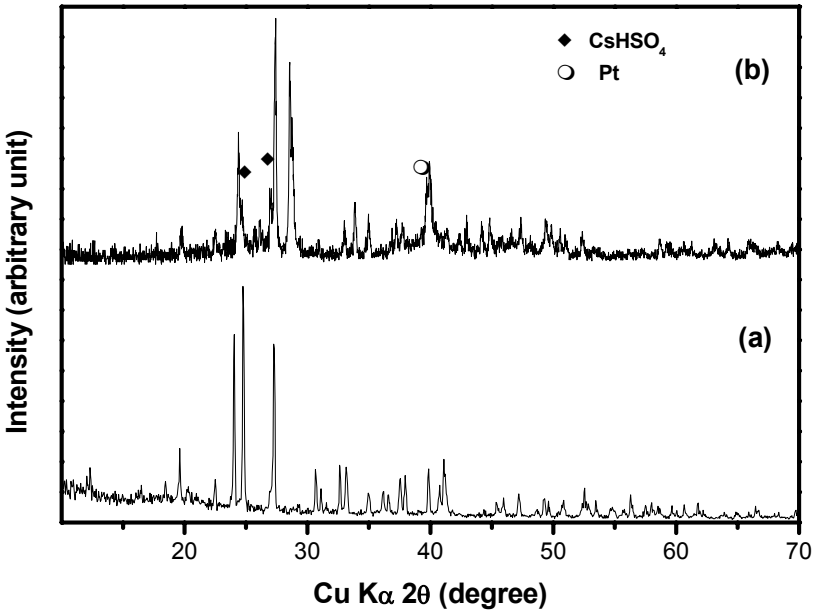

Figure 6.2 X-ray diffraction patterns of (a) as-prepared $CsHSO_4$ after drying at 100 °C in air and (b) $CsHSO_4$ Pt/C mixture after heating at 150 °C in H_2 atmosphere for 48 h. All the reflections in (a) correspond to $CsHSO_4$ (Phase II) and the unmarked reflections in (b) correspond to Cs_2SO_4.

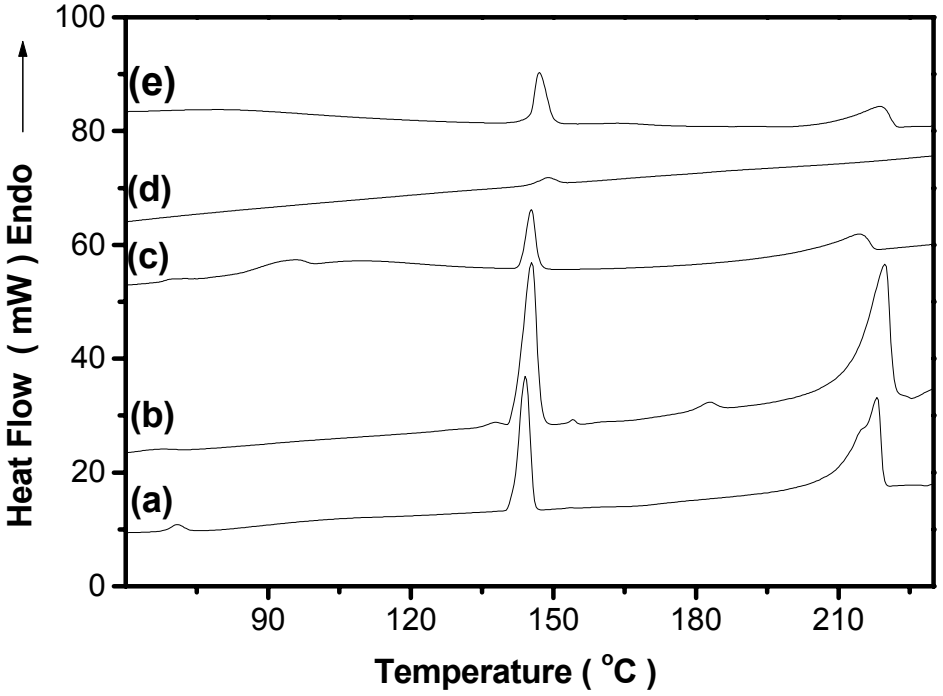

Figure 6.3 DSC plots of (a) as-prepared $CsHSO_4$, (b) $CsHSO_4$ after heating at 150 °C in H_2 atmosphere for 48 h, (c) $CsHSO_4$-Pt/C mixture before heating, (d) $CsHSO_4$-Pt/C mixture after heating at 150 °C in H_2 atmosphere for 48 h, and (e) $CsHSO_4$-Pt/C mixture after heating at 150 °C in air for 48 h.

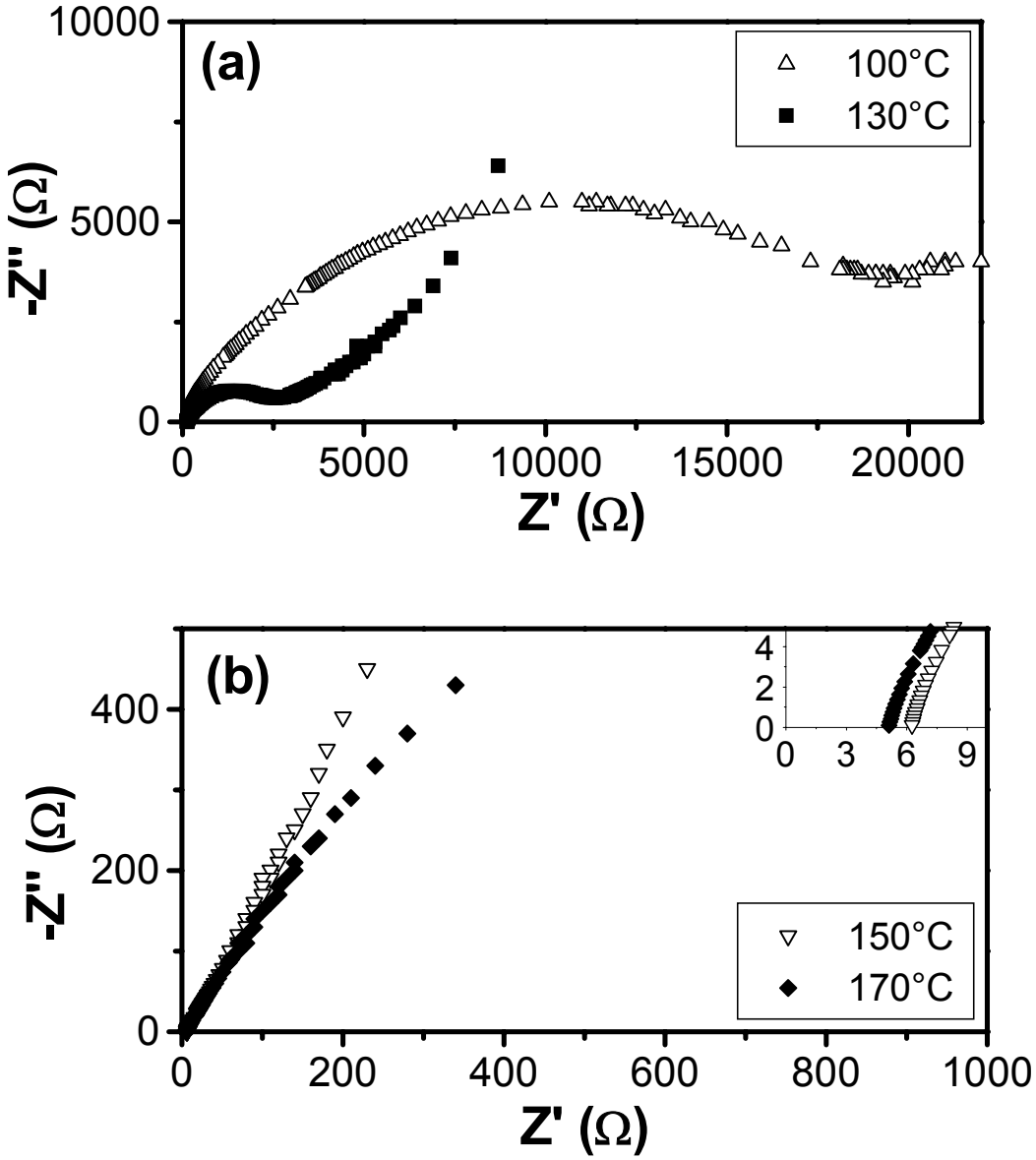

Figure 6.4 Typical impedance diagrams of PVDF/$CsHSO_4$ composite membrane consisting of 70 vol% $CsHSO_4$: (a) below the superprotonic transition temperature, (b) above the superprotonic transition temperature.

The typical impedance diagrams of $CsHSO_4$/PVDF composite membranes at various temperatures are shown in Fig. 6.4. It can be seen that, for 70 vol % $CsHSO_4$ - 30 vol % PVDF composite membrane, the impedance diagrams exhibit a depressed semicircle as shown in Fig. 6.4a below the superprotonic transition temperature, which is around 141 °C. The low frequency interception value of the semicircle with the real axis is taken as the bulk resistance of the membrane. However, when the measuring temperature is above the superprotonic transition temperature, the impedance diagram appears as a straight line at low frequency as shown in Fig. 6.4b, and the effective dc resistance of the sample was obtained from an extrapolation of the intersection of this line with the real axis.

Fig. 6.5 shows the variations of proton conductivity with temperature for two composite membrane compositions consisting of 50 and 70 vol% $CsHSO_4$. The conductivity of the composites is quite poor at low temperatures. However, the high-temperature conductivity of the high $CsHSO_4$ content composites (in dry atmospheres) is comparable to that of highly humidified Nafion. The conductivity data also confirm the superionic transition occurring around 141 °C with high conductivity values of around 10^{-3} S/cm at T > 150 °C, which is adequate for fuel cell applications. It can also be seen that the temperature of the transition is hardly affected by the presence of the polymer. The data in Fig. 6.5 also indicate that the conductivity of the composite membranes increases with increasing amount of $CsHSO_4$ as one would expect. The conductivity values could be improved further if stronger membranes could be fabricated with higher vol% $CsHSO_4$ in the composite membrane.

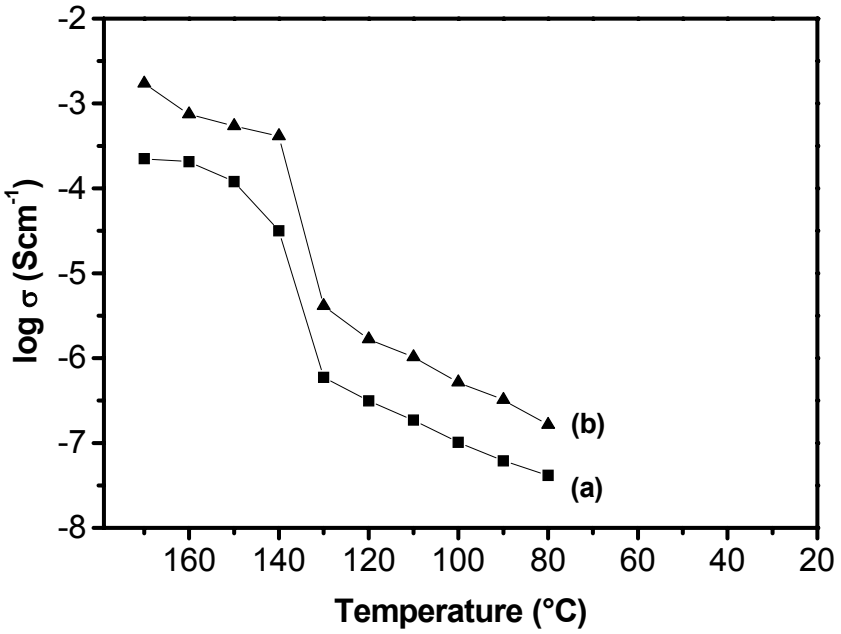

Figure 6.5 Arrhenius plots of the variations of proton conductivity with temperature of $CsHSO_4$ - PVDF composite membranes: (a) 50 % $CsHSO_4$ - 50 % PVDF and (b) 70 % $CsHSO_4$ - 30 % PVDF.

6.3.2 Chemical Stability Investigation of $CsHSO_4$

Table 6.1 compares the weight losses observed on heating $CsHSO_4$, Pt/C, and the $CsHSO_4$-Pt/C mixture (3:1 wt. ratio) at 150 °C for 48 h in H_2 atmosphere and air. All the three samples show a small weight loss (≤ 3 %) on heating in air, which could be due to adsorbed water and other volatile impurities. In contrast, while the Pt/C catalyst alone and $CsHSO_4$ alone show low weight losses (< 3 %) on heating in H_2 atmosphere similar to that on heating in air, the $CsHSO_4$-Pt/C mixture exhibits a significantly larger weight loss of 12.7 % on heating in H_2 atmosphere. The weight loss experienced by the $CsHSO_4$-Pt/C mixture in H_2 atmosphere is much higher than that expected (2.65

%) based on the weight loss values observed separately for $CsHSO_4$ and Pt/C in H_2 atmosphere (Table 6.1). In fact, the weight loss experienced by $CsHSO_4$ alone in presence of Pt/C in H_2 atmosphere is 16 % compared to 2.6 % in the absence of Pt-C catalyst, assuming the Pt/C catalyst experiences identical weight loss values in the presence and absence of $CsHSO_4$ in H_2 atmosphere. The higher weight loss observed for the $CsHSO_4$-Pt/C mixture in H_2 suggests that $CsHSO_4$ could be undergoing degradation in presence of the electrocatalyst Pt/C in H_2 atmosphere.

In order to understand the origin of the higher weight loss value observed for $CsHSO_4$ in presence of the Pt/C catalyst in H_2 atmosphere, we characterized both by X-ray diffraction and DSC the products obtained after heating in H_2 atmosphere at 150 °C for 48 h, and the results are presented in Figs. 6.2 and 6.3. While $CsHSO_4$ still maintains a strong endothermic peak around 140 °C corresponding to the superionic transition after heating in the absence of the Pt/C catalyst at 150 °C in H_2 atmosphere (Fig. 6.3b), the endothermic peak is almost eliminated on heating under identical conditions in the presence of Pt/C catalyst (Fig. 6.3d). For a comparison, the DSC plot recorded for the $CsHSO_4$-Pt/C mixture before heating is given in Fig. 6.3c, which indicates the presence of the endothermic peak. The data clearly indicate that $CsHSO_4$ undergoes degradation in presence of H_2 and Pt.

Fig. 6.2b shows the X-ray diffraction pattern of the $CsHSO_4$-Pt/C mixture after heating in H_2 at 150 °C. The data indicate the formation of Cs_2SO_4 (JCPDS card No.

01-0685) after heating in the presence of H_2 and Pt/C. Based on the X-ray data, the degradation reaction could be envisioned as

$$2\ CsHSO_4 + 4\ H_2 \xrightarrow{\text{Pt catalyst}} Cs_2SO_4 + H_2S + 4\ H_2O \qquad (6.1)$$

Based on such a decomposition reaction, one would anticipate a weight loss of 21.3 % for $CsHSO_4$ in presence of Pt/C, which is slightly higher than the observed weight loss of 16 % for $CsHSO_4$ alone in the $CsHSO_4$-Pt/C mixture. The discrepancy could be due to the incomplete decomposition of $CsHSO_4$ under our experimental conditions of 150 °C for 48 h as shown in Fig. 6.2b.

Another possibility that could be considered for the weight loss and the degradation of $CsHSO_4$ to form Cs_2SO_4 is a simple dehydration reaction catalyzed by Pt as shown below:

$$2\ CsHSO_4 \xrightarrow{\text{Pt catalyst}} Cs_2SO_4 + H_2O + SO_3 \qquad (6.2)$$

If so, then one would anticipate the reaction 6.2 to occur in the absence of H_2 as well. However, the $CsHSO_4$-Pt/C mixture on heating in air exhibits a much smaller weight loss (1.9 %) than that observed in H_2 atmosphere (12.7 %) as seen in Table 1, indicating that $CsHSO_4$ does not decompose in the absence of H_2. The 1.9 % loss found in air for the $CsHSO_4$-Pt/C mixture is mainly due to the adsorbed water and volatile impurities. Also, the $CsHSO_4$-Pt/C mixture exhibits a prominent endothermic peak in DSC (Fig. 6.3e) after heating in air unlike after heating in H_2 (Fig. 6.3d), confirming further that $CsHSO_4$ does not decompose in presence of Pt without H_2. These results clearly rule out reaction 6.2 and demonstrate that $CsHSO_4$ undergoes reduction in H_2

atmosphere in presence of Pt in accordance with reaction 6.1. This conclusion was also supported by the characteristic odor of H_2S during heating in H_2 atmosphere and the formation of a black copper sulfide precipitate on passing the purge gas through copper sulfate solution. The formation of copper sulfide is due to the reaction of the evolved H_2S gas with the Cu^{2+} ions in solution. Although one may anticipate a potential reaction of the evolved H_2S with the Pt catalyst that is present in contact with the $CsHSO_4$ solid to give PtS, the heating temperature of 150 °C is too low for such a reaction to occur and no PtS was observed in the X-ray pattern (Fig. 6.2b).

The experimental data presented here demonstrate that although $CsHSO_4$ is quite stable at elevated temperatures in H_2 atmosphere, it is prone to rapid degradation evolving H_2S in presence of the Pt/C catalyst. It is clear that Pt catalyzes the decomposition reaction of $CsHSO_4$ and lowers the temperature of decomposition. The voltage drop observed at higher current densities by Haile *et al.* [34,113] could partly be related to this decomposition. Based on the data presented here, we believe that it is difficult to use $CsHSO_4$ as an electrolyte in PEM fuel cells with the conventional Pt-based electrocatalysts. However, it is possible that the decomposition may not occur at ~ 160 °C in presence of other non-platinum alloy or transition metal oxide catalysts.

6.3.3 Challenge in Preparing of Dense Membrane with $CsHSO_4$

Another challenge with $CsHSO_4$ is to fabricate dense, gas impervious membranes without porosity that will be suitable for fuel cell application. Our experiments indicate

that the composite membranes fabricated with the PVDF polymer are permeable to gas due to porosity (see Fig. 6.6) and are not quite suitable for fuel cell applications at this time. The porosity may be caused by the fast evaporation of acetone during the drying process of the membrane. To solve this problem, we used another polymer matrix, sulfonated poly(etheretherketone) with 54 % degree of sulfonation (SPEEK-54) (see chapter 4 for the details of the preparation), with DMAc as the solvent, which has a high boiling point of 166 °C. The typical surface photographs of 80 wt% $CsHSO_4$ - 20 wt % SPEEK-54 are shown in Fig. 6.7. It can be seen that, this composite membrane is much denser that PVDF/$CsHSO_4$ composite membrane. Due to the instability of $CsHSO_4$ with the Pt/C catalyst and the lack of gas permeability properties of the membranes, the evaluation of these membranes in real high temperature PEMFC was not conducted.

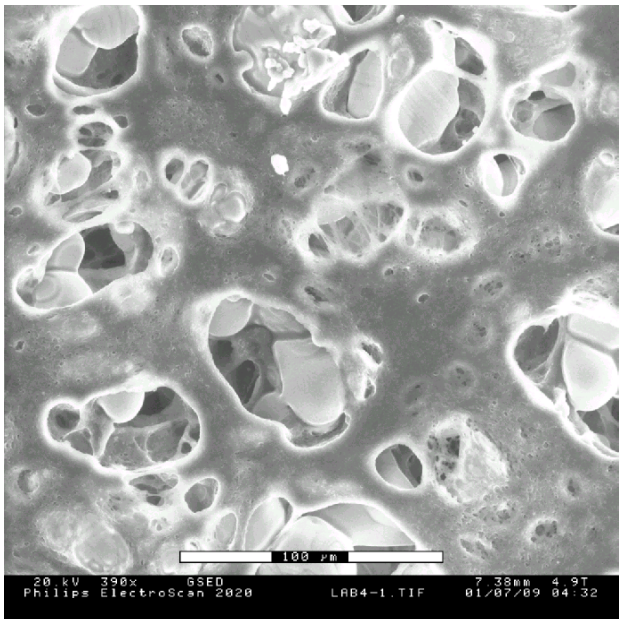

Figure 6.6 SEM photograph of the 70 % $CsHSO_4$/30 % PVDF composite membrane.

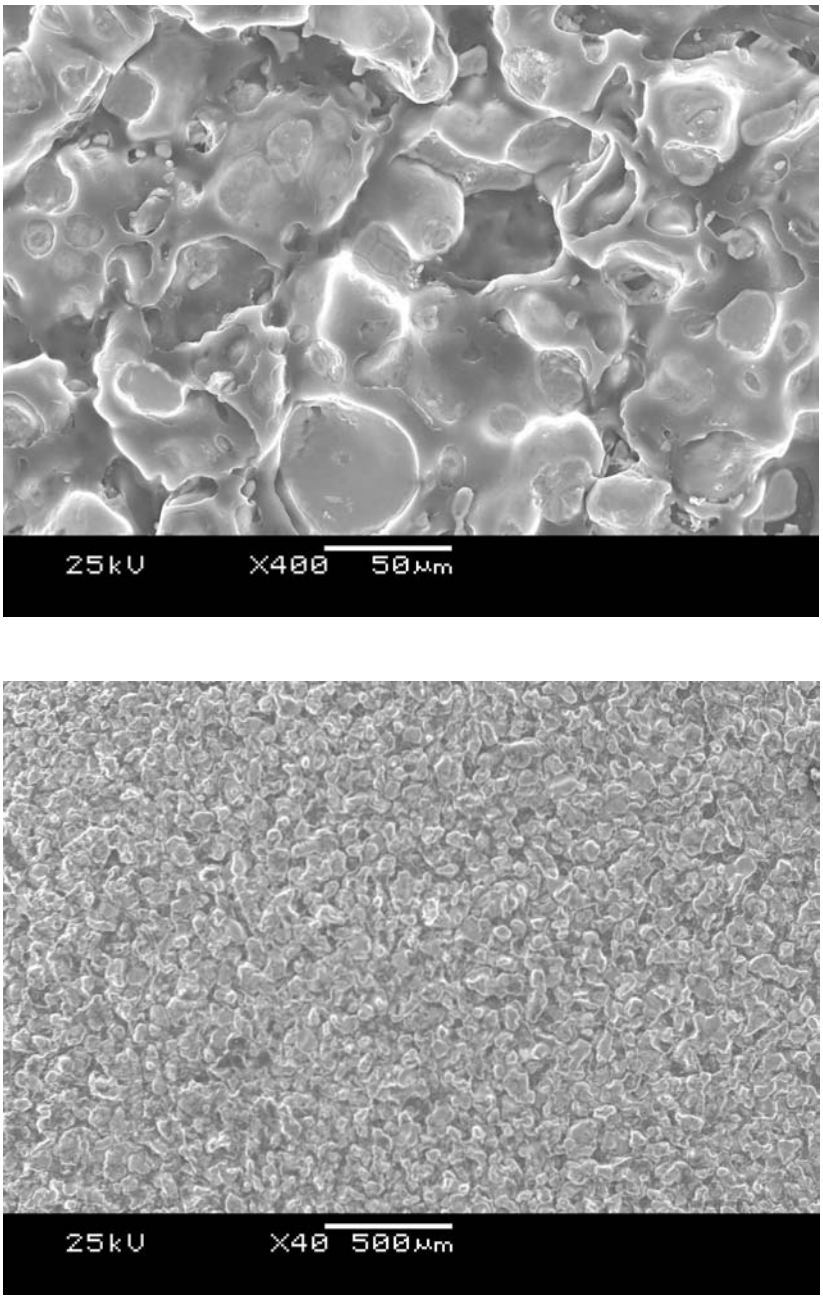

Figure 6.7 SEM photographs of the 80 wt% $CsHSO_4$/20 wt% SPEEK-54 composite membrane.

6.4 CONCLUSIONS

Composite membranes made with the dry proton conductor $CsHSO_4$ and PVDF exhibit high proton conductivity adequate for fuel cell applications. However, $CsHSO_4$ is found to experience chemical instability, decomposing to Cs_2SO_4 and H_2S, in hydrogen atmosphere in the presence of the electrocatalyst Pt/C. Development of alternative non-platinum alloy or transition metal oxide catalysts that can be compatible with $CsHSO_4$ and offer good catalytic activity is needed in order for $CsHSO_4$ to be useful as an electrolyte in fuel cells. Alternatively, analogous dry proton conductors based on phosphates instead of sulfates could offer good chemical stability in hydrogen atmosphere in presence of Pt. The $(PO_4)^{3-}$ groups are much more difficult to reduce compared to the $(SO_4)^{2-}$ groups as P is less electronegative than S. Furthermore, the membrane fabrication procedures need to be optimized with these ceramic proton conductors to obtain dense, gas impermeable membranes without porosity. Successful development of compatible dry proton conductor - electrocatalyst assembly could increase the operating temperatures of PEMFC and DMFC to 150 - 200 °C and thereby provide several advantages such as higher efficiency and elimination of CO poisoning and humidifiers.

Chapter 7

Operation of Thin Nafion Based Self-Humidifying Membrane in Proton Exchange Membrane Fuel Cell with Dry H_2 and O_2

7.1 INTRODUCTION

The state-of-the-art PEMFCs operate at around 80 °C with H_2 and O_2/air as the reactants. The presently used Nafion electrolyte membranes need to be wet to provide satisfactory proton conductivity because of the hydrophilic nature of the sulfonic acid groups attached to the polymer backbone and the necessity to hydrate the ionic clusters. Therefore, for the fuel cell to function properly, the reactants are usually humidified through external humidification subsystem prior to entry into the cell. However, operation of PEMFC without external humidification can reduce the overall weight while offering significant cost saving as discussed in Section 6.1. Also, the operation of PEMFC without the humidification subsystem can simplify the water and thermal management in the cell.

To suppress the dehydration of the membrane during operation with dry reactants, Watanabe *et al.* [26,185,186] proposed self-humidifying membranes with highly dispersed nanometer sized Pt. The Pt particles in the membrane were conceived to act as water generation sites by catalytic recombination of hydrogen and oxygen reactant gases permeating through the membrane from the anode and the cathode. The

generated water can directly humidify the membrane. However, the presence of Pt particles through the whole membrane increases the risk of short circuit and/or fire due to hot spots within the fuel cell. In addition, it is difficult to control the amount of Pt in the membrane using Watanabe's method. Recently, Liu *et al.* [187] reported a self-humidifying composite membrane prepared by casting a mixture of Nafion solution and Pt/C catalyst onto a porous PTFE film. Although gravity may lead to a gradient distribution of Pt/C through the membrane, the possibility of short circuit due to the electronically conducting Pt/C particles is still a concern.

As we discussed in chapter 3, the water balance in a PEMFC involves the following several mechanisms (see Fig. 3.1): (1) water supply from the reactants if an external humidification subsystem is applied, (2) water electro-osmotic drag from the anode to the cathode with proton conduction, (3) water produced at the cathode due to the cell reaction, and (4) water back-diffusion from the cathode to the anode due to the water concentration gradient. Numerical simulation of water management models indicates that water production associated with a current density of 1000 mA/cm^2 is sufficient to completely hydrate a dry 50 μm thick Nafion 112 membrane in roughly 10 s [188]. Thus, theoretically, it is possible to operate the PEMFC without external humidification by carefully controlling the operating conditions.

Buchi *et al.* [189] operated PEMFC without external humidification using Nafion 115 as the electrolyte and found that the back-diffusion of the product water from the cathode to the anode is the dominant process for water management in the cell over a wide range of operating conditions. However, the cell performance obtained without

humidification was much lower than that obtained with external humidification. This is probably due to the limited water back-diffusion through the thick Nafion 115 membranes (125 μm in dry state), which are now commonly replaced by Nafion 112 (50 μm in dry state) in PEMFCs.

In this chapter, we present a thin double-layer composite membrane consisting of one layer of plain Nafion and another layer of Pt/C catalyst dispersed recast Nafion. While the layer containing Pt/C was used on the anode side, the plain Nafion layer was used on the cathode side. This structure not only satisfies the requirement of self-humidifying the membrane close to the anode side, but also prohibits the short circuit through the membrane. The performances of the composite membrane and plain Nafion membrane in PEMFC are compared with an aim to identify the optimum dry operating conditions for the composite membrane.

7.2 EXPERIMENTAL

Nafion/Pt-C composite membrane was prepared by the recasting method with 5 wt% Nafion solution and 20 % Pt/C (E-TEK) catalyst. The loading of Pt metal in the ~ 30 μm thick membrane thus prepared was 0.02 mg/cm^2. Another layer of plain Nafion membrane of around 30 μm was also prepared by a similar process, but without Pt/C. These two membranes were then hot-pressed to an integral film at 150 °C for 5 min with a force of 3 tons. For a comparison, a control Nafion membrane with two layers of plain recast Nafion membranes was also prepared in a similar way with the same

thickness. The double-layer composite and plain Nafion membranes thus prepared are designated hereafter, respectively, as N-NPtC and N-N.

Both the anode and cathode catalysts were commercial 20 % Pt/Vulcan (E-TEK). "Nafion-mixed electrodes" (Section 2.3.1.1) were prepared in this study and the Pt metal loading in all the electrodes was 0.4 mg/cm^2. For preparing the MEA with the double-layer composite membrane, the anode was pressed onto the side containing Pt/C powders and the cathode was pressed onto the plain Nafion side. For fuel cell tests, the pressures of the anode and cathode gases were both kept at 1 atmosphere through this study. Room temperature dry H_2 and O_2 were fed at 1.5 and 3 times of their stoichiometric requirements for a current density of 1000 mA/cm^2, respectively, into the anode and cathode. When humidification was applied, the humidifier temperature was kept the same as the cell temperature.

7.3 RESULTS AND DISCUSSION

7.3.1 Cell Resistance vs. Current Density

To operate the single cell with dry H_2 and O_2, the cell was usually kept at open circuit at the operating temperature for about half an hour; then the current density was increased slowly from a low value to a high value. The cell was operated at each current density for about 20 min, and ten cell resistance values were recorded in the last 5 min. A comparison of the variations of the cell resistance with the current density of the MEAs fabricated with N-NPtC and N-N membranes and operated with dry H_2 and

O_2 is shown in Fig. 7.1. It can be seen that the cell resistances are very high at low current densities due to the lack of the product water back-diffusion from the cathode to the anode. On slowly increasing the current density, more water is produced at the cathode and the increased water concentration gradient between the cathode and the anode enhances the water back-diffusion, hydrating the anode side and decreasing the cell resistance dramatically. From Fig. 7.1, it can also be observed that the cell with N-NPtC membrane has lower cell resistance at each current density compared to that with N-N membrane. Especially at low current densities, where the water back-diffusion effect is limited, the difference in cell resistance is large between the two cells, indicating the self-humidifying effect in the N-NPtC membrane. The large resistance fluctuations shown in Fig. 7.1 at low current densities in both the cases indicate poor water management in the cells when the water back-transport is limited.

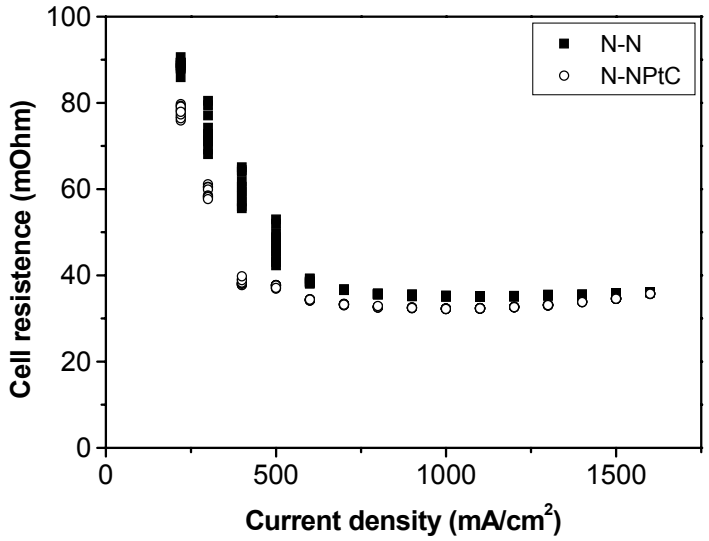

Figure 7.1 Variations of the cell resistance with the current density of the MEAs fabricated with the plain N-N and composite N-NPtC membranes and operated with dry H_2 and O_2 at 60 °C.

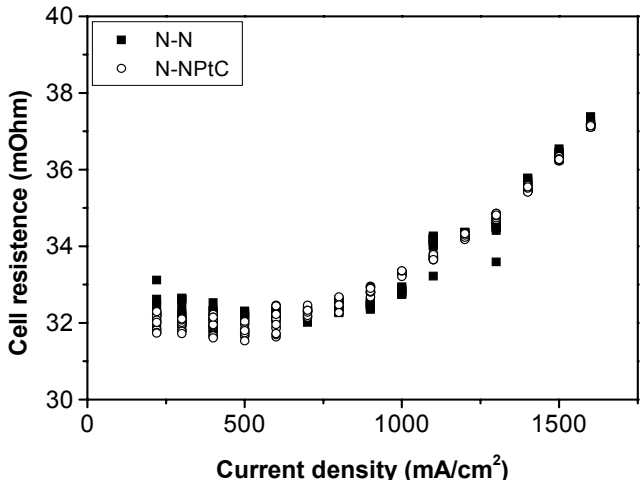

Figure 7.2 Variations of the cell resistance with the current density of the MEAs fabricated with the plain N-N and composite N-NPtC membranes and operated with humidified H_2 and O_2 at 60 °C.

Figure 7.2 compares the variations of the cell resistance with the current density of the cells fabricated with N-NPtC and N-N membranes and operated with humidified reactants at 60 °C. The results are different from those obtained with dry reactants. At low current densities, both electro-osmotic drag and back-diffusion effects are limited and the cell resistance is relatively low due to the external humidification. With an increase in the current density, more water is produced at the cathode side and the water back-diffusion effect prevails over the electro-osmotic effect, leading to a slight decrease in the cell resistance. However, when the current density is increased further, the insufficient compensation of the electro-osmotic drag by the back-diffusion of water to the anode leads to a drying out of the membrane at the anode side and an increase in the cell resistance. From Figs. 7.1 and 7.2, we also can observe that the cell resistances obtained with the dry reactants at high current density such as 1500

mA/cm^2 are very close to those obtained with humidified reactants, indicating that water produced at the cathode is sufficient to hydrate the thin film under proper operating conditions.

7.3.2 Relationship Between the Cell Voltage Output and Water Management

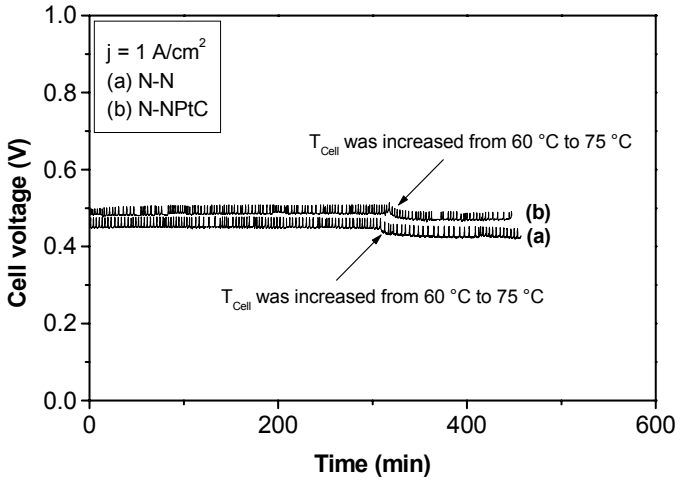

Figure 7.3 Variations of the cell voltage output with time of the MEAs fabricated with the plain N-N and composite N-NPtC membranes and operated with dry H_2 and O_2 at a constant current density of 1 A/cm^2.

Figure 7.3 compares the variations of the cell voltages with time for both the cells operated with dry H_2 and O_2 at a constant current density of 1000 mA/cm^2. It can be seen that the cell with the N-NPtC membrane has a higher cell voltage output than that with the N-N membrane, indicating a smaller cell resistance (Fig. 7.1). It may also suggest a suppressed H_2 and O_2 crossover in the former since the N-NPtC membrane could provide the sites for the catalytic recombination of H_2 and O_2 permeating through the membrane from the anode and the cathode, respectively, thus alleviating the mixed

potential problem associated with the crossover of the reactants. In this regard, open circuit voltage (OCV) values are good measurements of the fuel (H_2) and oxidant (O_2) crossover through the membranes. The electrodes used in both the cells were prepared identically and their activities can be assumed to be the same. Therefore, the cell with least fuel and oxidant crossover would lead to a higher OCV value. We had difficulty in obtaining stable OCV values when dry H_2 and O_2 were used due to the safety concerns arising from the serious crossover of reactants through the membrane in the dry state. However, we did record the OCV values of the two cells with humidified H_2 and O_2, and the results are given in Table 7.1. It is obvious that the cell with the N-NPtC membrane has higher OCV values at various temperatures from 50 °C to 75 °C, indicating that the incorporation of Pt/C catalyst powders into the Nafion membrane suppresses the crossover of reactants, most probably due to the effect of the catalytic recombination of the permeating H_2 and O_2 at the Pt particle sites inside the membrane.

Table 7.1 Comparison of the open circuit voltages (OCV) of cells fabricated with the plain N-N and the composite N-NPtC membranes at different temperatures with humidified H_2 and O_2.

Membrane	Open-circuit voltage (V)[a]		
	50 °C	60 °C	75 °C
N-N	0.878	0.879	0.883
N-NPtC	0.953	0.945	0.942

[a] The temperature values refer to the cell temperatures.

From Fig. 7.3, it can also be seen that when dry H_2 and O_2 are used, the cell voltage output shows periodic fluctuations. The fluctuations are believed to be related to the water management issue in the MEA during the cell operation. Although the incorporation of Pt/C powders could enhance the hydration of the membrane, water back-diffusion becomes dominant at high current densities, thus having a larger impact on the cell performance. A possible water transport cycle in the MEA and the corresponding cell performance are given in Fig. 7.4. The cycle starts with a cell operating at a constant high current (5 A) and a high cell voltage with a fairly hydrated initial state through the MEA. With dry H_2 and O_2, no external water is available due to the absence of humidification. The high current being delivered by the cell is accompanied with a large electro-osmotic drag transporting of water from the anode to the cathode. The initial small water concentration gradient through the MEA leads to limited water back-diffusion from the cathode to the anode. The combination of the two effects leads to an increased water concentration gradient through the MEA, resulting in a dramatic dehydration of the anode side. This dehydration is manifested as an increase in the overpotential at the anode, which leads to a decreased cell performance and lower cell voltage output. With the diminishing of the cell voltage output level, the water concentration gradient from the cathode to the anode side is increased further because the hydration state at the cathode is kept due to the constant current delivered by the cell; this facilitates the water back-diffusion from the cathode to the anode. Consequently, the rehydration of the anode side leads to a decrease in the resistance and anode overpotential, and the cell performance improves, which is

reflected by the increase in the cell voltage output at the same current. Thus the whole water transport cycle begins again, leading to the periodic fluctuation of the cell voltage output as observed in Fig. 7.3.

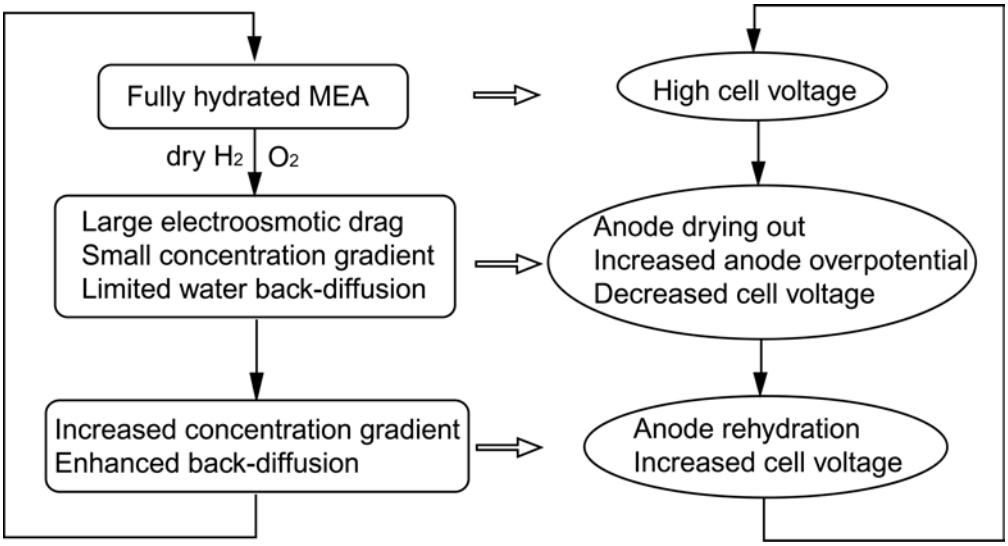

Figure 7.4 Scheme of water transports in the cell and the corresponding performance of a PEMFC operated at a constant high current density of 1 A/cm^2 with dry H_2 and O_2.

To verify the proposed water transport cycle indicated in Fig. 7.4, the change in the cell voltage output was investigated by varying the operating condition, and the results are shown in Fig. 7.5. At the initial state, the cell was operated with dry H_2 and O_2, and the cell voltage output fluctuation is obvious as shown in the beginning part of region (i) of Fig. 7.5. Then the anode H_2 was humidified while the cathode O_2 was kept dry. It can be seen that after some time of operation, the cell voltage fluctuations disappears and pretty stable output is obtained, indicating that the anode side is well hydrated due to the external humidification and confirming the water balance cycle given in Fig. 7.4.

When the H_2 is changed to be dry again, the fluctuations of the cell voltage start to be observed again as shown in region (ii) of Fig. 7.5. When O_2 instead of H_2 is humidified, the cell voltage fluctuation can still be observed as shown in region (iii) of Fig. 7.5, and the voltage value is slightly lower than those obtained in regions (i) and (ii). This is possibly due to the flooding problem at the cathode side. Product water from the cell reaction and the extra water due to the external humidification may fill the pores of the cathode, making the transport of the oxidant O_2 to the catalyst sites difficult.

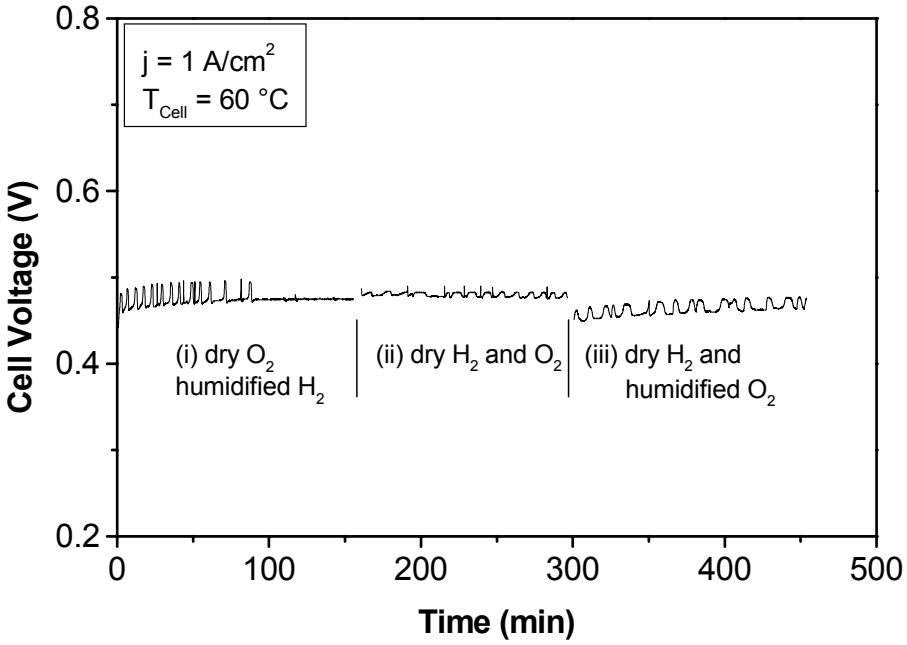

Figure 7.5 Variations of the cell voltage output of the MEAs fabricated with the composite N-NPtC membrane on changing the humidification state of the reactants. The cell was operated at 60 °C and 1 A/cm^2.

7.3.3 PEMFC Performance

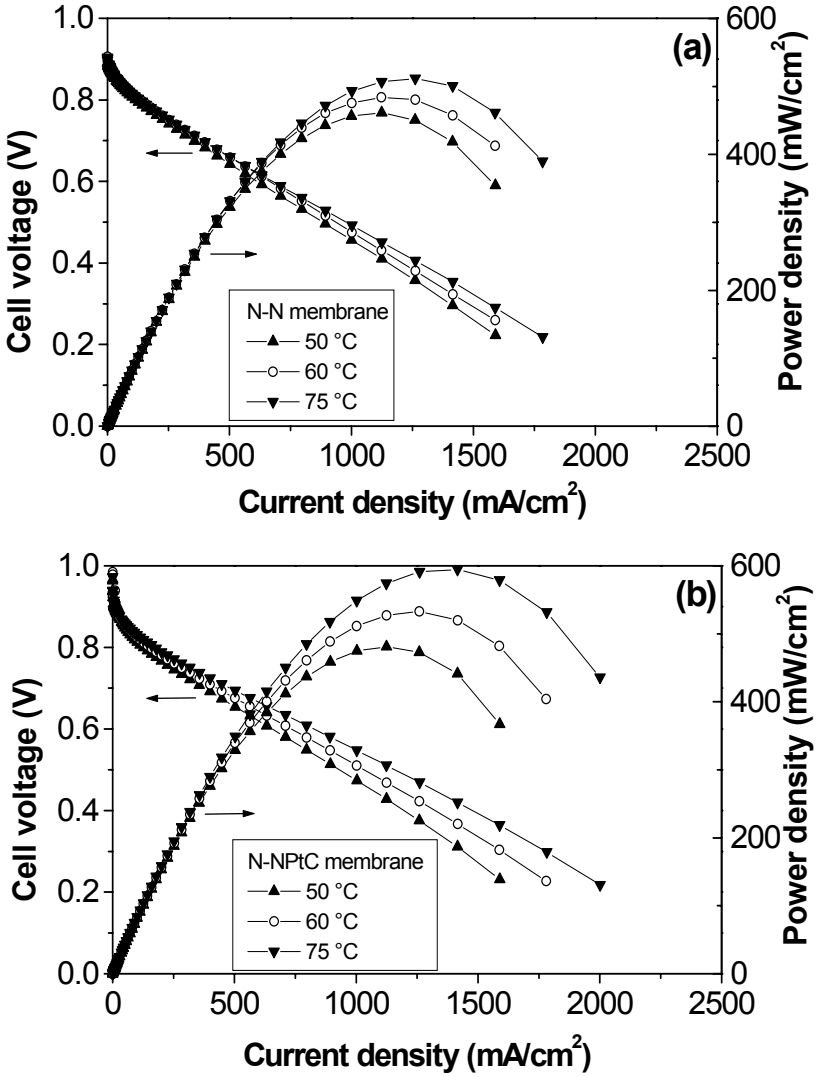

Figure 7.6 Polarization characteristics of the MEAs fabricated with the (a) plain N-N membrane and (b) composite N-NPtC membrane and operated with humidified H_2 and O_2 at different temperatures.

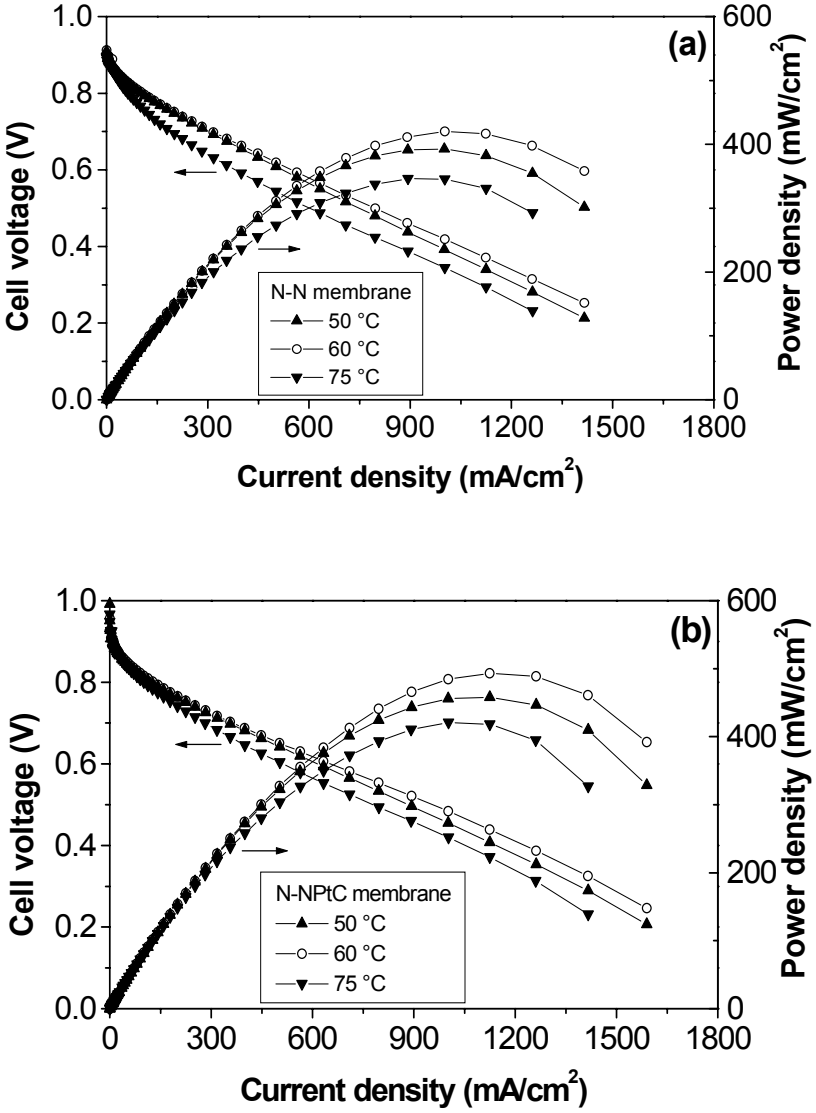

Figure 7.7 Polarization characteristics of the MEAs fabricated with the (a) plain N-N membrane and (b) composite N-NPtC membrane and operated with dry H_2 and O_2 at different temperatures.

Table 7.2 Comparison of the fraction of current density delivered by a PEMFC fabricated with the plain N-N and the composite N-NPtC membranes on operating with dry H_2/O_2.

Membrane designation	Cell Temperature (°C)	Fraction of current density at the voltage of[a]				
		0.8 V	0.7 V	0.6 V	0.5 V	0.4 V
N-N	50	90%	85%	85%	85%	85%
N-N	60	79%	81%	83%	85%	87%
N-N	75	48%	49%	56%	62%	67%
N-NPtC	50	97%	93%	94%	95%	96%
N-NPtC	60	85%	85%	89%	92%	93%
N-NPtC	75	59%	58%	62%	67%	71%

[a]The fraction of current density was calculated in comparison to that obtained on operating with humidified H_2 and O_2.

Figures 7.6 and 7.7 compare the polarization characteristics of the double-layer composite (N-NPtC) and plain Nafion (N-N) membranes in PEMFC with and without external humidification at various temperatures. These V-I curves were recorded after the cells had been operated at 1000 $mA \cdot cm^{-2}$ for at least half an hour and equilibrated states similar to that shown in Fig. 4 were obtained. It can be seen that the composite membrane shows better performance in both the cases of with and without external humidification. From Fig. 7.6, it can also be observed that when the fuel cell is operated with humidified H_2 and O_2, the performance improves with the cell operating

temperature due to the improved kinetics of the cell reaction and proton transport. However, when the dry reactants are used, the best performance is obtained at 60 °C for both the native membrane and the composite membrane (Fig. 7.7). This is because water loss due to vaporization becomes more serious at higher temperatures (75 °C), leading to a dehydration of the MEA and a decrease in cell performance.

The relative currents generated at different cell voltages with dry H_2 and O_2 as compared to those obtained with humidified reactants are compared in Table 7.2 for the MEAs fabricated with the plain N-N and composite N-NPtC membranes. For both the membranes, the fractions of current density decrease with increasing temperature due to the more serious water vaporization problem at higher temperatures although the maximum power density is obtained at 60 °C in both the cases when dry reactants are used (Fig. 7.7). At each temperature, the fractions of current density delivered by the PEMFC with the N-NPtC membrane are higher than those delivered by the PEMFC with the N-N membrane. For example, the cell with the N-N membrane on operating at 60 °C with dry reactants generate 79 to 87 % of the current generated with humidified reactants at the cell voltages of 0.8 to 0.4 V. On the other hand, the cell with the N-NPtC membrane generates 85 to 93 % of the current under similar conditions. These results indicate the pronounced effect of the incorporated Pt/C powder in self-humidifying the membrane and improving the cell performance with dry reactants.

7.4 CONCLUSIONS

The performances of thin double-layer composite membranes consisting of one layer of Pt/C catalyst dispersed Nafion and another layer of recast Nafion have been compared with those of plain Nafion membrane in PEMFC with dry and humidified H_2 and O_2 reactants. Although both the membranes could be operated with dry H_2 and O_2 due to the back-diffusion of the water produced at the cathode, the composite membranes show better performance than the plain Nafion membrane under both dry and humidified conditions. With dry H_2 and O_2, the composite membrane shows about 90 % of the performance obtained with the humidified reactants while the plain Nafion membrane shows about 80 % under similar conditions. The better performance with higher OCV values of the MEAs with the composite membrane is attributed to the catalytic recombination of H_2 and O_2 permeating through the membrane from the anode and cathode to produce water. The self-humidification fuel cell system presented here is more suitable for stationary applications where frequent starting and switch off of the system are not necessary.

Chapter 8

Summary

With an aim to better understand the proton conduction mechanisms in various proton conducting materials and overcome some of the difficulties of the presently used Nafion proton exchange membranes in both proton exchange membrane fuel cells (PEMFC) and direct methanol fuel cells (DMFC), systems such as hydrous Nafion/$Ta_2O_5 \cdot nH_2O$ composite membranes, sulfonated poly(etheretherketone) (SPEEK) based membranes, dry proton conductor $CsHSO_4$, and Nafion/Pt-C self-humidifying membranes have been developed and investigated.

Incorporation of the hydrous oxide into Nafion membrane was found to be an attractive and effective strategy to help the retention of water at temperatures > 100 °C. The presence of hydrous $Ta_2O_5 \cdot nH_2O$ in both the membrane and the electrodes allows the proper operation of the membrane-electrode assembly (MEA) at higher temperatures, which in turn is beneficial to alleviate the poisoning of the Pt catalysts by the CO impurities present in the fuel. The MEAs consisting of $Ta_2O_5 \cdot nH_2O$ modified membranes showed better cell performance than those with pristine Nafion membrane and high power densities of around 800 and 650 mW/cm^2 at 100 °C are obtained, respectively, with pure H_2 and H_2 - CO (150 ppm CO) fuels. The effects of the hydrous oxides are attributed to the existences of the lattice water and surface -OH groups which can easily absorb water from the environment. The presence of the lattice and

physically adsorbed water could enhance both the vehicle and Grotthuss mechanisms for proton conduction in the membrane at high temperatures with reduced humidity. To further increase the operating temperature and improve the proton conductivity of the membranes and the fuel cell performance at high temperatures, the properties, especially the surface properties, of the hydrous oxides deserve more fundamental studies. The knowledge will guide the preparation and optimization of the hygroscopic particles. In addition, proton conductive functional groups such as $-SO_3H$ can be tethered to porous oxides such as silica to increase the ion exchange capacity (IEC) of the oxides and gain high proton conductivity even at elevated temperatures. The incorporation of optimized hydrous inorganic oxides into the MEAs (membrane and electrodes) could prove to be a viable strategy to develop PEMFC for transportation applications with on-board reforming.

SPEEK membranes with a sulfonation level of around 50 % exhibit low methanol permeability and electrochemical performances comparable to that of Nafion membrane at around 60 °C. The lower cost and suppressed methanol crossover compared to that of Nafion make the SPEEK membranes promising alternatives for DMFC. The different methanol/water transport behaviors of SPEEK and Nafion membranes are revealed to be related to the different evolutions of the ionic clusters upon swelling. From *in-situ* small angle X-ray scattering (SAXS) in 2 M methanol solution and electrochemical impedance spectroscopic (EIS) data, it is found that with a sulfonation level of around 50 %, the SPEEK membranes have narrower pathways for methanol/water permeation at $T < 70$ °C, resulting in low methanol permeability. In

contrast, wide channels are easily formed in Nafion membranes even at low temperatures, which facilitates the transportation of methanol/water and thereby leads to serious methanol crossover problems in DMFC. The different ionic cluster evolutions of SPEEK and Nafion membranes are believed to be related to the different flexibilities of their structures. In Nafion membrane, the $-SO_3H$ groups are attached to the flexible side chains which provide enough flexibility and free volume for the clustering of ionic groups, while in SPEEK membranes, the $-SO_3H$ groups are attached to the main chain of the PEEK polymer which has high rigidity, leading to the difficulty of ionic clustering. The important insight obtained in this study regarding the different structural features of Nafion and SPEEK membranes upon swelling could provide help in designing and synthesizing new polymer membrane materials for the use in DMFC.

Multilayered membranes containing a thin inner layer of SPEEK polymer as a barrier and two outer Nafion layers have been fabricated and found to significantly reduce the methanol crossover in DMFC compared to plain Nafion membrane. Multilayered membrane containing an inner SPEEK layer with 44 % sulfonation level and a thickness of 25 μm was found to offer electrochemical performance comparable to that of Nafion despite a lower proton conductivity due to a 37 % reduction in methanol crossover compared to the native N-N-N multilayered membrane. The thin middle layer SPEEK membrane is well protected by the outer Nafion layers, leading to good strength. We believe that this multilayered approach to membrane fabrication is a promising strategy to circumvent the methanol crossover problems in DMFC. Future

investigations to chemically bond the different layers could solve the delamination problem and further improve the electrochemical performance.

The spectacular superprotonic transition of the solid acid $CsHSO_4$ at 414 K has been confirmed and high proton conductivity was obtained above this transition temperature with a PVDF/$CsHSO_4$ composite membrane. However, $CsHSO_4$ was found to experience chemical instability in contact with the Pt/C electrocatalyst and decompose to Cs_2SO_4 and H_2S in hydrogen atmosphere. For $CsHSO_4$ to be used in high temperature PEMFC, compatible catalyst materials with good catalytic activity need to be explored. In this regard, non-platinum catalysts are appealing as less active catalysts could become more active at higher temperatures. Alternatively, analogous solid acids based on phosphates instead of sulfates could be compatible with Pt based catalysts in reducing hydrogen atmosphere because the $(PO_4)^{3-}$ groups are much more difficult to reduce compared to the $(SO_4)^{2-}$ groups as P is less electronegative than S. On the other hand, fabrication procedures need to be optimized with these solid acids to obtain dense membranes that can be safely used in practical high temperature PEMFC. The operating temperature of PEMFC could be increased to 150 - 200 °C by successfully developing compatible dry proton conductor-electrocatalyst assembly, alleviating the CO poisoning problem and eliminating the humidification subsystem.

The possibility of operating PEMFC with dry H_2 and O_2 has been investigated by comparing the performance of thin double-layer self-humidifying composite membranes containing dispersed Pt/C catalyst powder in one layer with that of plain Nafion membrane in PEMFC with dry as well as humidified reactants. It was found

that the back-diffusion of water produced at the cathode is sufficient to hydrate the thin electrolyte membrane, leading to the proper operation of PEMFC with dry H_2 and O_2. However, the MEA fabricated with the self-humidifying N-NPtC composite membrane showed better performance than the N-N plain Nafion membrane in both dry and humidified conditions. The better performance of the former was found to be due to the catalytic recombination of H_2 and O_2 permeating through the thin membrane at the Pt/C sites to produce water that directly humidifies the membrane. Although the self-humidifying fuel cell system may not be attractive for applications involving frequent startup such as automobiles, they could become appealing for stationary applications, providing important cost savings by eliminating the humidification system.

In summary, this investigation demonstrates that significant improvements in the performance of PEMFC and DMFC and important cost savings can be achieved by developing new proton exchange membranes. Successful development of high temperature membranes that can operate at 150 – 200 °C in the future can have a profound impact in the fuel cell technology. It can alleviate the CO poisoning problem considerably and could possibly allow the exploration of non-platinum catalysts. This can lower the fuel cell cleanup and raw materials costs significantly, and make the fuel cell technology more cost competitive with the other existing technologies like internal combustion engines (ICE). Reduction in cost can allow a rapid commercialization of the fuel cell technology and provide important environmental benefits. Development of alternate methanol impermeable membranes can also have significant impact in the direct methanol fuel cell technology by allowing the use of high concentration

methanol solution, which is important in increasing the energy density and fabricating miniaturized DMFCs for portable electronic device applications.

Bibliography

[1] K. Kordesch, G. Simader, Fuel Cells and Their Applications, VCH, 1996.

[2] P. Costamagna, S. Srinivasan, J. Power Sources 102 (2001) 242.

[3] P. Costamagna, S. Srinivasan, J. Power Sources 102 (2001) 253.

[4] S. Srinivasan, R. Mosdale, P. Stevens, C. Yang, Annu. Rev. Energ. Env. 24 (1999) 281.

[5] B.D. McNicol, D.A.J. Rand, K.R. Williams, J. Power Sources 100 (2001) 47.

[6] X. Ren, T. Zawodzinski, S. Gottesfeld, Abstr. Pap. Am. Chem. Soc. 217 (1999) 345.

[7] Y.H.L. Eisenberg A., Perfluorinated Ionomer Membranes, ACS Symposium Series 180, American Chemical Society, Washington, DC, 1982.

[8] S.R. Samms, S. Wasmus, R.F. Savinell, J. Electrochem. Soc. 143 (1996) 1498.

[9] A. Steck, In: O. Savadogo, P.R. Roberge, T.N. Veziroglu (Eds.), Proceedings of the First International Symposium on New Materials for Fuel Cell Systems, Montreal, Canada, July 9 -13, 1995, p. 74.

[10] H.L. Yeager, A. Steck, J. Electrochem. Soc. 128 (1981) 1880.

[11] F. Barbir, T. Gomez, Int. J. Hydrog. Energy 21 (1996) 891.

[12] Q.F. Li, R.H. He, J.O. Jensen, N.J. Bjerrum, Chem. Mater. 15 (2003) 4896.

[13] K.T. Adjemian, S.J. Lee, S. Srinivasan, J. Benziger, A.B. Bocarsly, J. Electrochem. Soc. 149 (2002) A256.

[14] Q.F. Li, R.H. He, J.A. Gao, J.O. Jensen, N.J. Bjerrum, J. Electrochem. Soc. 150 (2003) A1599.

[15] M.W. Verbrugge, J. Electrochem. Soc. 136 (1989) 417.

[16] R. Savinell, E. Yeager, D. Tryk, U. Landau, J. Wainright, D. Weng, K. Lux, M. Litt, C. Rogers, J. Electrochem. Soc. 141 (1994) L46.

[17] D. Chu, S. Gilman, J. Electrochem. Soc. 141 (1994) 1770.

[18] B. Bittinscattaneo, S. Wasmus, B. Lopezmishima, W. Vielstich, J. Appl. Electrochem. 23 (1993) 625.

[19] P. Colomban (Ed.), Proton Conductors: Solids, Membranes and Gels-Materials and Devices (Chemistry of Solid State Materials, No 2), Cambridge University Press, 1992.

[20] K.D. Kreuer, Solid State Ionics 136 (2000) 149.

[21] K.T. Adjemian, S. Srinivasan, J. Benziger, A.B. Bocarsly, J. Power Sources 109 (2002) 356.

[22] N. Miyake, J.S. Wainright, R.F. Savinell, J. Electrochem. Soc. 148 (2001) A898.

[23] P.L. Antonucci, A.S. Arico, P. Creti, E. Ramunni, V. Antonucci, Solid State Ionics 125 (1999) 431.

[24] A.S. Arico, P. Creti, P.L. Antonucci, V. Antonucci, Electrochem. Solid-State Lett. 1 (1998) 66.

[25] B. Baradie, J.P. Dodelet, D. Guay, J. Electroanal. Chem. 489 (2000) 101.

[26] M. Watanabe, H. Uchida, M. Emori, J. Phys. Chem. B 102 (1998) 3129.

[27] C. Trakanprapai, V. Esposito, S.L. Coccia, E. Traversa, V. Baglio, A.D. Blasi, A.S. Arico, V. Antonucci, P.L. Antonucci, Abstract No. 1080, The 204th Meeting of The Electrochemical Society, Orlando, FL, Oct. 12 -17, 2003.

[28] P. Costamagna, C. Yang, A.B. Bocarsly, S. Srinivasan, Electrochim. Acta 47 (2002) 1023.

[29] G. Alberti, M. Casciola, Solid State Ionics 97 (1997) 177.

[30] G. Alberti, M. Casciola, Annu. Rev. Mater. Res. 33 (2003) 129.

[31] M. Rikukawa, K. Sanui, Prog. Polym. Sci. 25 (2000) 1463.

[32] J. Roziere, D.J. Jones, Annu. Rev. Mater. Res. 33 (2003) 503.

[33] M.E. Schuster, W.H. Meyer, Annu. Rev. Mater. Res. 33 (2003) 233.

[34] S.M. Haile, D.A. Boysen, C.R.I. Chisholm, R.B. Merle, Nature 410 (2001) 910.

[35] D.A. Boysen, T. Uda, C.R.I. Chisholm, S.M. Haile, Science 303 (2004) 68.

[36] R.A. Zoppi, I.V.P. Yoshida, S.P. Nunes, Polymer 39 (1998) 1309.

[37] K.A. Mauritz, I.D. Stefanithis, S.V. Davis, R.W. Scheetz, R.K. Pope, G.L. Wilkes, H.H. Huang, J. Appl. Polym. Sci. 55 (1995) 181.

[38] P.L. Shao, K.A. Mauritz, R.B. Moore, Chem. Mater. 7 (1995) 192.

[39] G. Alberti, M. Casciola, R. Palombari, J. Membr. Sci. 172 (2000) 233.

[40] H.T. Wang, B.A. Holmberg, L.M. Huang, Z.B. Wang, A. Mitra, J.M. Norbeck, Y.S. Yan, J. Mater. Chem. 12 (2002) 834.

[41] P. Dimitrova, K.A. Friedrich, U. Stimming, B. Vogt, Solid State Ionics 150 (2002) 115.

[42] A.S. Arico, V. Baglio, A. Di Blasi, V. Antonucci, Electrochem. Commun. 5 (2003) 862.

[43] C. Yang, P. Costamagna, S. Srinivasan, J. Benziger, A.B. Bocarsly, J. Power Sources 103 (2001) 1.

[44] C. Yang, S. Srinivasan, A.S. Arico, P. Creti, V. Baglio, V. Antonucci, Electrochem. Solid-State Lett. 4 (2001) A31.

[45] J.A. Kerres, J. Membr. Sci. 185 (2001) 3.

[46] K.D. Kreuer, J. Membr. Sci. 185 (2001) 29.

[47] D.J. Jones, J. Roziere, J. Membr. Sci. 185 (2001) 41.

[48] J.M. Bae, I. Honma, M. Murata, T. Yamamoto, M. Rikukawa, N. Ogata, Solid State Ionics 147 (2002) 189.

[49] G. Alberti, M. Casciola, L. Massinelli, B. Bauer, J. Membr. Sci. 185 (2001) 73.

[50] B. Bonnet, D.J. Jones, J. Roziere, L. Tchicaya, G. Alberti, M. Casciola, L. Massinelli, B. Bauer, A. Peraio, E. Ramunni, J. New Mat.Electrochem. Syst. 3 (2000) 87.

[51] F. Lufrano, G. Squadrito, A. Patti, E. Passalacqua, J. Appl. Polym. Sci. 77 (2000) 1250.

[52] F. Lufrano, I. Gatto, P. Staiti, V. Antonucci, E. Passalacqua, Solid State Ionics 145 (2001) 47.

[53] B. Lafitte, L.E. Karlsson, P. Jannasch, Macromol. Rapid Commun. 23 (2002) 896.

[54] A.C. Tavares, R. Pedicini, I. Gatto, Y.A. Dubitsky, A. Zaopo, E. Passalacqua, J. New Mat.Electrochem. Syst. 6 (2003) 211.

[55] L.E. Karlsson, P. Jannasch, J. Membr. Sci. 230 (2004) 61.

[56] R.W. Kopitzke, C.A. Linkous, H.R. Anderson, G.L. Nelson, J. Electrochem. Soc. 147 (2000) 1677.

[57] B. Bauer, D.J. Jones, J. Roziere, L. Tchicaya, G. Alberti, M. Casciola, L. Massinelli, A. Peraio, S. Besse, E. Ramunni, J. New Mat.Electrochem. Syst. 3 (2000) 93.

[58] T. Kobayashi, M. Rikukawa, K. Sanui, N. Ogata, Solid State Ionics 106 (1998) 219.

[59] S.D. Mikhailenko, S.M.J. Zaidi, S. Kaliaguine, Catal. Today 67 (2001) 225.

[60] L. Li, L. Xu, Y.X. Wang, Acta Polymerica Sinica (2003) 452.

[61] P.X. Xing, G.P. Robertson, M.D. Guiver, S.D. Mikhailenko, K.P. Wang, S. Kaliaguine, J. Membr. Sci. 229 (2004) 95.

[62] E. Drioli, A. Regina, M. Casciola, A. Oliveti, F. Trotta, T. Massari, J. Membr. Sci. 228 (2004) 139.

[63] B. Lakshmanan, W. Huang, D. Olmeijer, J.W. Weidner, Electrochem. Solid-State Lett. 6 (2003) A282.

[64] X. Glipa, M. ElHaddad, D.J. Jones, J. Roziere, Solid State Ionics 97 (1997) 323.

[65] P. Staiti, F. Lufrano, A.S. Arico, E. Passalacqua, V. Antonucci, J. Membr. Sci. 188 (2001) 71.

[66] C. Genies, R. Mercier, B. Sillion, N. Cornet, G. Gebel, M. Pineri, Polymer 42 (2001) 359.

[67] X.X. Guo, J.H. Fang, T. Watari, K. Tanaka, H. Kita, K.I. Okamoto, Macromolecules 35 (2002) 6707.

[68] C.A. Linkous, Int. J. Hydrog. Energy 18 (1993) 641.

[69] X.G. Jin, M.T. Bishop, T.S. Ellis, F.E. Karasz, British Polymer Journal 17 (1985) 4.

[70] J. Lee, C.S. Marvel, J. Polym. Sci., Polym. Chem. Ed. 22 (1984) 295.

[71] R.Y.M. Huang, P.H. Shao, C.M. Burns, X. Feng, J. Appl. Polym. Sci. 82 (2001) 2651.

[72] D. Daoust, J. Devaux, P. Godard, Polym. Int. 50 (2001) 917.

[73] D. Daoust, J. Devaux, P. Godard, Polym. Int. 50 (2001) 925.

[74] D. Daoust, J. Devaux, P. Godard, Polym. Int. 50 (2001) 932.

[75] G. Hubner, E. Roduner, J. Mater. Chem. 9 (1999) 409.

[76] J. Kerres, W. Cui, S. Reichle, J. Polym. Sci., Polym. Chem. Ed. 34 (1996) 2421.

[77] T.S. Guth, J. Baurmeister, G. Frank, R. Knauf, International Patent WO 99/29763. In, 1999.

[78] C.A. Linkous, H.R. Anderson, R.W. Kopitzke, G.L. Nelson, Int. J. Hydrog. Energy 23 (1998) 525.

[79] S.M.J. Zaidi, S.D. Mikhailenko, G.P. Robertson, M.D. Guiver, S. Kaliaguine, J. Membr. Sci. 173 (2000) 17.

[80] B. Baradie, C. Poinsignon, J.Y. Sanchez, Y. Piffard, G. Vitter, N. Bestaoui, D. Foscallo, A. Denoyelle, D. Delabouglise, M. Vaujany, J. Power Sources 74 (1998) 8.

[81] J.H. Fang, X.X. Guo, S. Harada, T. Watari, K. Tanaka, H. Kita, K. Okamoto, Macromolecules 35 (2002) 9022.

[82] N. Cornet, O. Diat, G. Gebel, F. Jousse, D. Marsacq, R. Mercier, M. Pineri, J. New Mat.Electrochem. Syst. 3 (2000) 33.

[83] S. Besse, P. Capron, O. Diat, G. Gebel, F. Jousse, D. Marsacq, M. Pineri, C. Marestin, R. Mercier, J. New Mat.Electrochem. Syst. 5 (2002) 109.

[84] P. Genova-Dimitrova, B. Baradie, D. Foscallo, C. Poinsignon, J.Y. Sanchez, J. Membr. Sci. 185 (2001) 59.

[85] P. Staiti, M. Minutoli, J. Power Sources 94 (2001) 9.

[86] P. Staiti, M. Minutoli, S. Hocevar, J. Power Sources 90 (2000) 231.

[87] Y. Park, M. Nagai, Solid State Ionics 145 (2001) 149.

[88] H. Nakajima, I. Honma, Solid State Ionics 148 (2002) 607.

[89] Y.L. Ma, J.S. Wainright, M.H. Litt, R.F. Savinell, J. Electrochem. Soc. 151 (2004) A8.

[90] P. Donoso, W. Gorecki, C. Berthier, F. Defendini, C. Poinsignon, M.B. Armand, Solid State Ionics 28 (1988) 969.

[91] J. Przyluski, A. Zalewska, J. Maron, W. Wieczorek, Polish J. Chem. 71 (1997) 968.

[92] M.F. Daniel, B. Desbat, F. Cruege, O. Trinquet, J.C. Lassegues, Solid State Ionics 28 (1988) 637.

[93] R. Tanaka, H. Yamamoto, A. Shono, K. Kubo, M. Sakurai, Electrochim. Acta 45 (2000) 1385.

[94] D. Rodriguez, C. Jegat, O. Trinquet, J. Grondin, J.C. Lassegues, Solid State Ionics 61 (1993) 195.

[95] J.S. Wainright, J.T. Wang, D. Weng, R.F. Savinell, M. Litt, J. Electrochem. Soc. 142 (1995) L121.

[96] J.S. Wainright, J.T. Wang, R. Savinell, M. Litt, H. Moaddel , C. Rogers, In: S. Srinivasan, D.D. Macdonald, A.C. Khandkar (Eds.), Electrode Materials and Processes for Energy Coversion and Storage, Pennington, NJ, 1995, p. 255.

[97] D. Weng, J.S. Wainright, U. Landau, R.F. Savinell, J. Electrochem. Soc. 143 (1996) 1260.

[98] Q.F. Li, H.A. Hjuler, N.J. Bjerrum, J. Appl. Electrochem. 31 (2001) 773.

[99] T.A. Zawodzinski, T.E. Springer, J. Davey, R. Jestel, C. Lopez, J. Valerio, S. Gottesfeld, J. Electrochem. Soc. 140 (1993) 1981.

[100] T.F. Fuller, J. Newman, J. Electrochem. Soc. 139 (1992) 1332.

[101] X. Glipa, B. Bonnet, B. Mula, D.J. Jones, J. Roziere, J. Mater. Chem. 9 (1999) 3045.

[102] R.H. He, Q.F. Li, G. Xiao, N.J. Bjerrum, J. Membr. Sci. 226 (2003) 169.

[103] J.T. Wang, R.F. Savinell, J. Wainright, M. Litt, H. Yu, Electrochim. Acta 41 (1996) 193.01

[104] J.T. Wang, J.S. Wainright, R.F. Savinell, M. Litt, J. Appl. Electrochem. 26 (1996) 751.

[105] Q.F. Li, H.A. Hjuler, C. Hasiotis, J.K. Kallitsis, C.G. Kontoyannis, N.J. Bjerrum, Electrochem. Solid-State Lett. 5 (2002) A125.

[106] K.D. Kreuer, Solid State Ionics 97 (1997) 1.

[107] K.D. Kreuer, A. Fuchs, M. Ise, M. Spaeth, J. Maier, Electrochim. Acta 43 (1998) 1281.

[108] H.G. Herz, K.D. Kreuer, J. Maier, G. Scharfenberger, M.F.H. Schuster, W.H. Meyer, Electrochim. Acta 48 (2003) 2165.

[109] W. Munch, K.D. Kreuer, W. Silvestri, J. Maier, G. Seifert, Solid State Ionics 145 (2001) 437.

[110] M. Schuster, W.H. Meyer, G. Wegner, H.G. Herz, M. Ise, K.D. Kreuer, J. Maier, Solid State Ionics 145 (2001) 85.

[111] M.F.H. Schuster, W.H. Meyer, M. Schuster, K.D. Kreuer, Chem. Mater. 16 (2004) 329.

[112] K.D. Kreuer, ChemPhysChem 3 (2002) 771.

[113] D.A. Boysen, C.R.I. Chisholm, S.M. Haile, S.R. Narayanan, J. Electrochem. Soc. 147 (2000) 3610.

[114] E.B. Easton, B.L. Langsdorf, J.A. Hughes, J. Sultan, Z.G. Qi, A. Kaufman, P.G. Pickup, J. Electrochem. Soc. 150 (2003) C735.

[115] A. Sungpet, J. Membr. Sci. 226 (2003) 131.

[116] M.A. Smit, A.L. Ocampo, M.A. Espinosa-Medina, P.J. Sebastian, J. Power Sources 124 (2003) 59.

[117] T. Shimizu, T. Naruhashi, T. Momma, T. Osaka, Electrochemistry 70 (2002) 991.

[118] N.Y. Jia, M.C. Lefebvre, J. Halfyard, Z.G. Qi, P.G. Pickup, Electrochem. Solid-State Lett. 3 (2000) 529.

[119] B. Bae, B.H. Chun, H.Y. Ha, I.H. Oh, D. Kim, J. Membr. Sci. 202 (2002) 245.

[120] F. Finsterwalder, G. Hambitzer, J. Membr. Sci. 185 (2001) 105.

[121] W.C. Choi, J.D. Kim, S.I. Woo, J. Power Sources 96 (2001) 411.

[122] L.J. Hobson, H. Ozu, M. Yamaguchi, S. Hayase, J. Electrochem. Soc. 148 (2001) A1185.

[123] L.J. Hobson, H. Oozu, M. Yamaguchi, S. Hayase, J. New Mat.Electrochem. Syst. 5 (2002) 113.

[124] P. Staiti, A.S. Arico, V. Baglio, F. Lufrano, E. Passalacqua, V. Antonucci, Solid State Ionics 145 (2001) 101.

[125] D.H. Jung, S.Y. Cho, D.H. Peck, D.R. Shin, J.S. Kim, J. Power Sources 106 (2002) 173.

[126] N. Miyake, J.S. Wainright, R.F. Savinell, J. Electrochem. Soc. 148 (2001) A905.

[127] C. Genies, R. Mercier, B. Sillion, R. Petiaud, N. Cornet, G. Gebel, M. Pineri, Polymer 42 (2001) 5097.

[128] C. Manea, M. Mulder, J. Membr. Sci. 206 (2002) 443.

[129] K. Ramya, K.S. Dhathathreyan, J. Appl. Polym. Sci. 88 (2003) 307.

[130] K. Ramya, B. Vishnupriya, K.S. Dhathathreyan, J. New Mat.Electrochem. Syst. 4 (2001) 115.

[131] B. Vishnupriya, K. Ramya, K.S. Dhathathreyan, J. Appl. Polym. Sci. 83 (2002) 1792.

[132] L. Jorissen, V. Gogel, J. Kerres, J. Garche, J. Power Sources 105 (2002) 267.

[133] B. Yang, A. Manthiram, Electrochem. Solid-State Lett. 6 (2003) A229.

[134] L. Li, J. Zhang, Y.X. Wang, J. Membr. Sci. 226 (2003) 159.

[135] S.P. Nunes, B. Ruffmann, E. Rikowski, S. Vetter, K. Richau, J. Membr. Sci. 203 (2002) 215.

[136] B. Ruffmann, H. Silva, B. Schulte, S.P. Nunes, Solid State Ionics 162 (2003) 269.

[137] L. Li, L. Xu, Y.X. Wang, Mater. Lett. 57 (2003) 1406.

[138] M. Takami, Y. Yamazaki, H. Hamada, Electrochemistry 69 (2001) 98.

[139] D.H. Jung, Y.B. Myoung, S.Y. Cho, D.R. Shin, D.H. Peck, Int. J. Hydrog. Energy 26 (2001) 1263.

[140] F.G. Wilhelm, I.G.M. Punt, N.F.A. van der Vegt, H. Strathmann, M. Wessling, J. Membr. Sci. 199 (2002) 167.

[141] J. Kerres, W. Zhang, L. Jorissen, V. Gogel, J. New Mat.Electrochem. Syst. 5 (2002) 97.

[142] J. Kerres, W. Zhang, A. Ullrich, C.M. Tang, M. Hein, V. Gogel, T. Frey, L. Jorissen, Desalination 147 (2002) 173.

[143] L. Xiong, A.M. Kannan, A. Manthiram, Electrochem. Commun. 4 (2002) 898.

[144] X. Ren, T.E. Springer, S. Gottesfeld, J. Electrochem. Soc. 147 (2000) 92.

[145] H. Meng, C.Y. Wang, J. Electrochem. Soc. 151 (2004) A358.

[146] L. Krishnan, C.A. Marozzi, K.T. Adjemian, A.B. Bocarsly, S. Srinivasan, Abstract No. 92. The 201st Meeting of the Electrochemical Society, May 12-17, Philadelphia, PA, 2002.

[147] M. Yamashita, S. Kim, C. Yang, S. Srinivasan, A.B. Bocarsly, Abstract No. 100. The 201st Meeting of the Electrochemical Society, May 12-17, Philadelphia, PA, 2002.

[148] R.C.T. Slade, J. Barker, T.K. Halstead, Solid State Ionics 24 (1987) 147.

[149] R.P. Singh, J. Electron. Mater. 30 (2001) 1584.

[150] G. Pourcelly, A. Oikonomou, C. Gavach, H.D. Hurwitz, Journal of Electroanalytical Chemistry 287 (1990) 43.

[151] R.S. Yeo, J. Electrochem. Soc. 130 (1983) 533.

[152] J. Halim, F.N. Buchi, O. Haas, M. Stamm, G.G. Scherer, Electrochim. Acta 39 (1994) 1303.

[153] T.E. Springer, T.A. Zawodzinski, M.S. Wilson, S. Gottesfeld, J. Electrochem. Soc. 143 (1996) 587.

[154] V.A. Paganin, C.L.F. Oliveira, E.A. Ticianelli, T.E. Springer, E.R. Gonzalez, Electrochim. Acta 43 (1998) 3761.

[155] M. Ciureanu, H. Wang, J. New Mat.Electrochem. Syst. 3 (2000) 107.

[156] M. Ciureanu, H. Wang, J. Electrochem. Soc. 146 (1999) 4031.

[157] M. Ciureanu, H. Wang, Z.G. Qi, J. Phys. Chem. B 103 (1999) 9645.

[158] A. Parthasarathy, S. Srinivasan, A.J. Appleby, C.R. Martin, J. Electroanal. Chem. 339 (1992) 101.

[159] J. Lipkowski, P.N. Ross (Eds.), Electrochemistry of Novel Materials, VCH, 1994.

[160] W.A. England, M.G. Cross, A. Hamnett, P.J. Wiseman, J.B. Goodenough, Solid State Ionics 1 (1980) 231.

[161] S.N. Lvov, Abstract No. 972. In: 241th Meeting of the Electrochemical Society, Orlando, FL, Oct. 12 - 17, 2003.

[162] K.D. Kreuer, M. Ise, A. Fuchs, J. Maier, J. Phys. IV 10 (2000) 279.

[163] F.J. Waller, R.W. Vanscoyoc, Chemtech 17 (1987) 438.

[164] M.A. Harmer, W.E. Farneth, Q. Sun, J. Am. Chem. Soc.118 (1996) 7708.

[165] P. Argyropoulos, K. Scott, W.M. Taama, J. Power Sources 87 (2000) 153.

[166] P. Argyropoulos, K. Scott, W.M. Taama, Electrochim. Acta 45 (2000) 1983.

[167] T.D. Gierke, G.E. Munn, F.C. Wilson, J. Polym. Sci., Polym. Phys. Ed. 19 (1981) 1687.

[168] M. Fujimura, T. Hashimoto, H. Kawai, Macromolecules 14 (1981) 1309.

[169] M. Fujimura, T. Hashimoto, H. Kawai, Macromolecules 15 (1982) 136.

[170] G. Gebel, J. Lambard, Macromolecules 30 (1997) 7914.

[171] J. Kao, R.S. Stein, W.J. Macknight, W.P. Taggart, G.S. Cargill, Macromolecules 7 (1974) 95.

[172] W.J. Macknight, W.P. Taggart, R.S. Stein, J. Polym Sci.: Polym Phys. 45 (1974) 113.

[173] D.J. Yarusso, S.L. Cooper, Macromolecules 16 (1983) 1871.

[174] D.J. Yarusso, S.L. Cooper, Polymer 26 (1985) 371.

[175] C.L. Marx, D.F. Caulfield, S.L. Cooper, Macromolecules 6 (1973) 344.

[176] G. Gebel, P. Aldebert, M. Pineri, Polymer 34 (1993) 333.

[177] L. Prado, H. Wittich, K. Schulte, G. Goerigk, V.M. Garamus, R. Willumeit, S. Vetter, B. Ruffmann, S.P. Nunes, J Polym Sci B: Polym Phys. 42 (2004) 567.

[178] A. Eisenberg, Macromolecules 3 (1970) 147.

[179] G. Gebel, Polymer 41 (2000) 5829.

[180] S. Schlick, G. Gebel, M. Pineri, F. Volino, Macromolecules 24 (1991) 3517.

[181] H.W. Li, S. Schlick, Polymer 36 (1995) 1141.

[182] A.V. Belushkin, R.L. McGreevy, P. Zetterstrom, L.A. Shuvalov, Physica B 241 (1997) 323.

[183] A.V. Belushkin, W.I.F. David, R.M. Ibberson, L.A. Shuvalov, Acta Cryst B 47 (1991) 161.

[184] M. Friesel, A. Lunden, B. Baranowski, Solid State Ionics 35 (1989) 91.

[185] M. Watanabe, H. Uchida, M. Emori, J. Electrochem. Soc. 145 (1998) 1137.

[186] M. Watanabe, H. Uchida, H. Igarashi, Macromol. Symp. 156 (2000) 223.

[187] F.Q. Liu, B.L. Yi, D.M. Xing, J.R. Yu, Z.J. Hou, Y.Z. Fu, J. Power Sources 124 (2003) 81.

[188] P. Berg, K. Promislow, J. St Pierre, J. Stumper, B. Wetton, J. Electrochem. Soc. 151 (2004) A341.

[189] F.N. Buchi, S. Srinivasan, J. Electrochem. Soc. 144 (1997) 2767.